Interplay between ATM and ATR for the regulation of cellular responses to DNA damage

Inaugural-Dissertation

zur
Erlangung des Doktorgrades
Dr. rer. nat.
der Fakultät
Biologie und Geografie
an der Universität Duisburg-Essen

vorgelegt von

Xiaoxiang Fan
aus China

Essen, im November 2009

Die der vorliegenden Arbeit zugrunde liegenden Experimente wurden am Institut für Medizinische Strahlenbiologie der Universität Duisburg-Essen durchgeführt.

1. Gutachter:	Prof. Dr. phil. nat. George Iliakis
2. Gutachter:	Prof. Dr. Perihan Nalbant
3. Gutachter:	Prof. Dr. Jürgen Thomale
Vorsitzender des Prüfungsausschusses:	Prof. Dr. Perihan Nalbant
Tag der mündlichen Prüfung:	21.04.2010

1 Abstract

Cell cycle checkpoints are critical regulatory processes ensuring the proper traversal of a cell through the cell cycle. Activation of checkpoints in response to different types of DNA damage arrests the normal cell cycle progression at different stages, presumably to allow time for repair. ATM (Ataxia-telangiectasia mutated) and ATR (ATM and Rad3-related) are critical players in G2 checkpoint response. It is still unknown whether the contribution of ATM and ATR to checkpoint activation is through independent inputs from parallel signaling cascades, or whether the two kinases contribute in a sequential manner, in the sense that the activation of one is enhanced by the activation of the other.

Here, we use flow cytometry-based measurement of DNA-content and mitotic index variations to detect G2 checkpoint activation and maintenance after exposure of cells with different genetic background to ionizing radiation (IR). Extensive experiments using different cell lines and an array of inhibitors confirm that ATR signaling plays a dominant role in the development of a full scale G2 arrest, while ATM signaling ensures the maintenance of a full scale G2 arrest.

In response to IR, ATRIP (ATR interacting protein) and ATM phosphorylated at serine 1981 (ATM-pS1981) show local accumulation on chromatin that is detected in the form foci by immunofluorescence microscopy. Immunofluorescence detection of ATRIP and ATM-pS1981 foci reveals a linkage between foci formation and G2 checkpoint activation. Although ATR plays a dominant role in G2 checkpoint signaling, its activation for G2 arrest may not coincide with foci formation since visible foci form relatively late (1 h after IR). The contribution of ATM to G2 arrest, as indicated by the formation of ATM-pS1981 foci, is strongly dependent on the cell cycle phase in which the cell is irradiated. To investigate this aspect in greater detail, we introduced multicolor staining protocols utilizing appropriate cell cycle makers that allow cell cycle stage characterization before and after irradiation. By combining ATM-pS1981 foci kinetics with cell cycle information, we observed an apparent requirement for about 20 foci for the maintenance of the G2 arrest for cells irradiated in the G2-phase. There is no apparent correlation between ATM-pS1981 foci and G2 arrest for cells irradiated in the G1-phase, as in this case foci disappear relatively

quickly. Interestingly, cells irradiated throughout S-phase, show a response similar to that observed with G2 cells and not, as one would expect, a mixed response reflecting subpopulations responding like G1 and subpopulations responding like G2 cells.

Key words, ATM, Chk2, ATR, Chk1, phosphorylation, ATM foci, G2 checkpoint

2 Introduction

2.1 Cell cycle progression and Checkpoint activation

Cell cycle checkpoints are critical regulatory processes ensuring the proper traversal of a cell through the cell cycle. They include responses that enforce the right sequence in cell progression through the cell cycle, contribute to the repair of DNA damage, ensure the high fidelity of DNA replication, and assist in the proper chromosome segregation at mitosis (1,2). Checkpoints are highly conserved in all eukaryotes (3). Activation of checkpoints in response to different types of DNA damage arrests the normal cell cycle progression at different phases, presumably to allow time for repair. Checkpoint deficiency causes genomic instability and has been implicated in carcinogenesis (3). The cell cycle and checkpoints are illustrated in Figure 1.

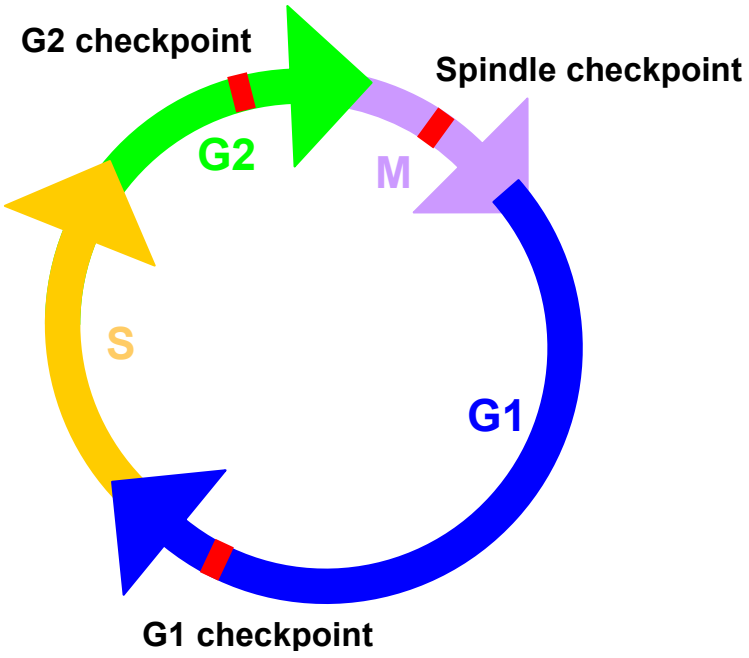

Figure 1. Cell cycle and checkpoint control. Four cell cycle stage and three checkpoints are depicted. Because the intra-S checkpoints are distributed throughout the S-phase, they do not show in the picture.

2.1.1 The G1 checkpoint

It is generally thought that the tumour suppressor p53 plays an essential role in controlling the G1/S checkpoint (4). After the occurrence of DNA damage, p53

mediates transcriptional up-regulation of p21. p21 binds a series of Cdk-cyclin complexes, like for example cdk4-cyclin D, Cdk6-cyclin D, Cdk2-cyclin E, as well as Cdk2-cyclin A, and inhibits their activities. This inhibition transiently arrests cells in their transition from G1 into S (4-7).

2.1.2 G2 checkpoint

The activation of the G2 checkpoint delays mitotic entry in the presence of DNA damage. Because the spindle checkpoint at mitosis only responds to spindle damages or mis-attached chromosomes (8), the G2 checkpoint is the last chance for correcting genomic damage prior to cell division (9). This fact probably explains its importance in the overall checkpoint response. The proteins participating in the activation of the G2 checkpoint are highly conserved in eukaryotes (10). It is well documented that the ultimate target of the initiated G2 checkpoint signal transduction pathway is Cdc2 (Cdk1) (1,11-13). In G2, this cyclin dependent kinase (Cdk) is activated after binding to cyclin B1, by a phosphorylation at Threonine-161 and a dephosphorylation at Threonine-14/Tyrosine-15 (1). In this stage, Cdk1 is associated with cyclin B1 and forms the so called mitosis promotion factor (MPF). Checkpoint mediated delay in G2 can be enhanced by a delay in the removal of the inactivating phosphorylation in Thr-14/Tyr-15 (see above). Furthermore, several variations in the signal transduction cascade upstream of Cdk1 have been proposed, depending on the presence of p53 (14). p53 and p21 are believed to contribute to the G2 checkpoint by up-regulating the 14-3-3 proteins. High levels of 14-3-3 inhibit MPF by inhibiting the activity of Cdc25C, which is responsible for the dephosphorylation of Cdk1 at Tyr-15 (15). Interaction of Cdc25C with 14-3-3 proteins is increased after phosphorylation of Cdc25C by Chk1 or Chk2 and leads to the translocation of Cdc25C to the cytoplasm and its subsequent degradation. Ataxia-telangiectasia mutated (ATM) and ATM and Rad3-related (ATR) are putative critical players in G2 checkpoint activation independently of p53; ATR and ATM mediate the activation of Chk1 and Chk2, respectively (16-18).

2.1.3 DSBs are very effective to activate checkpoints

The DNA double-strand breaks (DSBs) are the principle cytotoxic lesions induced by ionizing radiation (IR). They are also induced as a consequence of chemical treatments (hydroxyurea, etoposide, bleomycin) (19,20), as well as of mechanical

stress (21). They can also be accidentally induced by abrogation of normal biological events, such as the collapse of a replication fork, and are produced in a programmed fashion during V(D)J and class switch recombination in developing lymphoid cells, as well during meiosis (22-24). DSBs must be properly handled. Unrepaired or misrepaired DSBs can lead to mutations or genomic instability (25). DSBs are very effective in triggering the activation of cell cycle checkpoints, presumably to provide time for repair (3,26,27).

2.2 ATM-Chk2 and ATR-Chk1 signaling in G2 checkpoint

ATM and ATR are key players in checkpoint response and their activations are essential for the maintenance of genomic integrity after DNA damage (10,28,29). ATM, ATR, as well as the DNA dependent protein kinase catalytic subunit (DNA-PKcs) are large protein kinases with molecular weight of 370, 301 and 450 KD respectively. They share sequence homology with the phosphoinositide-3 lipid family of kinases (PI-3Ks) but work exclusively on proteins (30-32) by phosphorylating serines and threonines at the consensus sites SQ/TQ. All three proteins contain themselves clusters of SQ/TQ motifs (33) allowing thus autophosphorylation, Figure 2. As a result of the preference of these kinases for SQ/TQ motifs, they are considered structural hallmarks of DNA-damage-response proteins (34-36). Due to their high rank in the DSB induced signal transduction cascade, all PI-3Ks (ATM, ATR and DNA-PKcs) are considered sensors of cellular genotoxic stress (37).

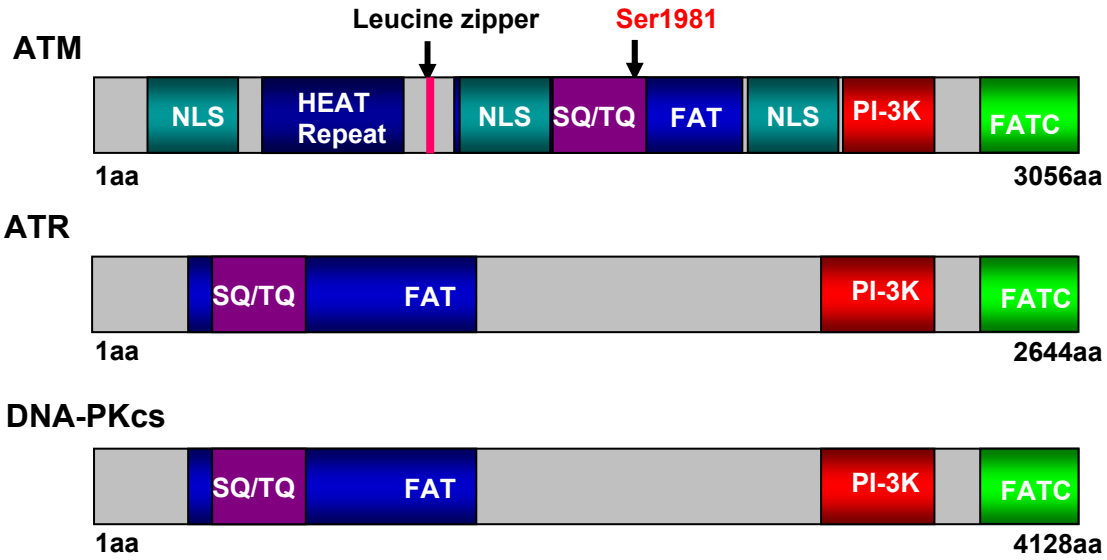

Figure 2. The Structure of PI-3K like family members. Conserved domains of PI-3K like family members are depicted in different colours. In detail: FAT (FRAP, ATM, TRRAP domain); FATC (FAT C-terminal domain); PI3-K (phosphatidylinositol 3-kinase domain); HEAT Repeat (Huntingin, elongation factor 3 (EF3), protein phosphotase 2A (PP2A), TOR1 domain); NLS: (Nuclear Localization Signal domain). SQ/TQ: SQ/TQ cluster. Ser1981 indicates Serine 1981, which is the major phosphorylation site of ATM, see below.

2.2.1 The ATR-Chk1 signaling pathway

Although ATR is activated in response to many different types of DNA damage, the ssDNA (single-stranded DNA) which is generated as a result of stalled DNA replication or during processing of chromosomal lesions appears to be central to the activation of ATR. Several alternative mechanisms are reported in the activation of ATR (38,39). But RPA (replication protein A)-coated ssDNA (single-stranded DNA) is crucial for the localization of ATR to sites of DNA damage, which is observed in both human and budding yeast systems (40,41). ATR is recruited to DNA lesions in part through its association with ATR-interacting protein (ATRIP) (41,42), which in turn interacts with RPA (40,43,44). Although RPA–ssDNA might be sufficient to localize the ATR–ATRIP complex, it is not sufficient for ATR activation (45,46). ATR signaling is dependent on the colocalization of the ATR–ATRIP complex with the 9-1-1 complex (RAD9–RAD1–HUS1 complex), a heterotrimeric ring-shaped molecule that is related in structure and sequence to PCNA (proliferating cell nuclear antigen) (47-50). Rfc2-Rfc5 (a component of the replication factor-C complex), as well as Rad17 replacing Rfc1, are also reported involved in ATR activation (50,51).

In S. cerevisiae, the 9-1-1 complex has been reported to directly activate ATR (52). But there is no evidence that this direct activation occurs in other organisms (18). The 9-1-1 complex brings TOPBP1 (topoisomerase-binding protein-1) to ATR (53,54). TOPBP1 is a breast cancer-1 (BRCA1) C-terminal (BRCT)-domain-containing protein that is necessary for ATR activation in vitro (55). The mechanism by which TOPBP1 binding activates ATR remains to be elucidated. The primary binding site for the activation domain of TOPBP1 on the ATR complex is within ATRIP, and mutations in this region of ATRIP block the activation of ATR (56,57).

Although the majority of RPA-coated ssDNA is generally present only during DNA replication, activation of ATR is not restricted to S-phase cells (45,58,59). In G1 and G2-phase, ATR activation might still require formation of RPA-coated ssDNA, through mechanisms, which might be different from those operating during S-phase (28). IR induced DSBs will be rapidly processed to ssDNA by various exonucleases,

including Mre11 (60). The recruitment of replication RPA to ssDNA facilitates the recruitment of several complexes of checkpoint proteins (40,61). In this context, ATR is activated and then phosphorylates Chk1, activating it in the process and allowing it to enforce a block in mitotic entry (28). Chk1, a serine/threonine protein kinase, is phosphorylated at serines 317 and 345 (SQ/TQ site) and thus activated by ATR (51,62,63). Several proteins are required for this process (10). Claspin is crucial for this activation, functioning to bring ATR and CHK1 together (48).

As indicated above, activated Chk1 targets its major substrate Cdc25C to negatively regulate its activity by facilitating its degradation (64-66). Low level Cdc25C suppresses dephosphorylation of Tyr-15 on Cdk1, which keeps MPF inactive, thus blocking progression into M. This final event completes the signal transduction from the DNA damage to the ultimate cell cycle arrest (67,68). Chk1 is not only required for checkpoint initiation but it is also needed to maintain the G2 checkpoint (69). Inactivation of Chk1 during G2 leads to a premature termination of the checkpoint that frequently results in catastrophic mitotic events (70).

2.2.2 The ATM-Chk2 signaling pathway

Exposure of cells to IR triggers ATM kinase activity, and this function is required for the complete activation of checkpoints in G1, S and G2 phases of the cell cycle (71,72). The quick induction of ATM kinase activity following IR suggests that it might act at an early stage of signal transduction in mammalian cells (73). DNA DSBs lead to the accumulation of the MRN (Mre11, Rad50 and Nbs1) complex, which binds to DSBs as a heterotetramer (74). MRN complex accumulation at DSB end is MDC1 (mediator of DNA-damage checkpoint protein-1) dependent (75). The retention of the MRN complex at the sites of DSBs increases its local concentration. ATM also arrives early at the DSB site (76). Interaction of MDC1 through its FHA domain with ATM regulates the accumulation of ATM at damage sites (77).

The expression level of ATM remains stable throughout the cell cycle and is not changed in response to IR; and the regulation of ATM mainly occurs through post translational modifications (78). ATM is held inactive in unirradiated cells as a dimer or a higher-order multimer in a form that masks the serine-1981 (an “SQ/TQ”) site (36). IR triggers the rapid autophosphorylation of serine-1981 (ATM-pS1981) that causes dimer dissociation and initiates monomer formation (78). Evidence suggest

that ATM kinase activity elevation is not regulated by this phosphorylation but rather by the disruption of the dimer, which allows access and phosphorylation of down stream ATM substrates (78). Although DSBs can elevate ATM kinase activity, it remains unclear precisely how ATM is activated by DSBs. Some evidence suggests that it is not activated by binding directly to DSBs, but by the alterations in higher-order chromatin structure (78-80). Others suggest that direct binding ATM to DSB ends is a crucial step in its activation (81).

Several substrates of the ATM kinase participate in checkpoints activated throughout the cell cycle. These include p53, Mdm2 and Chk2, Nbs1, Brca1, FancD2 and SMC1, hRad17, H2AX and others (29,73,78,82,83). The MRN complex (Mre11/Rad50/NBS1), is not only involved in the activation of ATM, but it is also a target for ATM kinase in downstream signaling to the DNA-repair machinery and the cell-cycle checkpoints (84). It is now well established that NBS1 is rapidly recruited to a DSB, where it remains stably bound (85). The stable binding of MRN to the break site and its co-localization with ATM makes it an ideal candidate to facilitate downstream substrate phosphorylation (75).

With the involvement of MRN complex, ATM transduces a genotoxic stress signal by activating its downstream substrate Chk2 (86). Chk2, the mammalian homolog of the *Saccharomyces cerevisiae* Rad53 and *Schizosaccharomyces pombe* Cds1 protein kinases, is required for the overall DNA damage response and specifically for the activation of the DNA replication checkpoints (87). Such activation occurs by phosphorylation of Chk2 at Thr68, a SQ/TQ site by ATM (17,88). Chk2 transduces the signal by phosphorylating Cdc25C at serine-216, a site known to be involved in the negative regulation of Cdc25C (89-91). The same site is phosphorylated by Chk1, which suggests that, in response to DNA damage and DNA replication stress, the ATR-Chk1 and ATM-Chk2 pathways converge at phosphorylating Cdc25C to prevent entry into mitosis (90,92).

2.2.3 The significance of two converging signaling pathways

The deficiency of ATM and ATR are associated with distinct consequences at the cell level. ATR is essential for early embryonic development, with $Atr^{-/-}$ embryos dying at an early developmental stage. $Art^{-/-}$ blastocysts cycle into mitosis but soon thereafter fail to expand and die of caspase-dependent apoptosis (93). However, individuals

partially defective in ATR can survive but suffer from the Seckel syndrome, a microcephalic primordial dwarfism syndrome. Seckel cells show high radiosensitivity and an impaired G2 checkpoint (94). Unlike mammalian cells, ATR deficiency is not lethal in plant cells but elicits abnormal G2 arrest in response to IR (95). In yeast, however, the essential function of Mec1, the ATR homologue, has little to do with cell-cycle arrest or origin firing, but is related to the fork-stabilization activity of the protein (96). Chk1 deficiency is embryonic lethal in mice (62). And the conditional knockout of Chk1 in cells using the cre-loxP system shows a defective G2 arrest (62). Complete depletion of Chk1 leads to premature activation of MPF that is followed by mitotic catastrophe (97). Chk1-deficient DT40 cells are viable, but fail to arrest in G2 in response to IR and are radiosensitive to killing (98).

Unlike ATR, deficiency in ATM is not embryonic lethal. The ATM deficiency associates with the human disease ataxia–telangiectasia (AT), and abrogates responses to ionizing radiation in mammalian cells. Cells from AT patients typically lack detectable ATM protein, contain abnormalities in telomere morphology and have abnormal responses to IR, including increased cell death, increased chromosomal breakage and cell-cycle checkpoint defects (99). AT patients exhibit progressive cerebellar ataxia, immune deficiencies, gonadal atrophy, oculocutaneous telangiectasias, radiation sensitivity, premature ageing and increased risk of cancers (71,100). Chk2-deficient mice are also viable but exhibit radioresistance and are defective in p53-mediated transcription (101). Cells derived from $Chk2^{-/-}$ mice were found significantly impaired in the IR-induced G1 checkpoint and in apoptosis. On the other hand, the checkpoints in G2 or S-phase appear normal (101,102). Chk2 cooperates with Brca1 in the induction of breast cancer (103). Chk2 mutations are also found in patients with Li-Fraumeni syndrome, a syndrome linked to mutations of the p53 tumor suppressor gene (104).

The above outlined pathways are highly conserved in different organisms, such as Drosophila and mammals (2,105,106), which suggests that they play important but different and possibly complementing roles in the checkpoint response (107). However Tel1 and Mec1 (the yeast ATM and ATR homologues, respectively) have been found redundantly implicated in the DNA damage repair and telomere integrity of Saccharomyces cerevisiae (108,109).

2.2.4 Cross talk and mutual regulation between the ATM-Chk2 and ATR-Chk1 signaling pathways

The standard dogma in the field of DNA damage response is that the ATR-Chk1 pathway is mainly activated by UV light-induced DNA damage and by stalled replication forks, while the ATM-Chk2 pathway is activated in response to IR-induced DSBs (110-113). However, evidence is emerging that ATR and ATM are not acting in an independent fashion in the checkpoint response but rather that they cooperate to induce and maintain the checkpoint response (114). A summary of the ATM-Chk2 and ATR-Chk1 pathways co-operating to maintain the G2 checkpoint signaling cascade is shown in Figure 3. Mec1 and Tel1 in yeast are reported to function redundantly in the DNA DSB repair and telomere length regulation (109,115). The overlap in substrate specificity between ATM and ATR also suggests the possibility for a crosstalk between the two pathways; BRCA1 and p53 are phosphorylated by both kinases (116-118).

The ATM and MRN complexes are required for the processing of DSBs and to generate RPA-coated ssDNA, which then mediates ATR/Chk1 activation (41,119). Efficient ATM-dependent ATR activation is restricted to the S and G2 phases of the cell cycle, and requires the CDK kinase activity (16,119). Some evidence suggests that ATM deficiency causes an elevation of ATR activity to sustain Chk2 phosphorylation in response to IR (120). Hence ATM may be located upstream of ATR (121).

The hallmark of ATM autophosphorylation at Ser1981 after IR is not observed after UV irradiation, or replication fork stalling. In this case, ATR alone, without ATM and the MRN complex, is required for checkpoint signaling (122). Furthermore, after depletion of endogenous ATM or ATR, a chimeric protein by fusing ATM to the ATRIP binding domain of ATR can partly restore checkpoint function, although the full complementation is not achieved (123). Detailed genetic analysis of Chk1 and Chk2 homologues in different species also reveals a cross talk between the ATM-Chk2 and ATR-Chk1 pathways in fungi, as well as in humans (124,125).

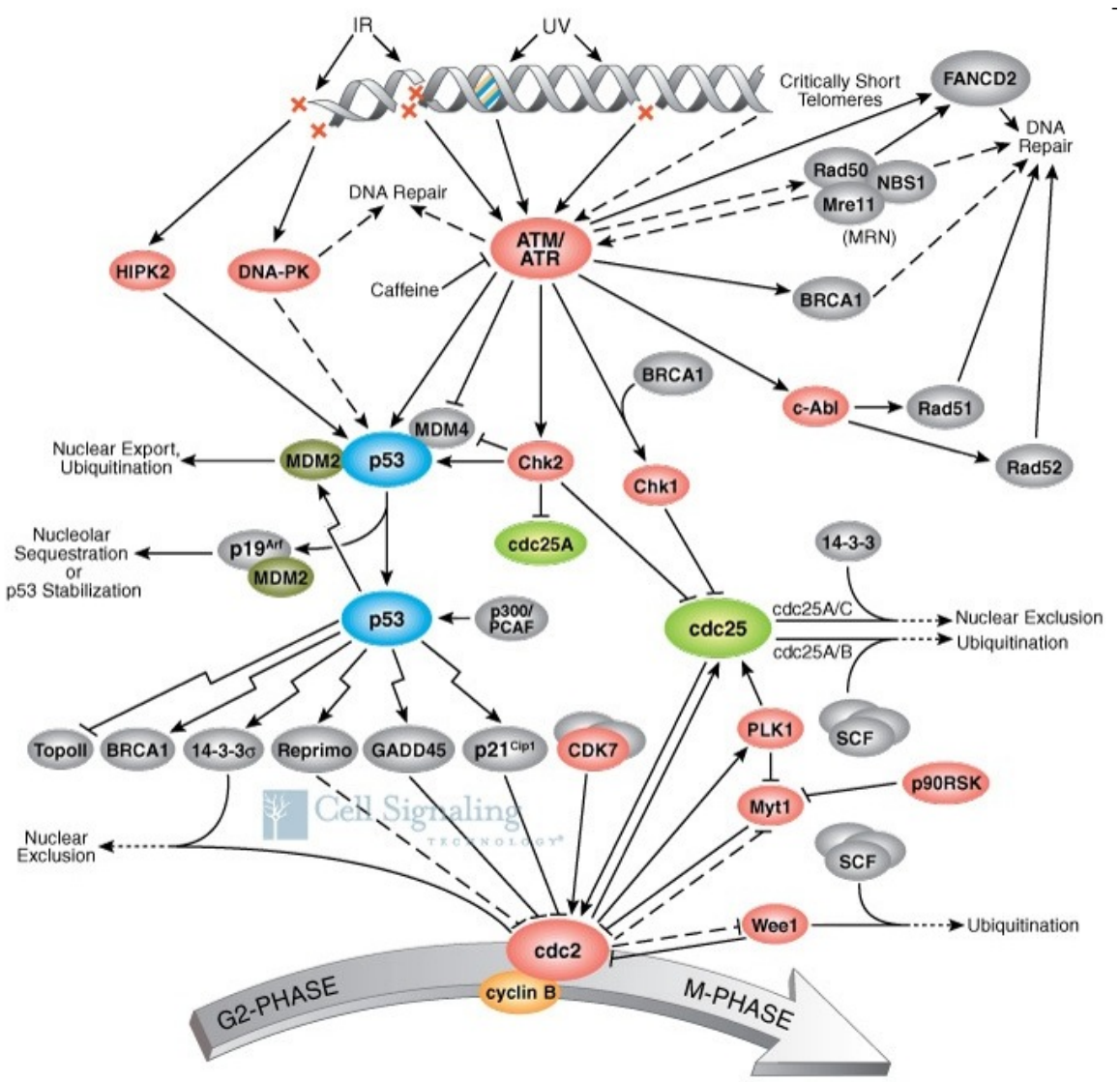

Figure 3. Putative G2 arrest signal transduction network (adapted from **Cell Signaling Technology®**). The G2 arrest signal transduction pathways in response to radiation (ionizing radiation and UV radiation). ATM and ATR play central roles in the G2 arrest pathway(s).

Crosstalk occasionally observed at the level of Chk1 and Chk2 (such as ATM-dependent Chk1 phosphorylation after exposure to IR (126)) probably result from interconversion of the DNA lesions. End resection converts DSBs into ssDNA structures that activate ATR, whereas nucleases can cleave ssDNA to yield DSBs that activate ATM (18).

2.3 Foci formation

In response to IR, many proteins involved in the response mounted by the cell show a local modification or accumulation, which can de detected under the microscope by

immunofluorescence staining as a “focus” forming in the nucleus. Proteins with such properties include H2AX-pS139 (γ-H2AX), ATF2-pS490/498, pSMC1-pS957，Chk2-pT68, 53BP1, PCNA, RAD51 etc (127-131). Among these modifications, phosphorylation at Ser139 of H2AX to generate γ-H2AX is the most well-documented case of foci forming after IR as a result of a local modification of a chromatin bound protein (132,133). γ-H2AX foci form in chromatin sites adjacent to DSBs and their initial number decreases concomitantly with DNA DSB repair, which makes them a good surrogate marker for studying DSBs and their repair (134-136).

γ-H2AX foci are conveniently detected by immunofluorescence microscopy and can be precisely scored by image processing, generating thus a sensitive technique for DSB-quantification (137-139). However, care must be taken not to equate a γ-H2AX focus with a DSB at all times (140). A pulsed-field gel electrophoresis (PFGE) method has been used to measure DSBs in mammalian cells after relative high doses (10–25 Gy) of ionizing radiation (141,142). Scoring of γ-H2AX foci is now generally accepted as an approach to evaluate of DSB repair kinetics at low radiation doses (135,143). Compared to PFGE and despite its weaknesses, use of γ-H2AX foci as a DSB marker remains a viable approach, particularly at low doses of radiation where PFGE can not be used (144).

Phosphorylated ATM also forms foci in response to IR (145). Other treatments, such as hypotonic shock, can also activate ATM but do not lead to foci formation (146). The kinetics of ATM-pS1981 foci formation is comparable to that of γ-H2AX. The induction of ATM-pS1981 foci shows a linear dose–response relationship between 0.1-1 Gy (147).

Although foci formation seems to be a general observation after IR, there is only very limited information regarding possible connections between foci formation and the signal transduction pathways leading to G2 arrest. It is reported that increased formation of γ-H2AX foci is detected in early thymocytes of aged mice as compared to young mice(148). Since senescence is usually accompanied by compromised checkpoint activation (149,150), a linkage between foci formation and checkpoint activation is suggested. Other evidence suggests that γ-H2AX regulates the 53BP1 foci formation, and that this regulation is strongly related to the levels of DNA damage present. Only sufficient accumulation of 53BP1 at DSB site can prevent entry of damaged cells into mitosis (151).

Persistent ATM-pS198 foci are found in the cell nucleus after IR. These persistent foci are lower in numbers as compared to those initially seen and display an altered geometry and size (152). All persistent ATM-pS1981 foci colocalize with the persistent foci of γ-H2AX, MDC1, 53BP1, and NBS1. Defective formation of the persistent IR-induced foci is observed in cells derived from AT and NBS patients, which are defective in the IR-induced G1 checkpoint. These results indicate that the development of the persistent foci plays a pivotal role in checkpoint activation especially during G1 arrest (152).

2.4 Prospects of this thesis

Checkpoint activation alters the normal distribution of cells through the cell cycle, which is easily detected by DNA content variation in flow cytometry. This technology is central to the present work. Mitotic index (MI) variation also reflects the G2 checkpoint activation and provides even higher sensitivity than G2 phase accumulation assayed by flow cytometry. In some experiments, a flow cytometry protocol was used to quantify checkpoint activation evaluating MI and DNA content simultaneously.

As tools to study interdependencies between DNA-PKcs, ATM, and ATR, extensive experiments were carried out using cell lines with the appropriate genetic background and an array of inhibitors. And the goal was to reveal the contributions of these kinases to the development and maintenance of the G2 checkpoint.

Foci formation of different components from the DNA damage response machinery offers a unique opportunity to study of the G2-checkpoint. In the present thesis, we will take advantage of these facts to build a connection between foci formation for specific proteins and G2 checkpoint activation. This is because, the major kinases implicated in this cellular regulatory function, DNA-PKcs, ATM, and ATR form foci around DSBs, which suggests not only that they have registered the presence of this dangerous lesion, but also that they have proceeded with their own activation. In the case of ATM, autophosphorylation at Serine 1981, which suggests the activation of ATM, is easily detected as foci at DSB sites; Localization around DSBs of ATR, as can be nicely documented using its partner ATRIP, allows confirmation of its presence in regions of DSBs. The aspect of foci formations are extensively used here to study the involvements of these kinases in the G2 checkpoint.

For this purpose, we examined carefully, mainly in G2, the kinetics of activation of each of these kinases in order to obtain information regarding their kinetics of engagement and their sequential activation. The relevance of these observations for G2 checkpoint activation and the coordination of the DSB repair pathways will be discussed.

3 Materials and methods

3.1 Cell culture

3.1.1 Tissue culture

Tissue culture was performed in SANYO MCO-18 O_2/CO_2 incubators at 37°C with 5% CO_2. A549 cells were maintained in McCoy's 5A medium (M4892, Sigma-Aldrich) supplemented with 10% fetal bovine serum (FBS) (S0615, BIOCHROM). AT5-BIVA cells were maintained in MEM medium (61100-087, GIBCO) supplemented with 10% FBS. GM847-ATRkd cells were maintained in MEM supplemented with 10% FBS. F02-98 primary human Seckel syndrome fibroblasts were maintained in MEM supplemented with 15% FBS. DK0064 lymphoblast cell from human Seckel syndrome was maintained in suspension form in RPMI1640 (R6504, Sigma-Aldrich) + 10% FBS. M059J and M059K cells were maintained in DMEM (D5523, Sigma-Aldrich) supplemented with 10% FBS. HCT116 DNA-PKcs$^{-/-}$ and HCT116 wt cells were maintained in McCoy's 5A medium supplemented with 10% FBS.

Cells were grown in 100 ml tissue culture dishes (664160, CELLSTAR) with 15ml growth media. Exponentially growing cells were passaged every 3 days while avoiding confluency levels above 80%. For passage, media were removed and cells were rinsed with cold PBS. Cells were rinsed with by 5 ml trypsin-EDTA solution and incubated for 5 min at 37°C. Detached cells were resuspended in 10 ml cold media supplemented with 10% FBS. Single cell suspensions were obtained by passing cells through the Pasteur pipette. Cells were counted and appropriate numbers of cells were further incubated for experiments or for subculture, see Appendix 2. When frozen cells were taken to subculture, they were passed at least 5 times before being used in experiments. Cells were discarded after about 50 passages, since their genomic stability could not be guaranteed.

3.1.2 Antibody production

ATRIP 3.51 hybridoma cells, a generous gift from Professor Thanos D. Halazonetis, Geneva, Switzerland, produces a monoclonal antibody which shows very high avidity against human ATRIP. 10^6/ml cells were seeded in 15 ml HSFM media (12040-077, Invitrogen) and were maintained in exponentially growing phase by passaging them

every 3 days. For antibody generation, 10^6/ml cells were incubated in the above growth medium for 15 days. Supernatant from these cultures was centrifuged at 4500 RPM to remove cell debris and was passed through a 0.22 µm filter to remove possible contamination. Sodium azide (S2002, Sigma-Aldrich) was added to a final concentration at 0.02% (w/v), and supernatant was stored at -80°C until use.

3.1.3 Drug treatments

Caffeine (C8960 Sigma-Aldrich) was dissolved in Milli-Q water (Z00QSV001, Millipore, 18.2 MΩ·cm at 25°C) to prepare a 200 mM stock solution. The solution was sterilized by passing through a 0.22 µm filter and stored in RT. 4 mM caffeine was used as the working concentration. 2-morpholin-4-yl-6-thianthren-1-yl-pyran-4-one (118500, Calbiochem, also known as KU-55933) was dissolved in DMSO (Dimethyl sulfoxide) (D8418, Sigma-Aldrich) to prepare a 10 mM stock solution that was stored at -20°C in the dark. 10 µM was used as the working concentration. 7-hydroxystaurosporine (539644, Calbiochem, also known as UCN-01) was dissolved in DMSO to prepare a 10 µM stock solution that was stored at -20°C in the dark. 100 nM was used as the working concentration. The Chk2 inhibitor II (220486, Calbiochem) was dissolved in DMSO to prepare a 10 µM stock solution that was stored at -20°C in the dark. 400 nM was used as the working concentration. 2-(Morpholin-4-yl)-benzo[h]chomen-4-one (N1537, Sigma-Aldrich, also known as NU-7026) was dissolved in DMSO to prepare a 10 mM stock solution that was stored at -20°C in the dark. 10 µM was used as the working concentration. All drugs were given to the cells 1 h before irradiation and maintained during the experiment.

Doxycycline Hyclate (D9891, Sigma-Aldrich) was dissolved in Milli-Q water to prepare a 5 mg/ml stock solution. The solution was sterilized by passing through a 0.22 µm filter and stored at -20°C in the dark. 5 µg/ml was used as working concentration. ATRkd expression was induced by incubating the exponentially growing GM847-ATRkd cells in doxycycline containing media for 36 to 48 h. The drug was maintained in the culture during the experiment.

3.1.4 Cell synchronization

Cell populations enriched in G1 cells were obtained by serum deprivation. Briefly, 0.15 million cells were seeded in 5 ml media supplemented with 10% FBS in 60 mm dishes. Medium was removed after 48 h. At this time, cells were in the exponential

phase of growth. Cells were washed twice with pre-warmed PBS and incubated in 5ml fresh serum-free medium for 24-36 h. Subsequently, cells were transferred in fresh growth medium supplemented with 10% FBS for 3 h before further manipulations. The distribution of cells through the cell cycle was measured by flow cytometry (see below). At this stage, at least 90% of the cells were in G1 phase.

Cell populations enriched in G1 or G2 cells were also obtained by a centrifugal elutriation. Briefly, 1 million cells were seeded in 15 ml growth media supplemented with 10% FBS in 100 mm dishes. At least, 40 dishes were prepared for each elutriation. After 48 h, cells were washed, trypsinized, suspended in the fresh growth medium supplemented with 10% FBS and counted. About 140 million exponentially growing cells could be collected for elutriation. Cells were loaded into an elutriation rotor (Avanti J-20 XP, BECKMAN COULTER). Fractions were collected by gradually reducing the rotor speed. Cell cycle analysis was carried out by flow cytometry. Typically, cell populations with at least 92% G1 cells were obtained in G1 fraction; and 75% G2 cells in G2 fraction.

Populations enriched in mitosis were obtained by treatment with nocodazole (M1404, Sigma-Aldrich). Briefly, 0.15 million cells were seeded in 5ml growth media supplemented with 10% FBS in 60mm dish and were allowed to grow for 48 h. At this time, cells were growing exponentially. Medium was replaced with 5ml fresh growth media supplemented with 10% FBS and 0.04 µg/ml nocodazole and incubated for 15-17 h. To release the nocodazole block, cells were washed twice with PBS and supplied with 5 ml pre-warmed fresh growth medium supplemented with 10% FBS. The cell cycle distribution was determined by flow cytometry. At least 75% cells were in mitosis at this stage.

3.1.5 Pulse labeling

BrdU and EdU are thymidine analogues that can be incorporated into DNA during DNA replication. They label S-phase cells with high specificity. Exponentially growing cells were pulsed labeled with 10 µM BrdU (B23151, Invitrogen) or 10 µM EdU (C10085, Invitrogen) at 37°C for 30 min. Cells were washed twice with pre-warmed PBS and supplied with pre-warmed fresh growth medium supplemented with 10% FBS. Cells could be used for the further manipulations.

3.2 Ionizing radiation (IR)

Cells were exposed to 320 kV X-rays with a 1.65 Al filter (GE-PANTAK). The dose rate was about 2 Gy/min. An even radiation was ensured by rotating the radiation table. Cells were returned to the incubator immediately after IR.

3.3 Flow cytometry

3.3.1 Cell cycle analysis by flow cytometry

Propidium iodide binds to DNA proportional to its mass. Cell cycle distribution was assessed by measuring propidium iodide (PI) fluorescence on a flow cytometer. Cells were washed with cold PBS and trypsinized at 37°C for 5 min. Single cell suspensions were prepared in 5ml cold fresh media. About 1 million cells were collected and centrifuged at 1500 RPM, 4°C for 5 min. The cell pellets were washed with cold PBS and fixed in 70% ethanol at -20°C overnight. Supernatant was removed by centrifugation at 1500 RPM for 5 min. Pellets were washed with cold PBS and incubated in PBS containing PI (40 µg/ml) (81845, Sigma-Aldrich) and RNase (62 µg/ml) (R4875, Sigma-Aldrich) at 37°C for 30 min in dark. Samples were measured on a flow cytometer (COULTER EPICS XL, BECKMAN COULTER) according to pre-established protocols, see Appendix 3. 20,000 cells per sample were counted and the single cell population was gated to obtain standard histograms. Histogram files (*.HST) were generated by counting the frequency of the cell with same PI signal intensity.

The fractions of cells in the different phases of the cell cycle were calculated using the Wincycle® software. HST files were loaded into the Wincycle®. The parameter “S-phase growing order” was carefully chosen between 0, 1 or 2, until the prediction model fitted the histogram shape. Cell cycle distributions were automatically calculated. G2 arrest kinetics was obtained by plotting the G2 fraction as a function of time after IR.

3.3.2 Bivariate flow cytometry

Bivariate flow cytometry was used to simultaneously measure DNA content and the levels of proteins of interest, e.g. phosphorylation of Histone 3 at serine 10 (H3-pS10), cyclin B1 and BrdU. Briefly, 0.6-0.8 million cells were prepared as single cell suspension in cold fresh media. After centrifugation at 1500 RPM, the cell pellets were washed with cold PBS and fixed in 70% ethanol at -20°C overnight.

Supernatants were removed by centrifugation at 1500 RPM for 5 min. Cells were further permeabilized in 2ml permeabilization solution (PBS + 0.25% Triton X-100) on ice for 15 min. Supernatants were removed by centrifugation at 1500 RPM and the pellets were washed with cold PBS. Cells were blocked in blocking buffer (PBS + 0.05% Tween-20 + 1% BSA (8076.2, ROTH)) at RT for 45 min in the dark with gentle agitation. Primary antibodies, e.g. H3-pS10 (06-570, upstate) and cyclin B1 (sc-752, Santa Cruz), were diluted 1:150 in blocking buffer. After centrifugation at 1500 RPM for 5 min, the pellets were suspended in 100 µl diluted primary antibody and incubated for 2 h at RT in the dark with gentle agitation. The primary antibody was diluted in 5ml PBS and the cells were washed 3 times with PBS. Secondary antibodies, such as Mouse IgG-FITC (F0257, Sigma), Rabbit IgG-FITC (AP307F, Chemicon), were diluted in blocking buffer (1:200). Cell pellets were incubated with 100 µl conjugated secondary antibody for 90 min at RT in dark. Secondary antibodies were removed by diluting in 5ml PBS and washing with PBS for three times. Cells were then incubated with PI plus RNase at 37°C for 30 min in the dark before measuring on a flow cytometer. Totally 20,000 cells were measured. Proper gating was applied to detect cyclin B1 positive, H3-pS10 positive cells and to calculate their fraction in the total population. Compensation was applied when necessary. Detailed information for program settings is available in Appendix 4.

Detection of BrdU incorporation was achieved using published protocols. Briefly, 0.8-1 M BrdU labeled cells were collected and fixed in ethanol. Cells were incubated in 2 ml 1M HCl for 10 min at RT for DNA denaturation. Acid was diluted with 5 ml PBS and cells were washed 3 times with PBS. BrdU primary antibody (1:200) (B23151, Beckson-Dickson), secondary antibody (1:300) were diluted in blocking buffer and sequentially applied. Finally, the cells were stained with PI-RNase staining solution as described above. Totally 20,000 cells per sample were measured on flow cytometry. Proper gating (BrdU positive cells) was applied to analyze the measured cell populations. Detailed information on program setting is available in Appendix 4.

3.4 Electrophoresis and Immunoblotting

3.4.1 Cell extracts preparation and protein concentration determination

Cells were collected and were washed twice with cold PBS. They were lysed for 20 min in ice cold RIPA buffer (89900, PIERCE, 1 ml RIPA per 5 million cells) with Halt Phosphatase Inhibitor Cocktail (78420, PIERCE) and Halt Protease Inhibitor Cocktail

(78410, PIERCE). Lysates were briefly sonicated and centrifuged at 12000 RPM, 4°C for 10 min. Supernatants were transferred into the fresh tubes and protein concentration were determined using the BCA (bicinchoninic acid) protein assay (Kit 23225, PIERCE) before aliquoting and storing at -20°C .

3.4.2 Electrophoresis

20 µg whole cell extract was mixed with 2x SDS-PAGE loading buffer. Samples were denatured at 95°C for 5 min and cooled down on ice for 5 min. They were centrifuged at 3000 RPM for 15 sec before loading. SDS-PAGE mini gels were cast (165-8000, Mini-PROTEAN Tetra Cell, BIO-RAD) by following the instructions from the manufacturer. Proteins were resolved in gels with different concentrations according to their sizes; for example 15% gel for proteins smaller 50 KD, 12% for proteins between 50-100 KD, 10% for proteins between 100-200 KD, and 8% for proteins larger than 200 KD. Samples were loaded and run at constant voltage (150 V) for 1.5 h at RT, see Appendix 5.

3.4.3 Immunoblotting

After the electrophoresis, the gels were removed from the cassette and briefly rinsed with MQ water. PVDF membranes (RPN303F, GE Healthcare) and the blotting paper (GB004 Waterman) were cut to the desired size. PVDF membranes were pre-soaked in 100% methanol for 1 min and rinsed in MQ water for 15 min. PVDF membranes, blotting paper and the transfer unit sponge were equilibrated in 1x transfer buffer (Glysine 200 mM (3908.2, ROTH), Tris 25 mM (4855.2 ROTH), 10% Methanol (32205, Sigmal-Aldrich)) at 4°C for at least 30 min. The Gel, blotting papers, sponge and PVDF membrane were assembled and loaded into an electro-transfer unit (170-3930, Mini Trans-Blot Electrophoretic Transfer Cell, BIO-RAD) according to the instructions from the manufacturer. Wet electro-transfers were run at 100 V, 0°C for 1 h. Detailed information is available in Appendix 5.

After completion of transfer, the unit was disassembled and the side of the membrane on which proteins were transferred was marked. PVDF membranes were briefly rinsed with PBST (PBS + 0.05% Tween-20) and blocked in blocking buffer (PBS + 0.05% Tween-20 + 5% milk (T145.2, ROTH) at RT for 1h with gentle agitation. Primary antibodies, for instance ATR (Ab2905, Biozol), Lamin A/C (Sc-7292 santa cruz), ATM (GTX77613, Gene Tex), ATM-pS1981 (4526, Cell Signaling)

were diluted in blocking buffer 1:800, GAPDH (Mab374, CHEMION), 1:20,000, ATRIP (culture supernatant) (1:10). Membranes were incubated with primaries antibodies at 4°C overnight with gentle agitation. The secondary antibodies, such as mouse IgG-HRP (7076, Cell Signaling), rabbit IgG-HRP (7074, Cell Signaling) were diluted 1:2000 in blocking buffer. After removing primary antibodies and washing with PBST (3 x 10 min), membranes were incubated with secondary antibodies at RT for 1 h. After washing with PBST (3 x 10 min), the membranes were ready for development. The ECL developing solution (RPN2132, GE Healthcare) was prepared according to the instructions from the manufacturer and evenly distributed on the side of the membrane on which the proteins were transferred. After 1 min incubation at RT in the dark, images were obtained using the molecular imager VersaDoc MP 4000 System (#170-8640, BIO-RAD).

3.5 Immunofluorescence and data analysis

3.5.1 Confocal microscopy

Sterilized cover slips (2 mm x 2 mm, 8404, Invitrogen) were incubated in 1 mg/ml poly-L-lysine (L7240, Biochrom) solution for 1 h. Solution was removed and cover slips were stored at 4°C in the dark. Cells were plated with 2 ml growth medium in a 35 mm dish with poly-L-lysine coated cover slips. At each time point, growth media were removed, cells were washed in cold PBS 3 times and fixed in 2% paraformaldehyde (PFA, 76240, FLUKA) for 15 min at RT. PFA was removed and cells were washed 3 times with PBS. Cells were permeabilized in P-solution (100 mM Tris pH7.4, 50 mM EDTA, 0.5% Triton X-100) for 10 min at RT. After washing 3 times with PBS, cells were blocking in the PBG solution (0.2% Gelatine, 0.5%BSA in PBS) at 4°C overnight.

Primary antibodies, such as ATM-pS1981 (Ab2888, Abcam), ATM-pS1981 (4526, Cell Signaling), Chk2-pT68 (18-785-210077, BIOZOL) were diluted 1:300 in PBG, ATRIP (culture supernatant) was diluted 1:5 in PBG. 100 µl diluted primary antibodies were dispensed on parafilm (52858-032-CS, The Lab Depot, Inc.). The cover slips were mounted on top of the solution containing the primary antibodies. After incubating at RT for 2 h in the dark, slides were returned to the dishes and washed with PBST (PBS+0.05%Tween 20) at RT 3 x 10 min. Conjugated secondary antibodies, such as Alexa488 mouse IgG (A11001, Invitrogen), Alexa488 rabbit IgG (A11008, Invitrogen), Alexa568 mouse IgG (A11004, Invitrogen), Alexa568 rabbit IgG

(A11011, Invitrogen) were diluted in PBG 1:400. Slides were incubated with 100 µl secondary antibody solution at RT for 1 h in the dark. After 3 washes in PBST, cells were counterstained with 100 ng/ml DAPI (D3571, Invitrogen) at RT for 5 min. The cover slips were washed 3 times with PBS and mounted on slides with 15 µl Prolong Antifade Mounting Media (P-7481, Invitrogen). The slides were kept in the dark at RT and allowed to solidify for 48 h before analysis.

Detection of EdU was performed according to a commercially available protocol, except for the staining sequence. Literature suggests that EdU staining should precede antibody-protein binding. In our experience, however, ATM-pS1981 foci were not detectable when following this order. EdU staining without compromising ATM-pS1981 foci detection could be achieved by changing the sequence and stain first for ATM-pS1981, then EDU and finally with DAPI.

Scanning of the slides was carried out on a Leica SP5 confocal microscope. For each slide, at least 5 fields were scanned (about 300 nuclei). Resolution was set at 512 x 512 and the zoom factor at 2. Bidirectional scans were applied to avoid bleaching of the fluorophore. Due to the differences in foci formation patterns, different proteins required different scanning parameters, such as laser intensity, PMT voltage, SMART GAIN offset, filter spectrum range, etc. The parameters used in each case are summarized in Appendix 6. LIF files were generated after each scan, which were used for foci quantification using the Imaris® software (see below). TIFF Images shown in the text were obtained from the maximum intensity projection of the field scanned.

3.5.2 Foci scoring

Foci numbers were enumerated using Imaris® (Imaris 6.0; Bitplane). At least 300 target nuclei were scored. The LIF files were loaded to Imaris using default settings. “Bright dots” with a size larger than 0.5 µm and intensity above the threshold value (between 17–21, summarized in Appendix 6) were confirmed as foci. Foci were grouped in each nucleus, and the number of foci per nucleus was obtained. In some cases, the mean number of foci per nucleus was calculated from data obtained by analyzing many nuclei. For data analysis, Microsoft Excel 2003® was used.

4 Results

4.1 Part 1. What is the contribution of ATM and ATR to G2 arrest?

After exposure to IR, cells experience a delay in their progression from the G2 into the M-phase of the cell cycle. As discussed above, the ATM-Chk2 and the ATR-Chk1 signaling pathways are thought to be integral to the signal transduction cascade underlying the development of the G2 checkpoint.

We set out to investigate the contributions of each of these pathways in the generation of the overall delay experienced in G2 by human cells exposed to IR. Diverse mutants as indicated and inhibitors of key players of this pathway (see below) were used for this purpose. UCN-01 is a rather specific inhibitor of Chk1 (IC_{50}=11 nM, IC_{50} stands for half maximal inhibitory concentration) with radiosensitizing properties and the ability to modulate G2 arrest (153,154). KU-55933, is a highly specific, new generation ATM inhibitor (IC_{50}=13 nM) (155). Chk2 inhibitor II is used to inhibit Chk2 kinase activity (156). Caffeine is the least specific inhibitor used in the present study, but it is known to inhibit both ATM as well as ATR and to exert inhibitory activity on DNA-PKcs as well (157).

A549 were used as control in these experiments. A549 is a human lung carcinoma cell line with no known defects in DNA repair or in cell signaling, and expresses a wild type form of p53. The results obtained with this cell line are summarized in Figure 04**.** Exposure of A549 cells to 4 Gy X-rays causes a delay in their progression from the G2 into the M-phase of the cell cycle, manifest by a gradual but transient accumulation of cells in G2, which are easily detectable by flow cytometry. In irradiated cultures, the fraction of cells in G2 increases from 8% to nearly 50% 12 h after exposure (Figure 5A). At later times, the fraction of cells in G2 gradually decreases indicating that cells overcome the checkpoint and resume progression through the cycle.

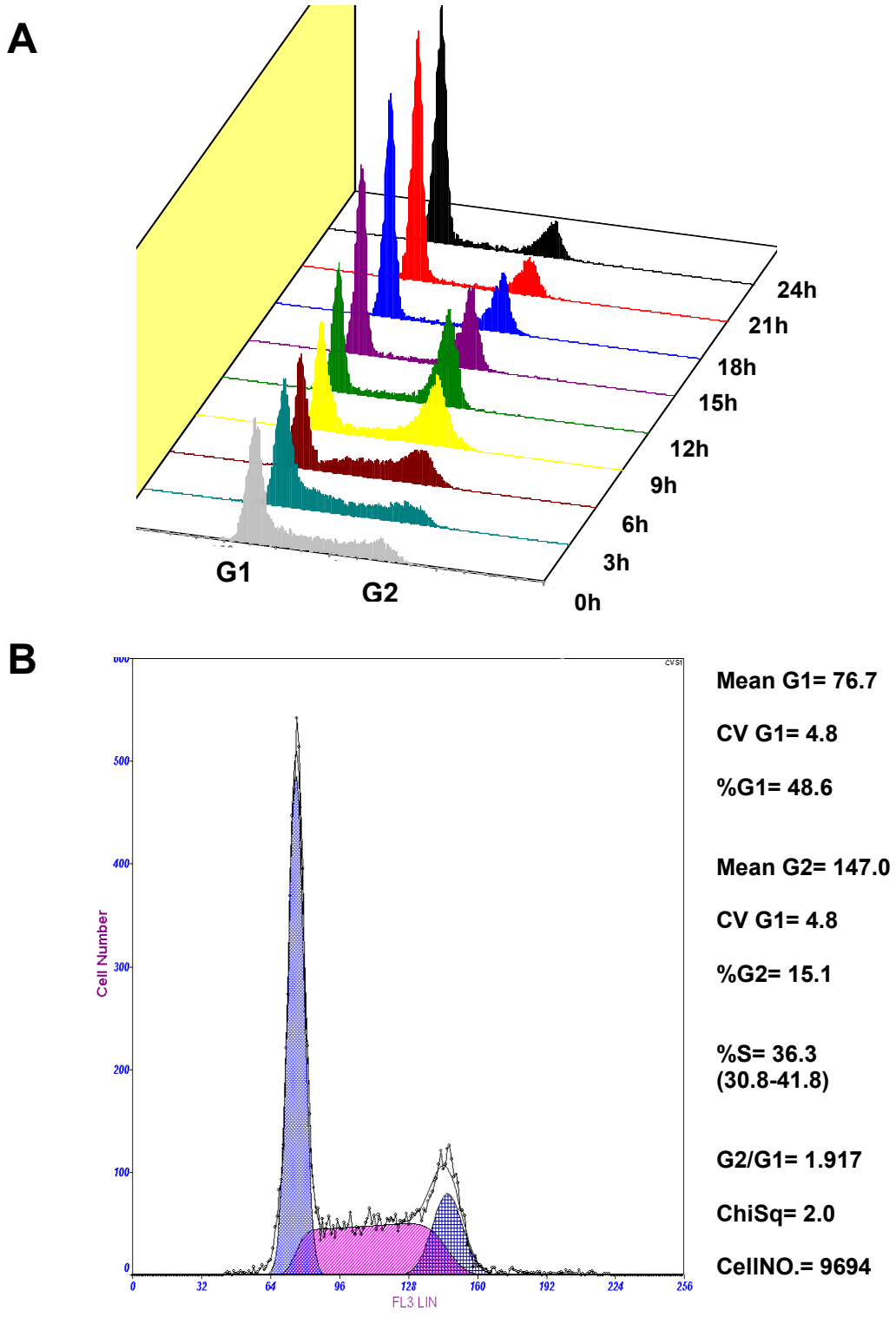

Figure 4. A549 G2 arrest pattern and cell cycle distribution analysis. Exponentially growing A549 cells were irradiated at 4 Gy. Cells were sampled every 3 h, fixed and stained with PI. PI signals were measured by flow cytometry. **(A)** Histogram of PI signal indicates the DNA content. **(B)** Cell cycle analysis on Wincycle®. S phase cells growing order can be either selected at 0, 1, or 2. In this case, "0" order prediction model fits the histogram very well. The calculations of cell cycle distributions are shown at the right panel.

Caffeine and UCN-01 are well documented to abrogate G2 checkpoint after IR (154,158), which are also confirmed in our experiment. The IR-induced G2 fractions fluctuations are dramatically reduced in presence of these drugs, (Figure 5A, 5C). Specific inhibition of ATM using KU-55933 delays the kinetics of accumulation in G2 with a peak now reached at 20 h, instead of 12 h, but persisting for longer periods of time. However, the maximum level of G2 accumulation achieved is comparable to that measured in irradiated cells that were not treated with the inhibitor (Figure 5B). This result may hint to an early involvement of ATM in developing G2 checkpoint. This KU-55933 mediated alteration of G2 arrest can be counteracted by caffeine, and simultaneous treatment with both inhibitors causes a response practically identical to that of caffeine alone, compare Figure 5A, 5B and 5E.

ATM functions in the G2 arrest by signaling to Chk2 (159). Therefore, inhibition of ATM or Chk2 is expected to generate similar results. Surprisingly, unlike KU-55933, 400 nM Chk2 inhibitor II (IC_{50} for Chk2 = 12.5 nM) (156) does not cause a measurable change in the pattern of G2 arrest after exposing cells to 4 Gy (Figure 5D). An additional experiment utilizing 800 nM of the drug also fails to demonstrate an effect (data not shown).

The results in Figure 5A and 5E demonstrate that administration of caffeine at 4 mM prevents the IR-induced accumulation in G2 almost entirely. Since caffeine is known to inhibit all kinases ($IC50_{ATM}$ = 0.2 mM, $IC50_{ATR}$ = 1.1 mM, $IC50_{DNA\text{-}pK}$ = 10 mM) (157)), these result directly indicate the implication of ATM, ATR as well as DNA-PKcs in the response.

4.1.1 The Role of ATM in G2 checkpoint response

To investigate the effect of ATM on the development of the G2 checkpoint in greater depth, we introduced mutants with defects in this protein. AT5-BIVA is an immortalized ATM mutant cell line generated by transfection of AT cells with SV40 DNA. The large tumor antigen (TAg) encoded by this viral DNA binds p53 and Rb and compromises their activities (160). The distribution of cells in G2 as a function of time after exposure to 4 Gy is summarized in Figure 06. IR induces a gradual accumulation of cells in G2 that reaches a maximum after about 20 h and causes a persistent arrest in this phase of the cell cycle (Figure 6A). This result is similar to that obtained with A549 cells exposed to KU-55933 (Figure 5B) and suggests that genetic or chemical inactivation of ATM give equivalent results.

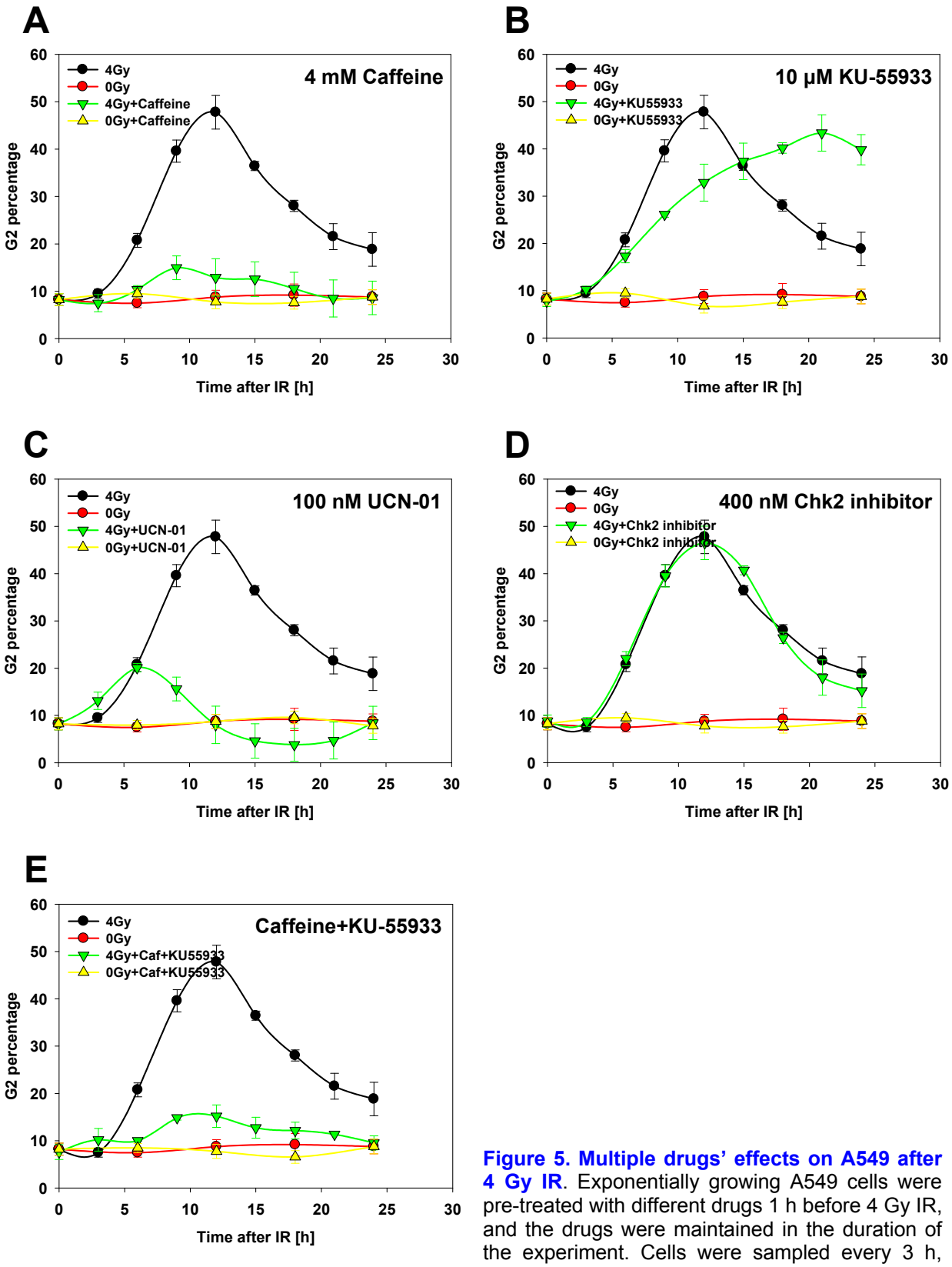

Figure 5. Multiple drugs' effects on A549 after 4 Gy IR. Exponentially growing A549 cells were pre-treated with different drugs 1 h before 4 Gy IR, and the drugs were maintained in the duration of the experiment. Cells were sampled every 3 h, fixed, permeabilized and stained with PI. The PI signal variations were measured by flow cytometry. Cell cycle distributions are calculated. G2 fractions obtained are plotted against time. **(A),** 4 mM caffeine; **(B),** 10 μM KU-55933; **(C),** 100 nM UCN-01; **(D),** 400 nM Chk2 inhibitor; **(E),** 4 mM Caffeine + 10 μM KU-55933. The results are from 3 repeated experiments. Error bar stands for standard deviation.

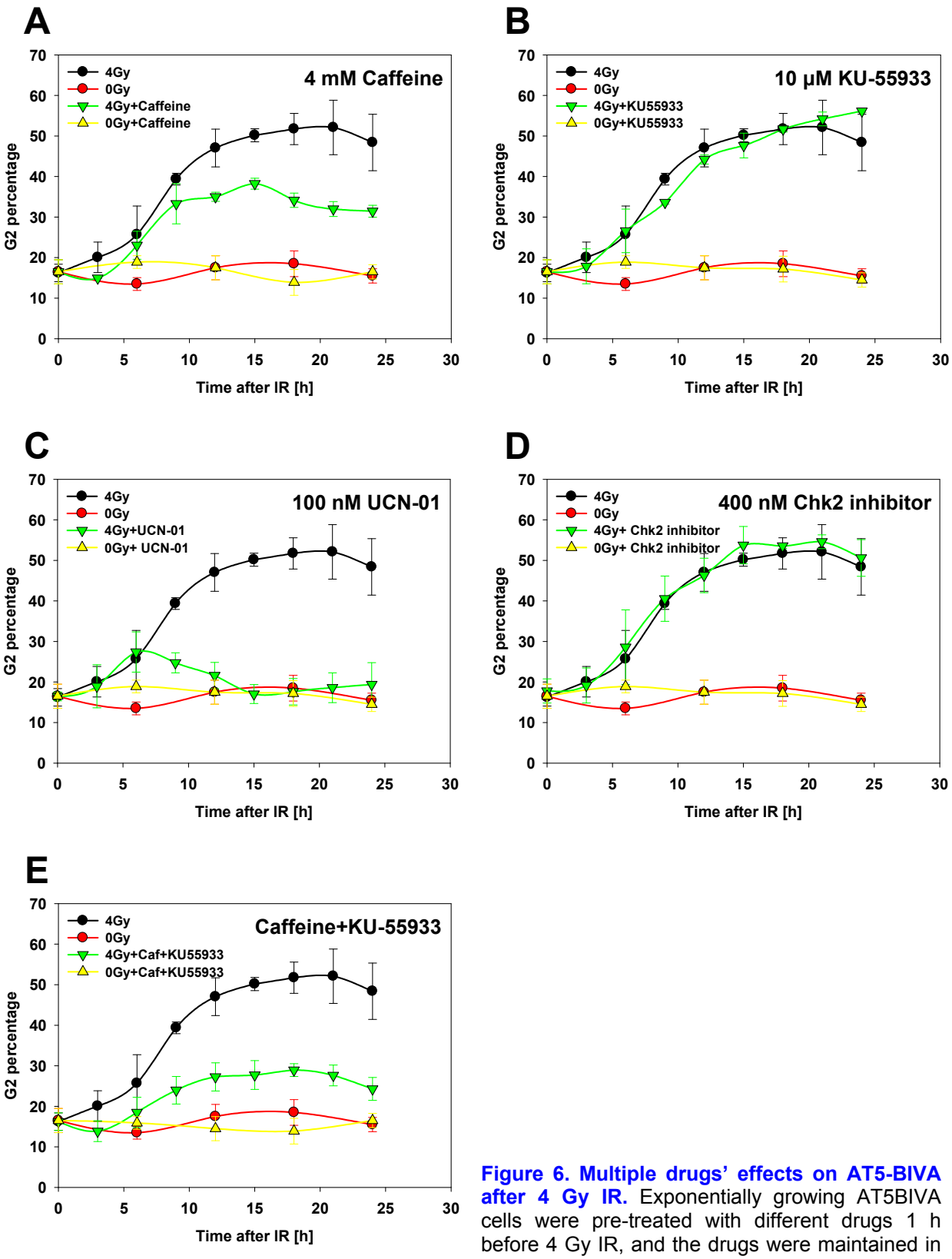

Figure 6. Multiple drugs' effects on AT5-BIVA after 4 Gy IR. Exponentially growing AT5BIVA cells were pre-treated with different drugs 1 h before 4 Gy IR, and the drugs were maintained in the duration of the experiment. Cells were sampled every 3 h, fixed, permeabilized and stained with PI. The PI signal variations were measured on flow cytometry. Cell cycle distributions were calculated. G2 fractions obtained are plotted against time. **(A),** 4 mM caffeine; **(B),** 10 μM KU-55933; **(C),** 100 nM UCN-01; **(D),** 400 nM Chk2 inhibitor; **(E),** 4 mM Caffeine + 10 μM KU-55933. The results are from 3 repeated experiments. Error bar stands for standard deviation.

The strong G2 arrest observation confirms the limited role of ATM in the development of the G2 checkpoint and is in line with the complete lack of effect observed in cells exposed to the Chk2 inhibitor. Not surprisingly KU-55933 remains inactive in these cells (Figure 6B), which provides a useful negative control since it demonstrates that the inhibitor has no detectable side effects. Notably, exposure of AT5-BIVA cells to caffeine causes a dramatic reduction in the accumulation of cells in G2 (Figure 6A) in line again with a contribution of ATR or DNA-PKcs in the development of the G2 checkpoint in ATM cells. Similar results are obtained after treatment with UCN-01 (Figure 6C), once again confirming the contribution of ATR/Chk1 signaling in the overall response.

4.1.2 The Role of DNA-PKcs in G2 checkpoint response

Although caffeine inhibits the functions of DNA-PKcs when tested in vitro (161), the in vivo effects of the drug are not compatible with inhibition of this kinase at physiological conditions. Thus, inhibition of DNA-PKcs by genetic or chemical means has a strong effect on the ability of cells to repair DSBs by NHEJ (162-164). On the other hand, treatment of cells with caffeine at the concentration typically used in such experiments (up to 10 mM) has no measurable effect on DSB rejoining (161). Thus, the in vitro inhibition by caffeine of DNA-PKcs may not be relevant for the actual signaling activity of DNA-PKcs (163), a conclusion that is also compatible with the IC50 for this kinase (10mM).

To explore the contribution of DNA-PKcs to the prolonged G2, M059J and M059K cells were used. M059J is human glioma mutant defective in DNA-PKcs. M059K, with competent DNA-PKcs, is used as a wild type counterpart (165). NU-7026 is a specific competitive inhibitor of DNA-PKcs (IC_{50}=0.23 μm) (166,167). By addition of NU-7026, DNA-PKcs can be inactivated in M059K.

As it is shown in summarized results, M059K cells show a transient G2 arrest after exposing to 2 Gy, which can be completely abrogated by 4 mM caffeine (Figure 7A). Inhibition of ATM with KU-55933 has a similar effect to that observed in A549 cells (Figure 7B). Significantly, inhibition of DNA-PKcs with NU-7026 also generates a significantly stronger and more persistent G2 arrest that is comparable to that measured after ATM inhibition, particularly when considering that in these experiments 2 Gy instead of 4 Gy IR were used (Figure 7C).

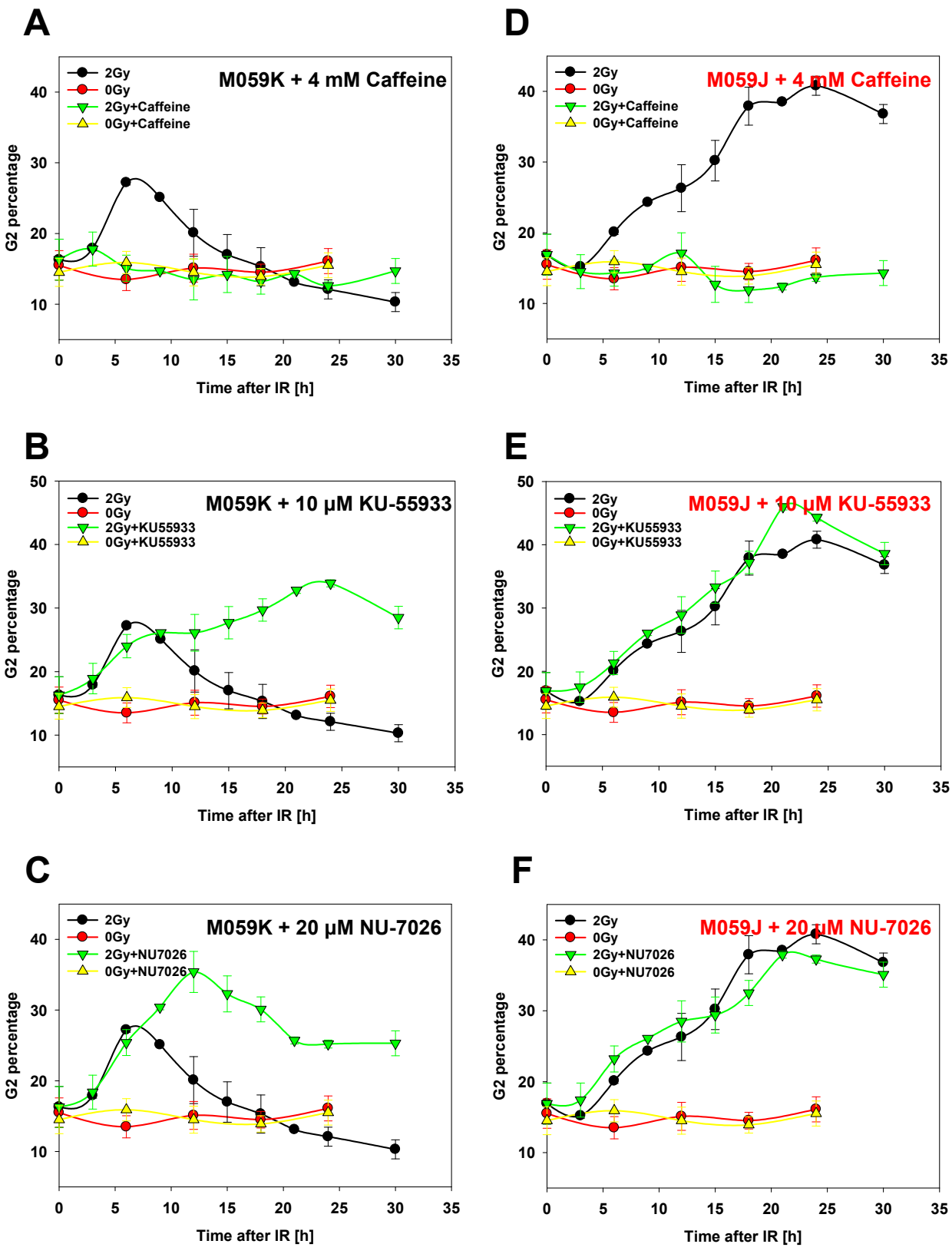

Figure 7. Multiple drugs' effects on M059J and M059K G2 arrest after 2 Gy IR. Exponentially growing M059J and M059K cells were pre-treated with different drugs 1 h before 2 Gy IR, and the drugs were maintained in the duration of the experiment.. Cell cycle distributions were calculated. G2 fractions are plotted against time. **(A)** M059K treated with 4 mM caffeine; **(B)** M059K treated with 10 μM KU-55933; **(C)** M059K treated with 20 μM NU-7026; **(D)** M059J treated with 4 mM caffeine; **(E)** M059J treated with 10 μM KU-55933; **(F)** M059J treated with 20 μM NU-7026. The results are from 3 repeated experiments. Error bar stands for standard deviation.

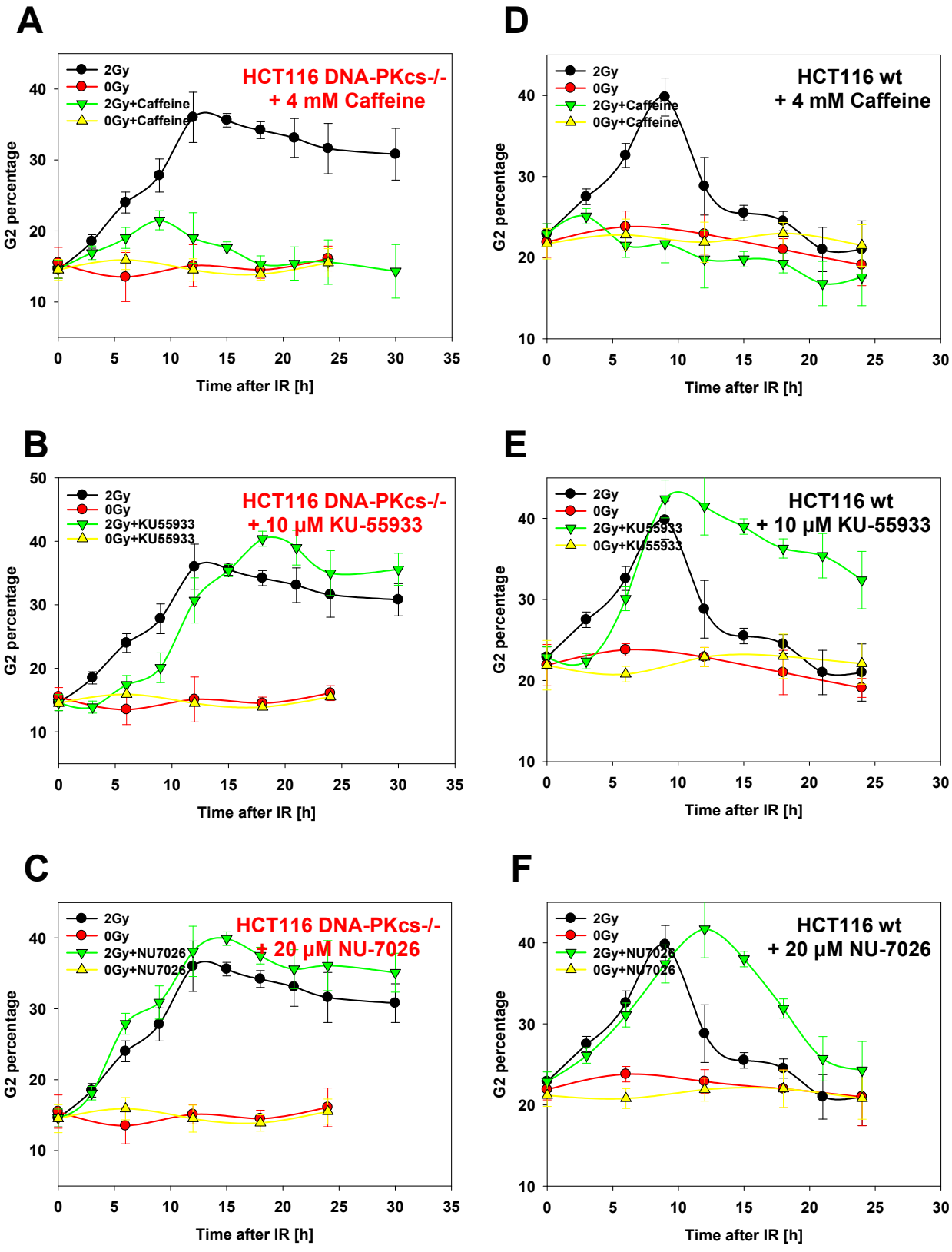

Figure 8. Multiple drugs' effects on HCT116 DNA-PKcs-/- and HCT116 wt G2 arrest after 2 Gy IR. Exponentially growing DNA-PKcs-/- and HCT116 wt cells were pre-treated with different drugs 1 h before 2 Gy IR, and the drugs were maintained in the duration of experiment. Cells were sampled every 3 h, fixed, permeabilized and stained with PI. The PI signal variations were measured on flow cytometry. Cell cycle distributions were calculated. G2 fractions obtained are plotted as a function of time. **(A)** HCT116 DNA-PKcs-/- treated with 4 mM caffeine; **(B)** HCT116 DNA-PKcs-/- treated with 10 μM KU-55933; **(C)** HCT116 DNA-PKcs-/- treated with 20 μM NU-7026; **(D)** HCT116 wt treated with 4 mM caffeine; **(E)** HCT116 wt treated with 10 μM KU-55933; **(F)** HCT116 wt treated with 20 μM NU-7026. The results are from 3 repeated experiments. Error bar stands for standard deviation.

This observation is further confirmed in M059J cells (Figure 7D) that shows a large increase in G2 arrest, as compared to M059K cells, which remains caffeine sensitive. Interestingly, in M059J cells, inhibition of ATM with KU-55933 has no further effect on G2 arrest suggesting that inhibition of ATM and DNA-PKcs leads to equivalent responses (Figure 7E). As expected, NU-7026 has no further effect on M059J cells (Figure 7F). The slightly smaller effect of NU-7026 on M059K cells compared to M059J cells tested in the absence of this drug may be due, either to incomplete inhibition of DNA-PKcs, or to drug inactivation at later incubation times.

We further performed a similar experiment by using HCT116 cells system, in which DNA-PKcs knockout mutant has been generated. The results shown in Figure 8 demonstrate that practically identical responses can be obtained. The ATM level is reported very low in M059J cells (168,169). A recent measurement in our laboratory indicates that HCT116 DNA-PKcs$^{-/-}$ cells also show low ATM levels. The observed long persistent G2 arrest might be also triggered by ATM, which may bias the results obtained. If it is true, it may suggest that there is a coupling between ATM and DNA-PKcs levels relevant to the responses investigated here.

4.1.3 The Role of ATR in G2 checkpoint response

Overall the above experiments leave ATR as the prime candidate kinase responsible for the development and maintenance of the G2 checkpoint, especially when ATM or DNA-PKcs are inactivated. In agreement with this postulate, inhibition of the down stream effectors of ATR, Chk1, using UCN-01 has an effect on the development of the G2 checkpoint in A549 cells that is quantitatively similar to that observed in cells treated with caffeine (compare results in Figure 5A, 5C). On the other hand, 200 nM of the Chk2 inhibitor II (IC50 for Chk2 = 12.5 nM) (156) has no effect on the development of the G2 checkpoint in A549 cells in agreement with the limited role of ATM in the response (Figure 5D). Increasing the concentration of this inhibitor to 800 nM did not alter the results, thus ruling out indirectly low concentration as the cause for the lack of an effect. Combined treatment with caffeine and KU-55933 (Figure 5E) gives results identical to caffeine alone suggesting that either caffeine completely inhibits ATM at the concentrations used so that KU-55933 is unable to add anything, and/or that ATM contributes less to the development of the G2 checkpoint.

Although the above results clearly point to a strong contribution of ATR to the development of the G2 checkpoint, all key conclusions are based on results obtained

with caffeine, a drug with pleiotropic effects. A powerful genetic system provides further evidence for the contribution of ATR in G2 checkpoint response. Since ATR inactivation is lethal in mammalian cells, only conditional inactivation generates useful model systems. In the GM847-ATRkd model, a Tet-on promoter is used to regulate the expression of exogenous ATR fragment in which kinase domain is inactivated (ATRkd). Administration of the tetracycline analog doxycycline in GM847-ATRkd cells causes the overexpression of ATRkd, which competes with the endogenous ATR and exerts a dominant negative effect (170).

The results in Figure 9 indicate that in the absence of doxycycline, GM847-ATRkd cells show a pattern of G2 arrest that is similar to that of A549, M059K and HCT116 wt cells (See Figure 9). Thus, inhibition of ATM causes a slightly delayed but overall stronger blockage in G2, and the Chk2 inhibitor remains ineffective. On the other hand caffeine and UCN-01 cause a nearly complete abrogation of the G2 arrest.

Addition of doxycycline for 48 h causes a strong induction of ATRkd, clearly demonstrated following Western blot analysis (Figure 10F). Notably, under these conditions no measurable arrest in G2 is measured (Figure 10A) and treatment with the entire collection of inhibitors including caffeine produces little additional effect (Figures 10A to 10E). This result strongly supports the contention that ATR is the key kinase initiating/maintaining the G2 arrest.

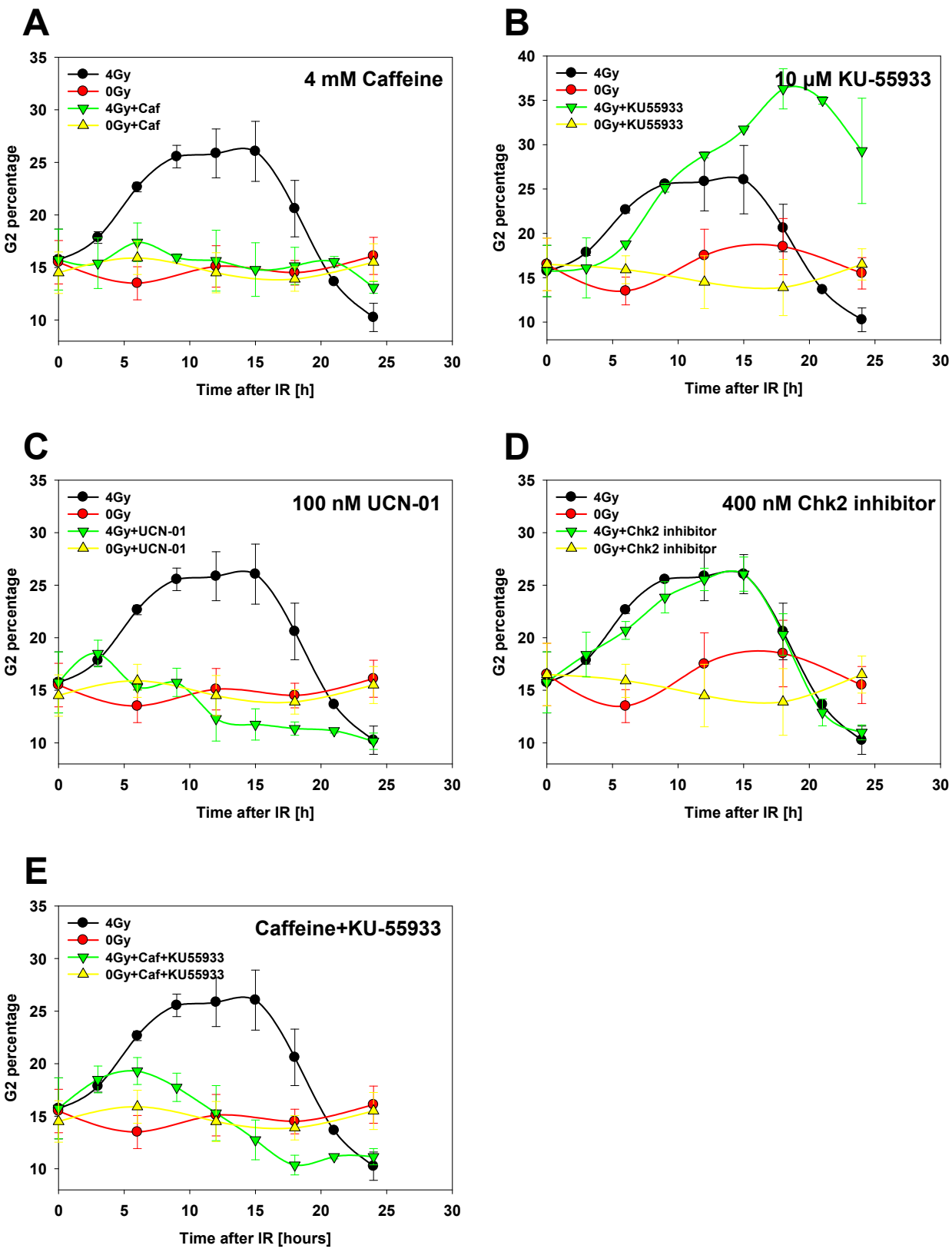

Figure 9. Multiple drugs' effects on GM847 ATRkd after 4Gy IR. Exponentially growing GM847 ATRkd cells were pre-treated with different drugs 1 h before 4 Gy IR, and the drugs were maintained in the duration of experiment. Cells were sampled every 3 h, fixed, permeabilized and stained with PI. The PI signal variations were measured on flow cytometry. Cell cycle distributions were calculated. G2 fractions are plotted as a function of time. **(A),** 4 mM caffeine; **(B),** 10 μM KU-55933; **(C),** 100 nM UCN-01; **(D),** 400 nM Chk2 inhibitor; **(E),** 4 mM Caffeine + 10 μM KU-55933). The results are from 3 repeated experiments. Error bar stands for standard deviation.

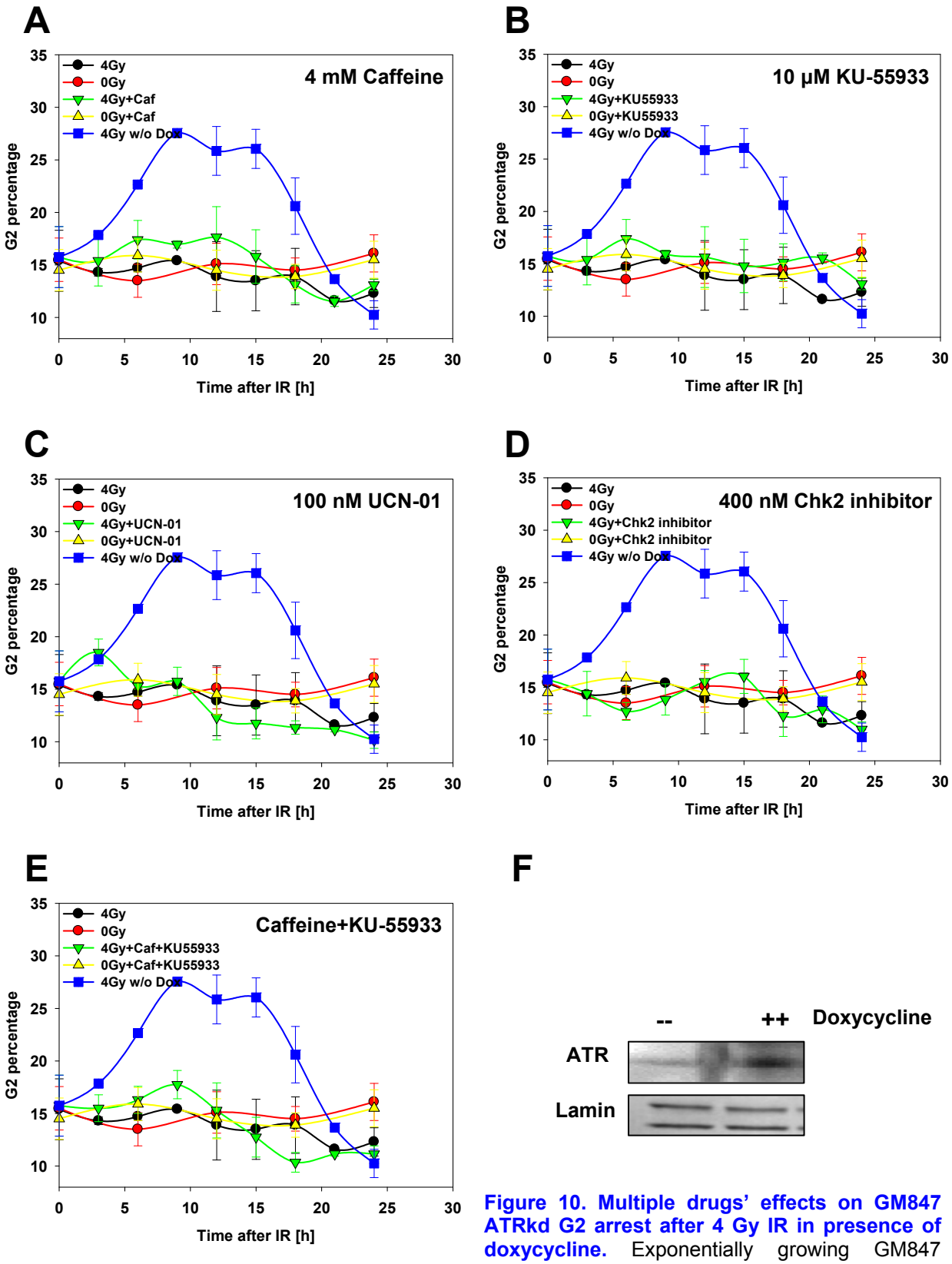

Figure 10. Multiple drugs' effects on GM847 ATRkd G2 arrest after 4 Gy IR in presence of doxycycline. Exponentially growing GM847 ATRkd cells were treated with 5 μg/ml doxycycline for 48 h. After induction, cells were pre-treated with different drugs 1 h before 4 Gy IR, and the drugs were maintained in the duration of experiment. Cells were sampled every 3 h, fixed, permeabilized and stained with PI. The PI signal variations were measured on flow cytometry. Cell cycle distributions were calculated. G2 fractions are plotted as a function of time. **(A),** 4 mM caffeine; **(B),** 10 μM KU-55933; **(C),** 100 nM, UCN-01; **(D),** 400 nM Chk2 inhibitor; **(E),** 4 mM Caffeine + 10 μM KU-55933). The results are from 3 repeated experiments. Error bar stands for standard deviation. A blue line shown in each graph is the G2 arrest response without doxyline treatment. **(F),** ATR expression level before and after induction. Western blot results suggested the expression of ATR were significantly increased after the induction by doxycycline.

4.1.4 The contribution of ATM, ATR and DNA-PKcs to G2 arrest

The relatively small contribution of ATM to the development of G2 checkpoint raises the question of possible artifacts in the above described experiments. In the results reported above, the G2 fraction was calculated by flow cytometry and the signal in the histogram attributed to G2 cells could also include mitotic and tetraploid cells, i.e. cells that are beyond the G2 arrest point. To address this limitation we searched for markers allowing the unequivocal identification of G2 cells.

At the beginning of mitosis, MPF is disrupted through ubiquitin-mediated degradation of cyclin B1 that is synthesized in high amounts starting at about the middle of S-phase and peaking during G2. Cyclin B1 can therefore be used as a rather specific G2 marker. Bivariate (DNA/cyclin B) analysis by flow cytometry of A549 and ATM deficient cells exposed to 4 Gy X-rays is shown in Figure 11. It is evident that even when the analysis is restricted to cyclin B positive cells and thus to true G2 cells, results similar to those discussed above are obtained.

The delayed G2 accumulation of irradiated ATM deficient cells probably reflects the combined effect of G2 cell division due to checkpoint abrogation, together with the subsequent accumulation in G2 of cells irradiated in G1 or S phase of the cell cycle. To address this possibility, we followed the accumulation in G2 of cells irradiated during the S-phase. 5-bromo-2´-deoxyuridine (BrdU), a thymidine analog, is widely used to pulse-label S-phase cells (171). By following the movement of the BrdU signal at different times after pulse-labeling, we confirmed that BrdU positive AT cells are arrested after IR in the G2-phase for relatively longer periods of time - as was also seen in the experiments described above. These results are summarized in Figure 12.

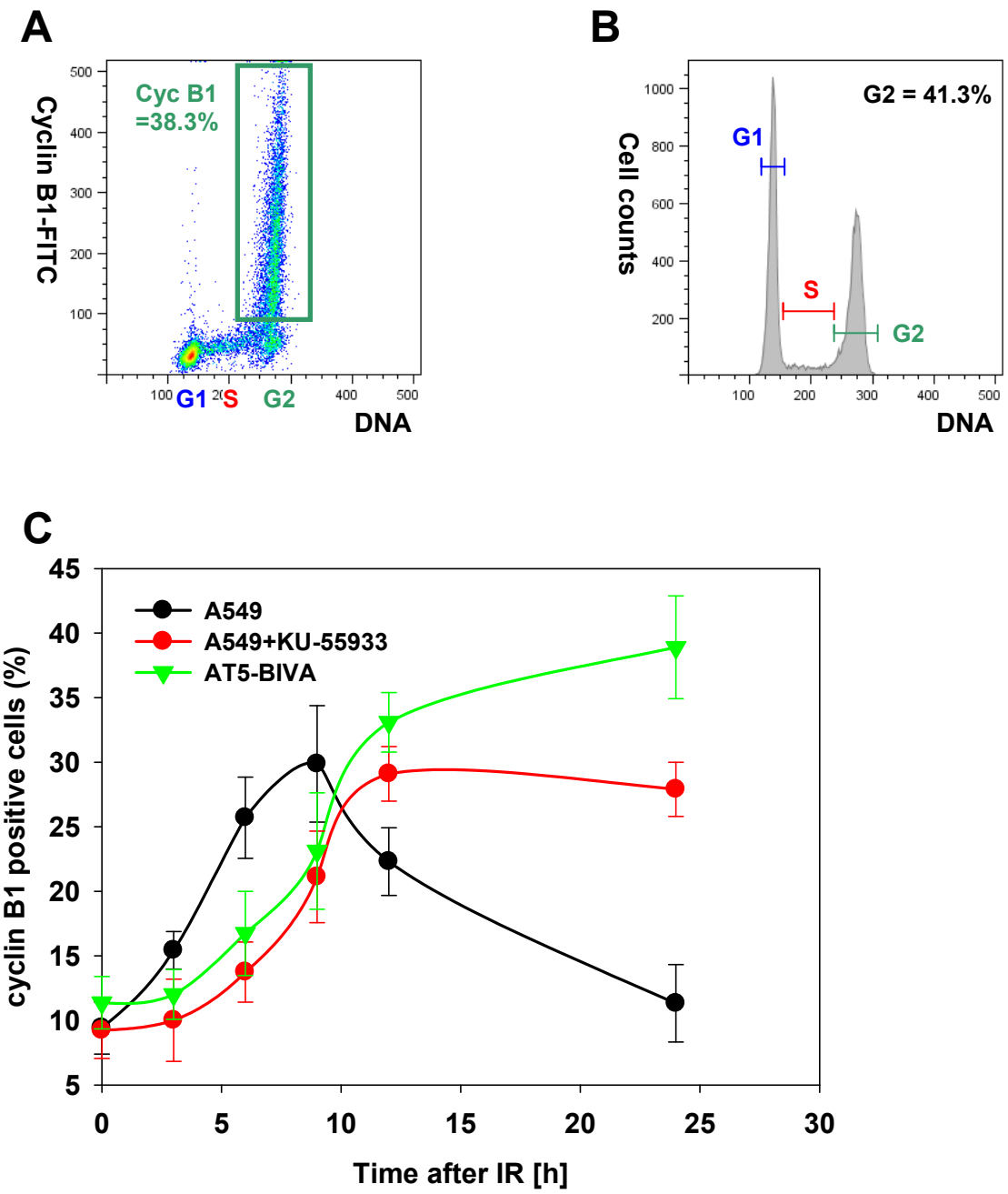

Figure 11.Cyclin B1 as a maker of G2 cells. Exponentially growing A549 and AT5-BIVA were treated with 10 μM KU-55933 followed by 4 Gy IR. Samples were taken every 3 h, fixed, permeabilized and stained with anti-cyclin B1 antibody and PI. Cyclin B1 positive fractions were gated and calculated. Bivariate flow cytometry was used to detect cyclin B1 expression level (FITC) and DNA content (PI) simultaneously. **(A)** A density plot of bivariate FACS. Gated populations indicate the cells expressing cyclin B1. **(B),** Cell cycle distributions of the sample **A**. **(C),** Cyclin B1 positive fractions are plotted as function of time .The results are from 3 repeated experiments. Error bar stands for standard deviation.

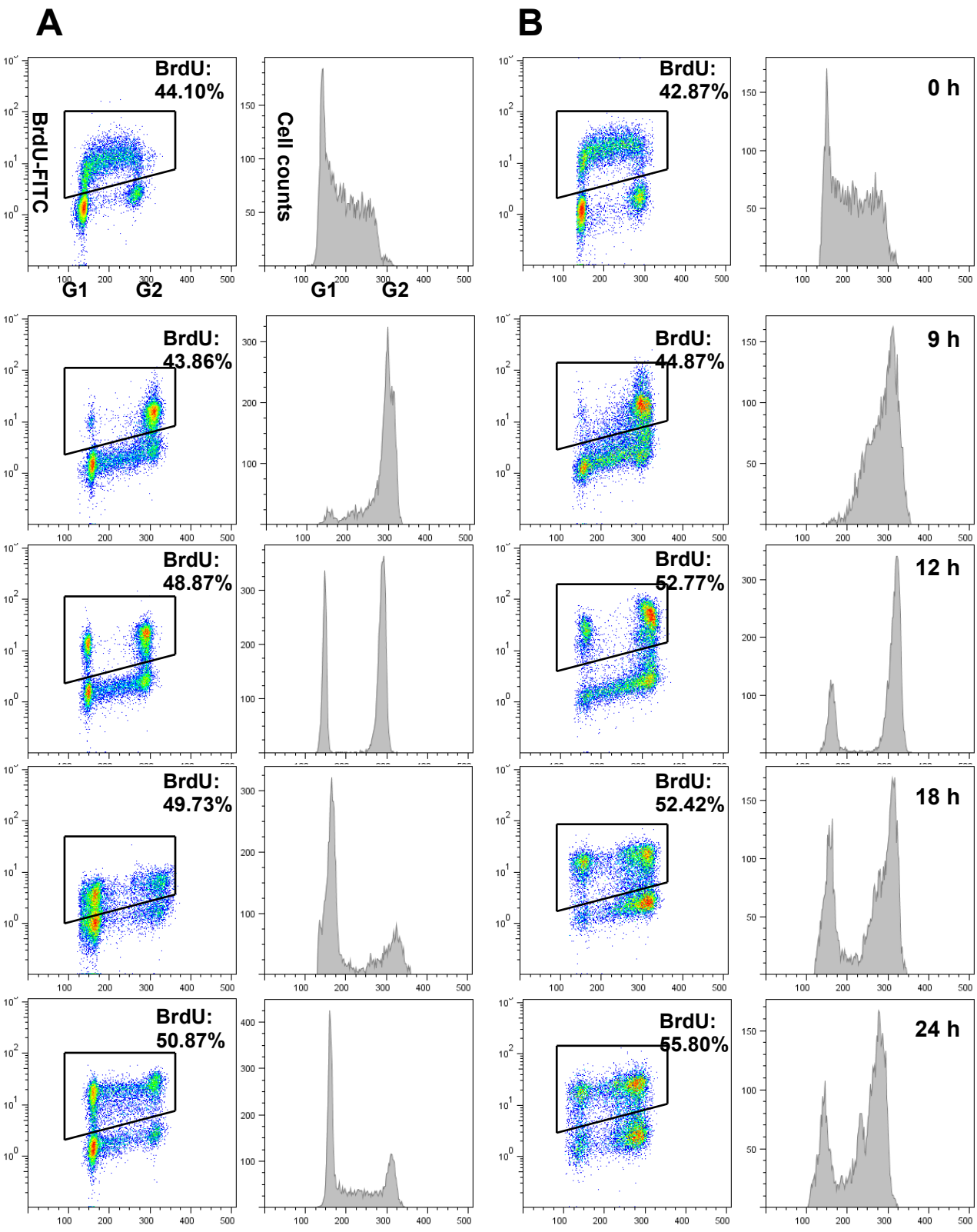

Figure 12. AT5-BIVA cells Irradiated during S-phase arrest in G2 for a longer duration compared to wild-type control. Exponentially growing A549 and AT5-BIVA cells were pulse labelled with10 μm BrdU for 30 min. BrdU were removed immediately after 4 Gy IR and cells were returned to the incubator. Cells were sampled every 3 h, fixed, permeabilized and stained with anti BrdU antibody and PI. Bivariate flow cytometry was used to detect the BrdU signal and the DNA content simultaneously. Gated populations are BrdU positive cells. Density dot plot is used to group cells with the same fluorescence density signals. Blue: low frequency; red: high frequency. Histogram is used to show the cell cycle distributions of BrdU positive cells. **(A),** The transition of BrdU labeled A549 cells in the cell cycle. **(B),** The transition of BrdU labeled AT5-BIVA cells in the cell cycle.

Thus, although ATM deficient cells irradiated in G2 may have defective activation of the G2 checkpoint (172), activation of the G2 checkpoint is possible in cells irradiated in preceding phases of the cell cycle, such as S and G1. The different response of ATM deficient cells regarding G2 checkpoint activation has led to the hypothesis that two forms of G2 checkpoint can be distinguished depending upon where in the cell cycle cells are irradiated (172). We wished to investigate further this possibility and employed for this purpose phosphorylation of histone H3 at Serine 10 (H3-pS10) as a marker (3). H3-pS10 is highly phosphorylated during M-phase and allows the easy discrimination by flow cytometry between G2 and M-cells. The results obtained are summarized in Figure 13. Under normal growth conditions the mitotic population remains stable according to bivariate (DNA/H3-pS10) flow cytometry analysis. Figure 13A shows the basis of discrimination of the mitotic cells according to this form of analysis. Figure 13B is a typical dot plot from flow cytometry which displays DNA content and H3-pS10 signal, as well as the gating used to identify mitotic cells.

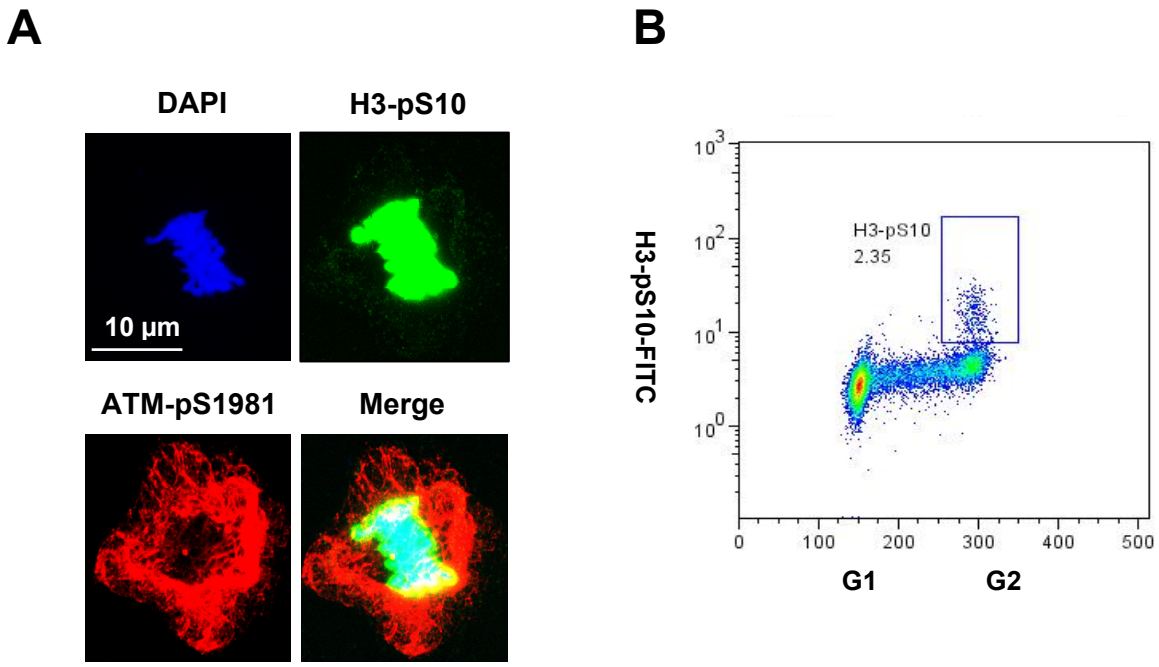

Figure 13. Detect mitotic cells by measuring phosphorylation of Histone3 at Serine 10. Exponentially growing A549 cells were fixed, permeabilized and stained anti H3-pS10, ATM-pS1981 antibodies and DAPI. Cells were visualized by confocal microscope. **(A),** Confocal image of stained mitotic cell. (Bar = 10 µm). Cells were fixed, permeabilized and stained an anti H3-pS10 antibody and PI. Bivariate flow cytometry was used to detect the H3-pS10 expression level and the DNA content simultaneously. MI was calculated by gating H3-pS10 positive fractions. **(B),** H3-pS10 expression levels in A549 cells.

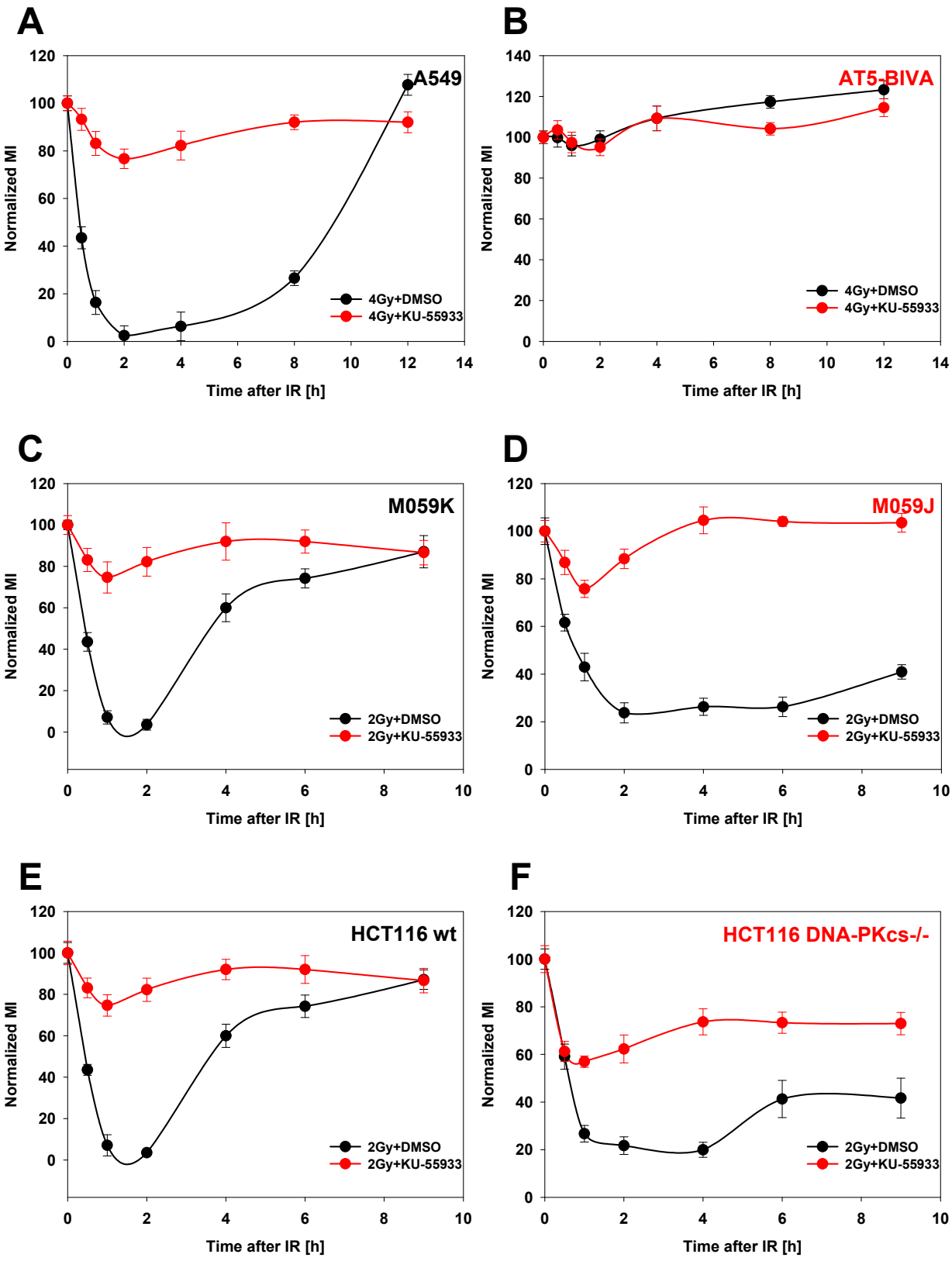

Figure 14. Mitotic index variations of A549 and AT5-BIVA, M059J, M059K HCT116 DNA-PKcs-/- and HCT116 wt in response to IR. Exponentially growing A549 and AT5-BIVA cells were pre-treated with KU-55933 1 h before 4 Gy IR. Exponentially growing M059J, M059K, HCT116 DNA-PKcs-/- and HCT116 wt cells were pre-treated with KU55933 1 h before 2 Gy IR. Cells were incubated with the drugs in the duration of the experiment. Cells were sampled at each time point, fixed, permeabilized and stained anti Histone 3- pSer10 antibody and PI. Bivariate flow cytometry was used to detect the H3-pS10 expression level and the DNA content simultaneously. Mitotic indexes are calculated by gating H3-pS10 positive fractions. MI was normalized by diving the MI of irradiated cells against non-irradiated cells. Normalized MI is plotted as a function of time. **(A),** Mitotic index variation of A549 cells

after IR. **(B),** Mitotic index variation of AT5-BIVA cells after IR. **(C),** Mitotic index variation of M059K cells after IR. **(D),** Mitotic index variation of M059J cells after IR. **(E),** Mitotic index variation of HCT116 wt cells after IR. **(F),** Mitotic index variation of HCT116 DNA-PKcs-/- cells after IR. The results are from 3 repeated experiments. Error bar stands for standard deviation.

Figure 14A summarizes the development of the mitotic index (MI) in A549 exposed to 4 Gy IR. The precipitous drop of MI within 1-2 h after IR is in line with a strong G2 arrest in cells irradiated in G2; it starts recovering 6-8 h later and reaches control levels 12 h after IR. This block in G2 is abrogated after treatment with KU-55933 implying the function of ATM in its development. Indeed, AT5-BIVA cells show no evidence for a drop in MI after IR and this effect is not further modified by KU-55933 (Figure 14B). The G2 arrest appears well active in DNA-PKcs deficient M059J cells (Figure 14D), as compared to their wild type counterpart (Figure 14C), and in both cases it is abrogated by the ATM inhibitor. Similar results are obtained with HCT116 model system (Figure 14E and 14F). In all these cases DNA-PKcs deficiency causes a prolonged drop in MI. These results suggest a strong dependence on ATM and minor dependence on DNA-PKcs of the initial development of the G2 arrest. However, they also suggest an involvement of DNA-PKcs in the recovery from the G2 arrest, as it was also described in experiment outlined above.

While the above results reproduce salient features of the ATM response in G2, they also raise a number of relevant questions. For instance, in AT cells MI has been the recovered to basal level from 15-24 h after IR, which is apparently contradicted to the observed strong G2 arrest. Such a controversy can be resolved if one considers that the MI (about 3%, data not shown) at the zero time point, which stems from the about 12-15% fraction of cells in G2 at that time. However, the same 3% MI at 15 h stems from an over 50% fraction of cells present in G2 at that time. Therefore, a significant reduction of G2 cells moving into M by a factor of three is observed, which suggests strong G2 arrest. To account for this perturbation from the variation of cell cycle, we calculated a MI normalized to the fraction of cells in G2 at any given time point. The results obtained are summarized in Figure 15. It is evident from the results that a clear reduction after later times in the normalized MI is observed in wild type cells treated with the ATM inhibitor, as well as ATM deficient cells. This observation reconciles the results obtained using G2 fraction analysis to those obtained using MI index analysis.

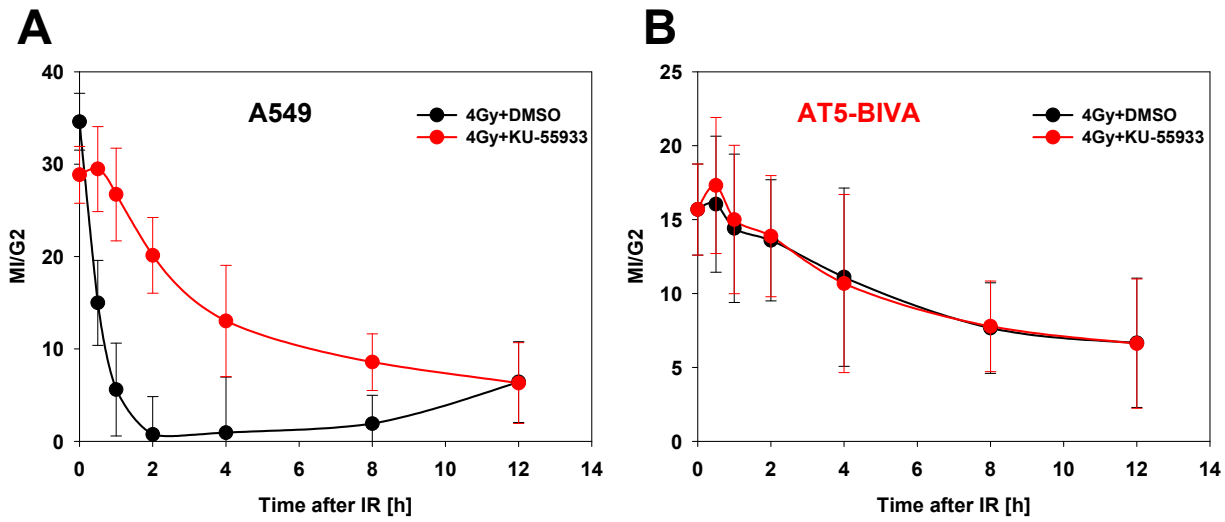

Figure 15. Normalized MI of A549 and AT5-BIVA in response to IR. The same experiment as in Figure 12. The MI was normalized by diving MI against G2 fraction. **(A),** Normalized MI of A549 after IR; **(B),** Normalized MI of AT5-BIVA after IR. The results are from 3 repeated experiments. Error bar stands for standard deviation.

But does ATM alone, instead of ATR, contribute the effect observed on MI? To address this question, we performed a similar analysis in GM847-ATRkd cells. The results in Figure 16 demonstrate that in the absence of doxycycline, when ATR is still active, these cells respond to IR in a manner comparable to that of A549 cells. MI drops to zero 2 h after IR and recovers 6-8h later (Figure 16A). The faster response of these cells when compared to A549 cells is partly explained by their higher constitutive MI, which suggests more active growth. This reduction in MI is significantly reduced after inhibition of ATM using KU-55933. However, after compromising ATR by treatment of the cells with doxycycline, the MI remains relatively unchanged after IR and is not further affected by the ATM inhibitor (Figure 16B). The same results were observed if we disrupted ATR function by caffeine treatment in many different genetic backgrounds (Figure 16C).

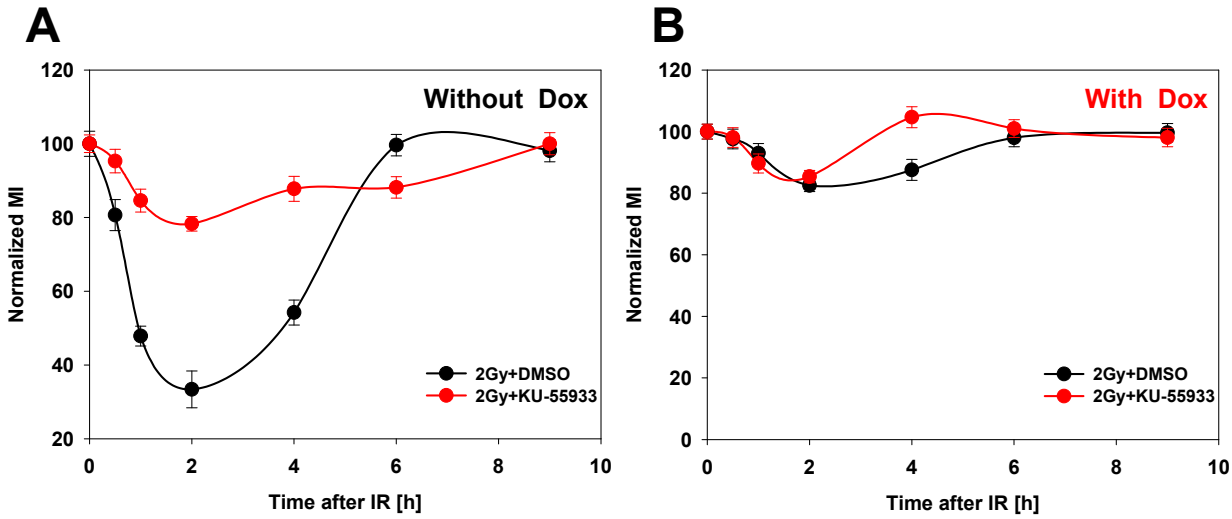

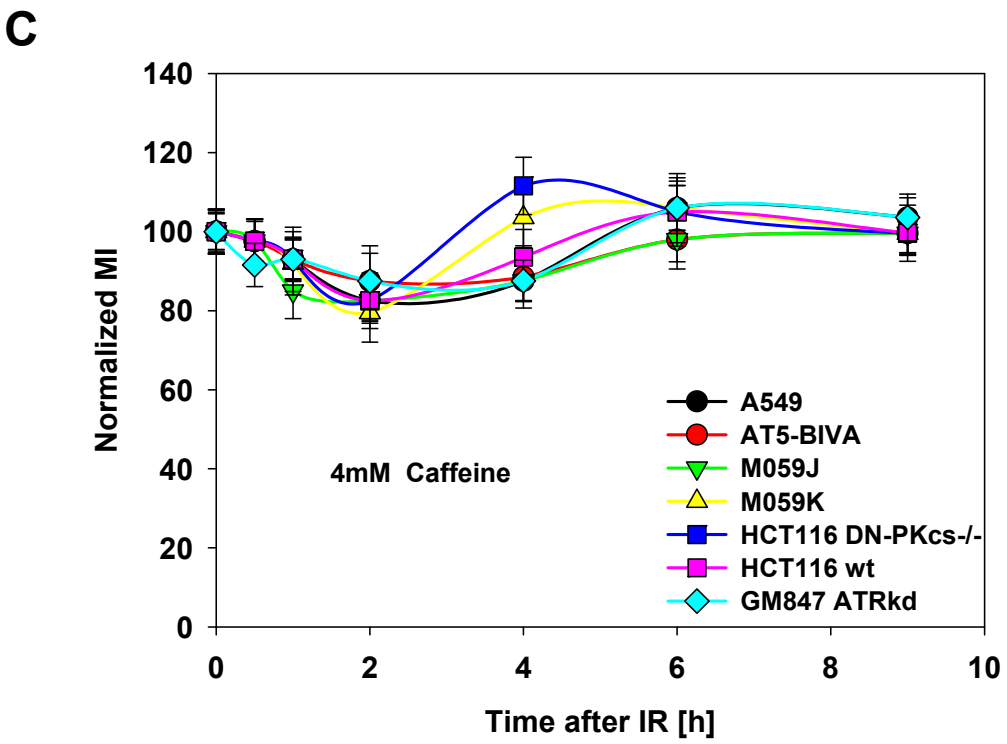

Figure 16. Mitotic index variations of GM847-ATRkd with or without doxycycline. Exponentially growing GM847 ATRkd cells with or without induction of doxycycline were pre-treated with KU-55933 1 h before 2 Gy IR. The drugs were kept for the duration of the experiment. MI is normalized by diving the MI from untreated samples. Normalized MI is plotted as a function of time. **(A),** Mitotic index variation of GM847 ATRkd cells in the absence of doxycycline. **(B),** Mitotic index variation of GM847 ATRkd cells in the presence of doxycycline. **(C),** Caffeine abrogated MI variation after 2 Gy IR. Exponentially growing A549, AT5-BIVA, M059J, M059K, HCT116wt, HCT16DNA-PKcs-/- and GM847 ATRkd were pre-treated with 4 mM caffeine for 1 h before IR. The results are from 3 repeated experiments. Error bar stands for standard deviation.

The persistently high levels of mitotic index in AT5-BIVA cells after IR opened the possibility that ATBIVA cells are blocked in M-phase of the cell cycle. Although no delays in M-phase have been observed in wild type cells exposed to IR, we wished to rule possible effects in the various mutants. For this purpose, we treated A549 and AT5-BIVA cells for 17 h with a highly specific inhibitor of microtubules polymerization, nocodazole, to generate a population of highly enriched M-phase cells. The results shown in Figure 17 confirmed such accumulation in M using bivariate staining with propidium iodide and H3-pS10 both for A549, as well as for AT5-BIVA cells. The synchronized cells were then exposed to either 0 or 4 Gy X-rays and their progression through the cycle was examined by following mitotic index as a function of time. There is no IR induced delay in A549 cells with more than 80% of the cells dividing within about 2 h. In AT5-BIVA cells, there is no radiation induced delay in cell division, but cell division overall is much slower than in the wild type A549 cells. Thus,

although ATM deficiency affects the release of cells from a nocodazole block, it does not alter the radiation response towards this end point.

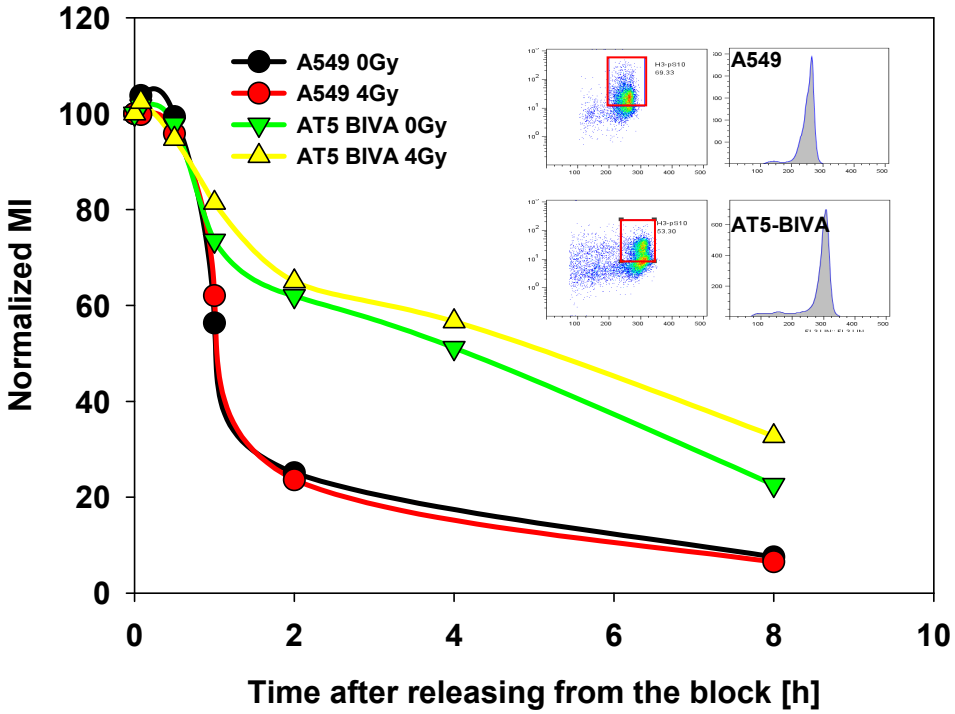

Figure 17. Mitotic index variation after releasing cells from nocodazole block. Exponentially growing A549 and AT5-BIVA cells were synchronized at M-phase by nocodazole (0.04 µg/ml) for 17 h. Cells were released from the block by washing with PBS and supplied with fresh media. After 4 Gy IR (if applied), cells were returned to the incubator. Samples were taken at different time; thereafter the MI was measured by flow cytometry. Histograms indicate the cell cycle distribution after synchronization. H3-pS10 positive populations are gated in the red square. Each MI is normalized by diving against the initial MI. The normalized MI is plotted as a function of time.

4.2 Part 2 How does ATM help to maintain the G2 arrest?

4.2.1 ATM, Chk2 and H2AX phosphorylation are early events in radiation response

In A549 cells exposed to 2 Gy and analyzed 1 h later, ATM-pS1981, Chk2-pT68 and γ-H2AX show rapid foci formation. Discrete foci can be detected 5 min post IR. The number and intensity of observed foci reaches a maximum 30-60 min after IR (Figure 18). Detailed analysis indicates that all Chk2-pT68 foci coincide with ATM-pS1981 foci and that such colocalization only occurs for a short period of time due to the rapid decay of Chk2-pT68 foci. There is also a high level of colocalization between ATM-pS1981 and γ-H2AX foci. As expected, there is no ATM-pS1981 foci formation after IR in AT5-BIVA cells, and as a result no Chk2-pT68 foci are forming either, which is in agreement with the epistatic nature of ATM over Chk2 (Figure 18C). Although γ-H2AX foci formation is not observed 5 min after IR in AT cells, they form robustly after 30 min.

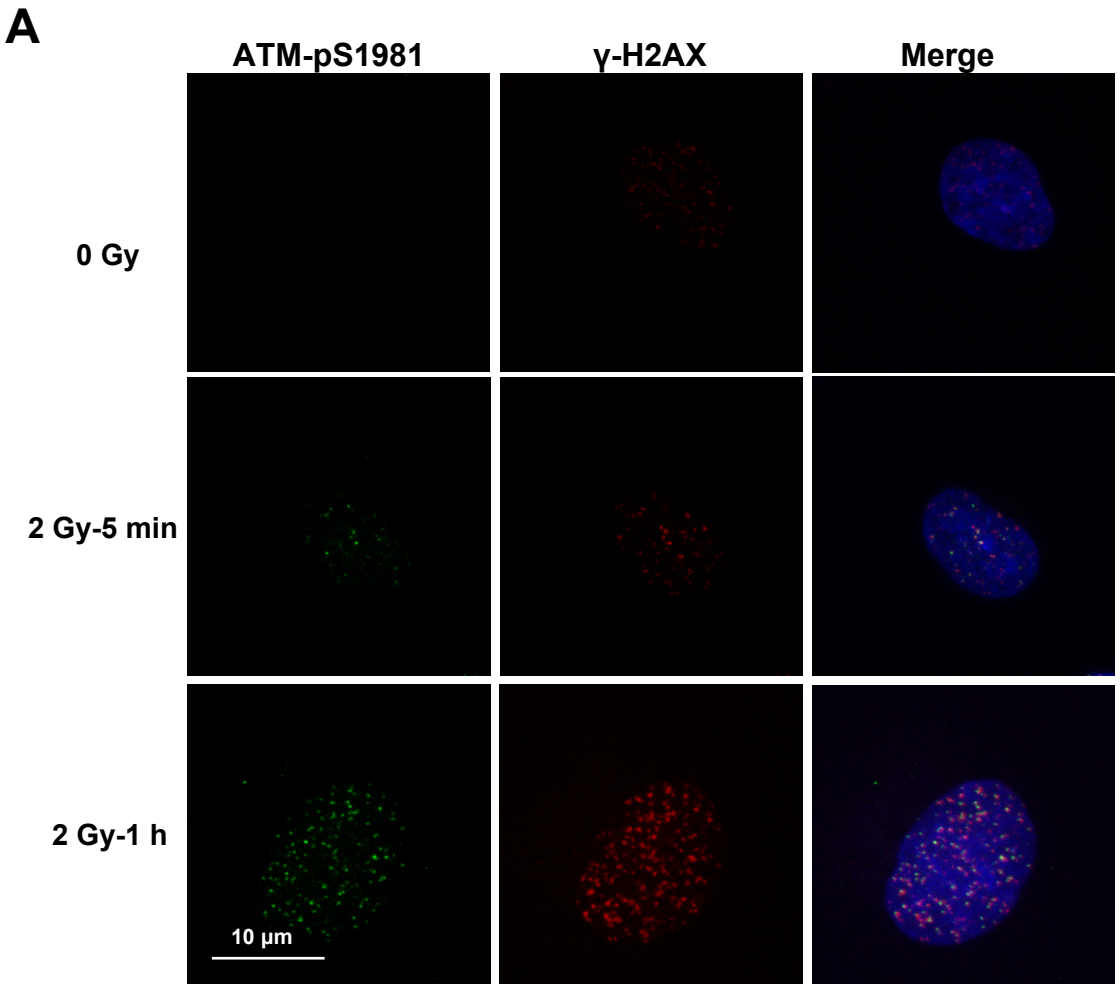

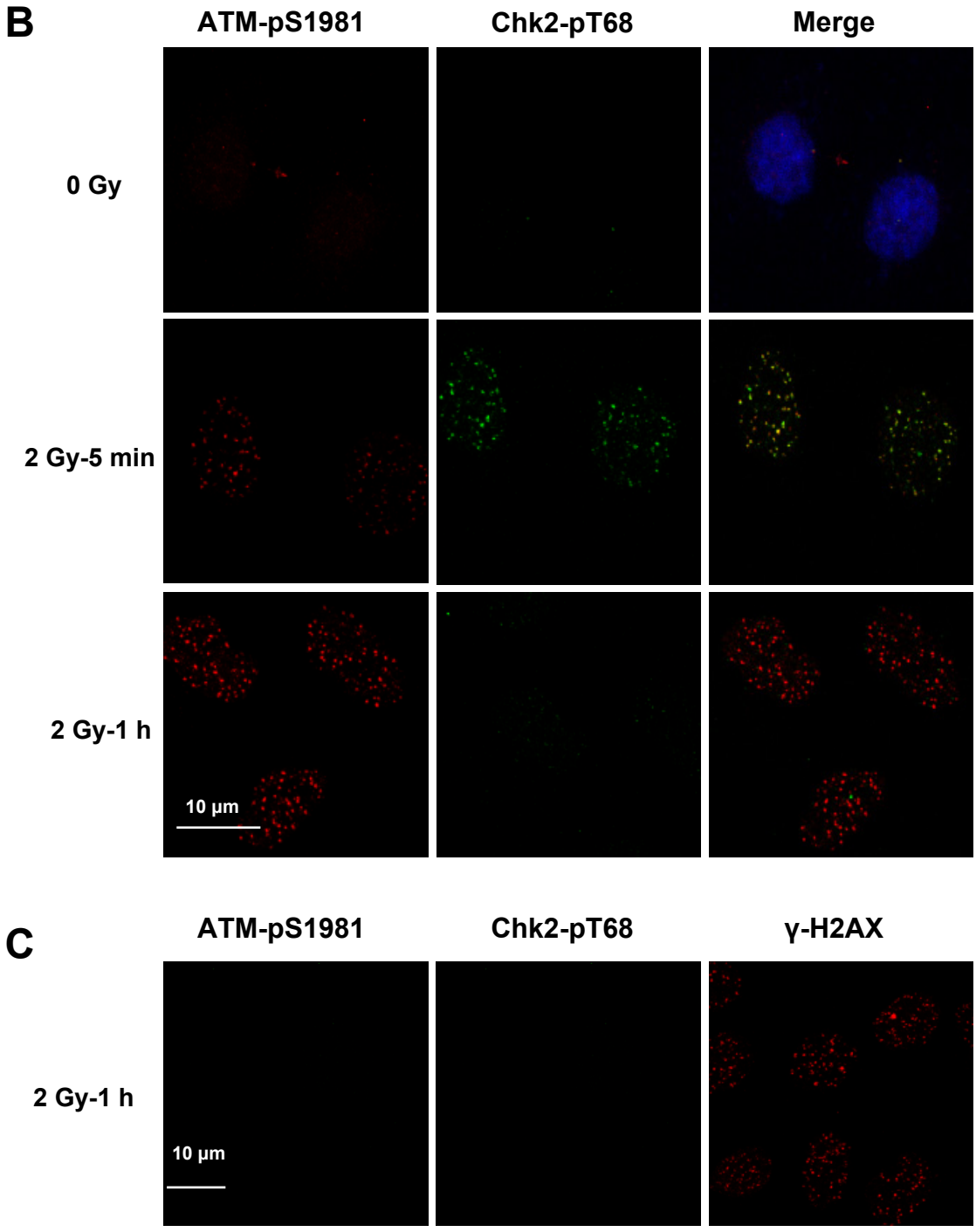

Figure18. Foci formation of different proteins. Exponentially growing A549 and AT5-BIVA were exposed to 2 Gy IR. After desired time, cells were fixed, permeabilized and stained with anti ATM-pS1981, Chk2-pT68 and γ-H2AX antibodies, respectively. Images were obtained using a confocal microscope. **(A);** ATM-pS1981 and γ-H2AX foci formation in A549 cells. **(B);** ATM-pS1981 and Chk2-pT68 foci formation in A549 cells. **(C);** ATM-pS1981, Chk2-pT68 and γH2AX foci formation in AT5-BIVA cells. (bar = 10µm)

4.2.2 ATM-pS1981 and Chk2-pT68 foci formation is independent from ATR function

The results of the previous section indicate important mechanistic connections between signaling pathways using different kinase inhibitors. We were therefore interested in investigating the effect of the same inhibitors on foci formation. The results shown in Figure 19A indicate that caffeine and UCN-01 do not modify detectably the formation of ATM-pS1981 foci in A549 cells exposed to IR. Neither foci intensity, nor foci number are affected following treatment with up to 4 mM caffeine and with up to 100 µM UCN-01. As expected, KU-55933 completely abrogates ATM-pS1981 and Chk2-pT68 foci formation. Interestingly, Chk2 inhibition leaves both the ATM-pS1981 and the Chk2-pT68 foci intact, which suggests that the inhibitor may not function, or that Chk2 activity is not required for foci formation. The above conclusions are also corroborated by the western blot analysis results summarized in Figure 19B, C.

As shown above, caffeine does not affect the formation of ATM-pS1981 and Chk2-pT68 foci after exposure to IR. Since we postulate that caffeine exerts its action by inhibiting ATR, we hypothesized that ATM-pS1981 and Chk2-pT68 foci formation are independent from ATR function. As discussed above, ATR knockout is lethal in higher eukaryotes, and therefore there is no clean system to study ATM functions in the absence of ATR. The GM847-ATRkd cell system used above contains endogenous ATRwt in parallel with the induced ATRkd after addition of doxycycline. Although IR induced ATM-pS1981 foci formation in GM847-ATRkd cells (in presence of 5 µg/ml doxycycline) is found intact (data not shown), we could not rule out the possibility that the endogenous ATRwt functions in a limited way and generates this result. Therefore we searched for alternative genetic systems to test this hypothesis.

Individuals suffering from the Seckel syndrome, a microcephalic primordial dwarfism syndrome, can survive but have a hypomorphic mutation in ATR that compromises, without completely abrogating, the activity of the protein (94). Cells from Seckel syndrome patients have impaired ATR signaling and show a compromised G2 arrest after exposure to IR (94). F02-98 and DK0064 are cells derived from the ATR-Seckel patients (94,122). Interestingly, both cell lines show comparable ATM-pS1981 and Chk2-pT68 foci formation. These results are summarized in Figure 20 and indicate that ATM-pS1981 foci formation occurs in the absence of fully active ATR. This foci

formation indicates that ATM becomes activated. However, despite the fact that the ATM kinase was activated, cells were unable to develop G2 arrest.

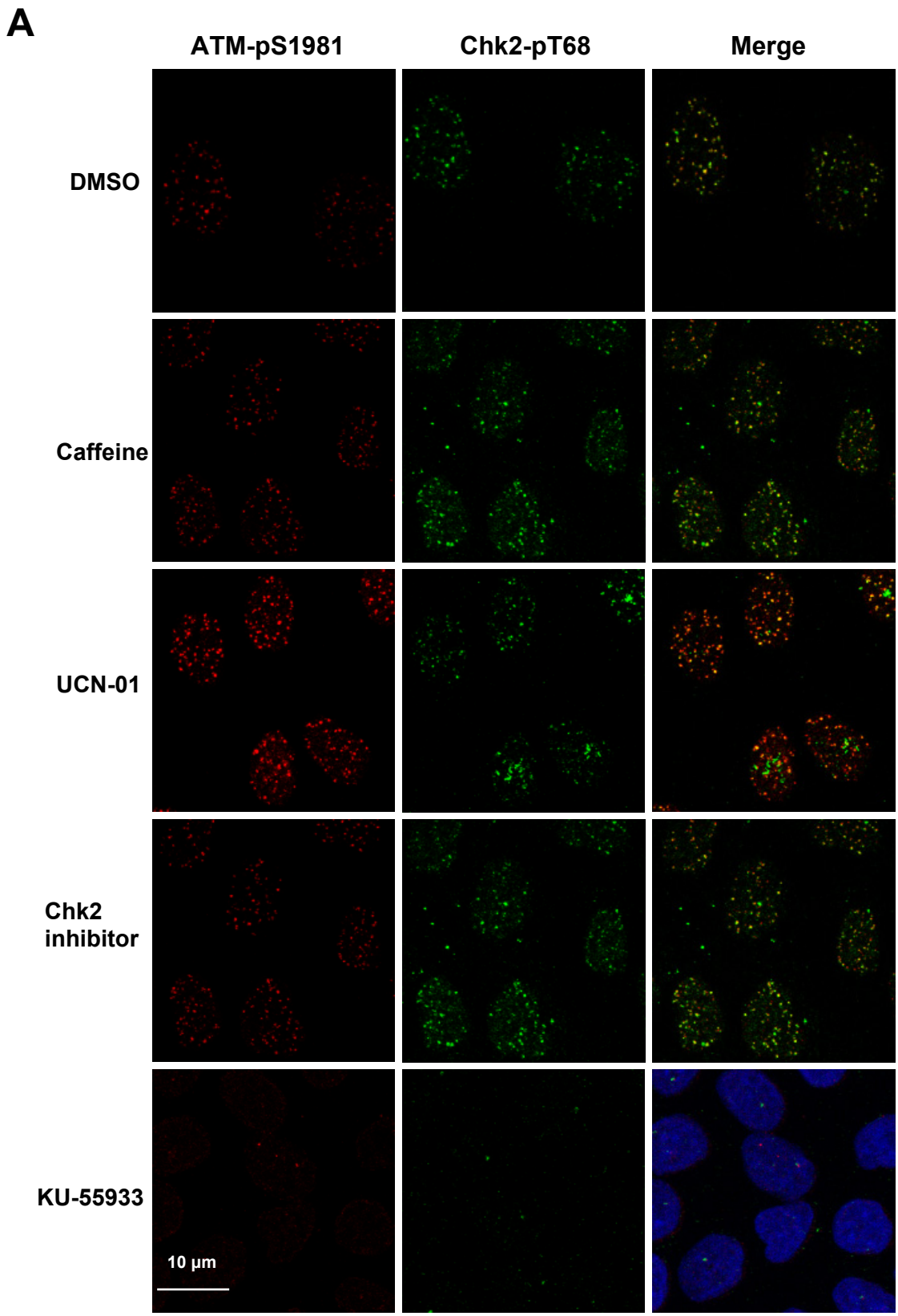

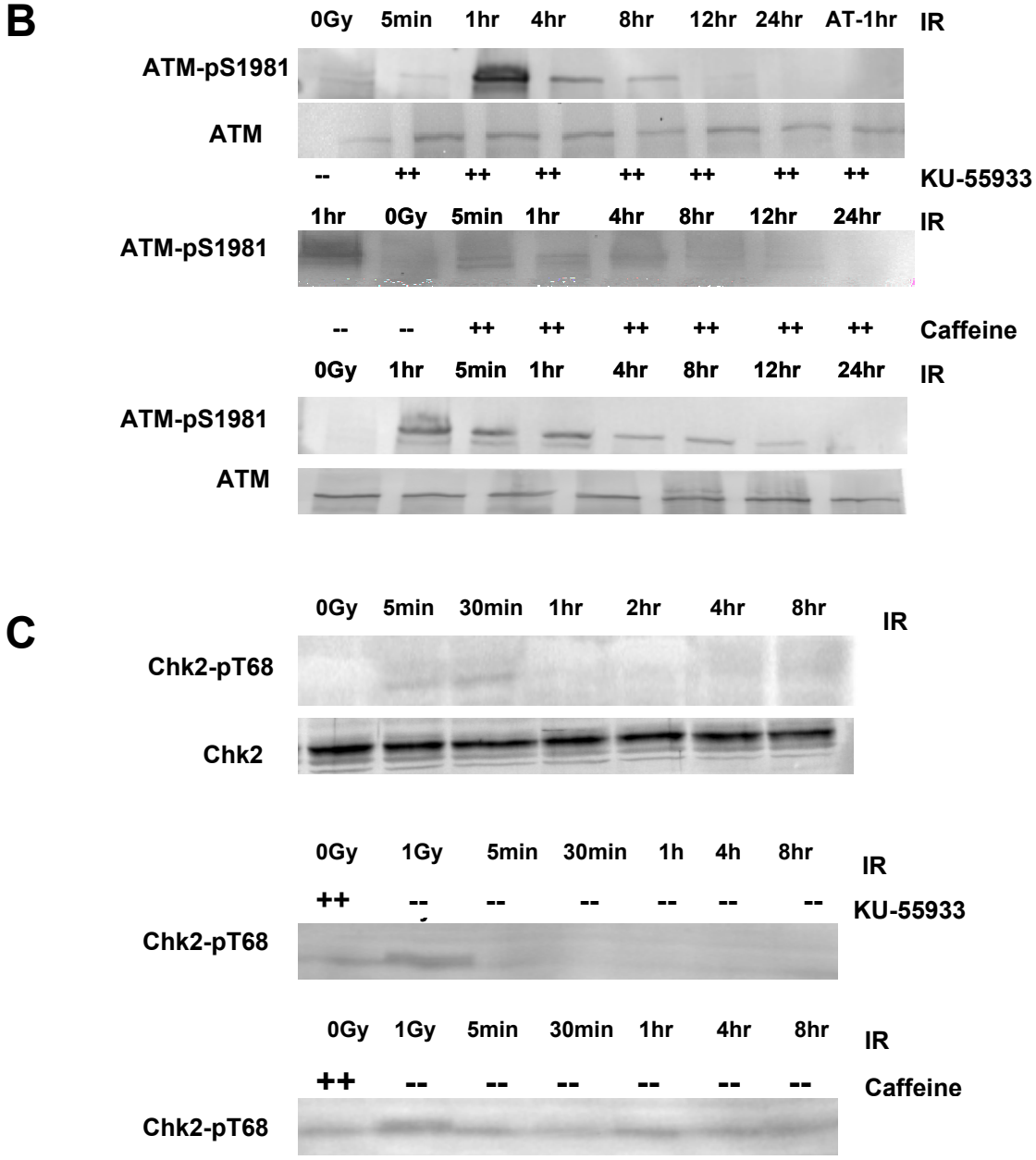

Figure 19 Effects on of different kinase inhibitors on the phosphorylation of ATM at serine 1981 and the phosphorylation of Chk2 at threonine 68 foci in A549 cells after IR. Exponentially growing A549 cells were pretreated with 4 mM caffeine, 100 nM UCN-01, 400 nM chk2 inhibitor, 10 μM KU-55933, respectively, 1 h before IR. After 30 min, the cells were fixed, permeabilized and stained with anti ATM-pS1981, and Chk2-pT68 antibodies. The inhibitors effects were also checked by western blot. **(A),** Drugs effects on foci formation. (bar = 10 μm) **(B),** Western blot to detect drugs effects on the phosphorylation of ATM at S1981. **(C),** Western blot to detect drugs effects on the phosphorylation of Chk2 at T68.

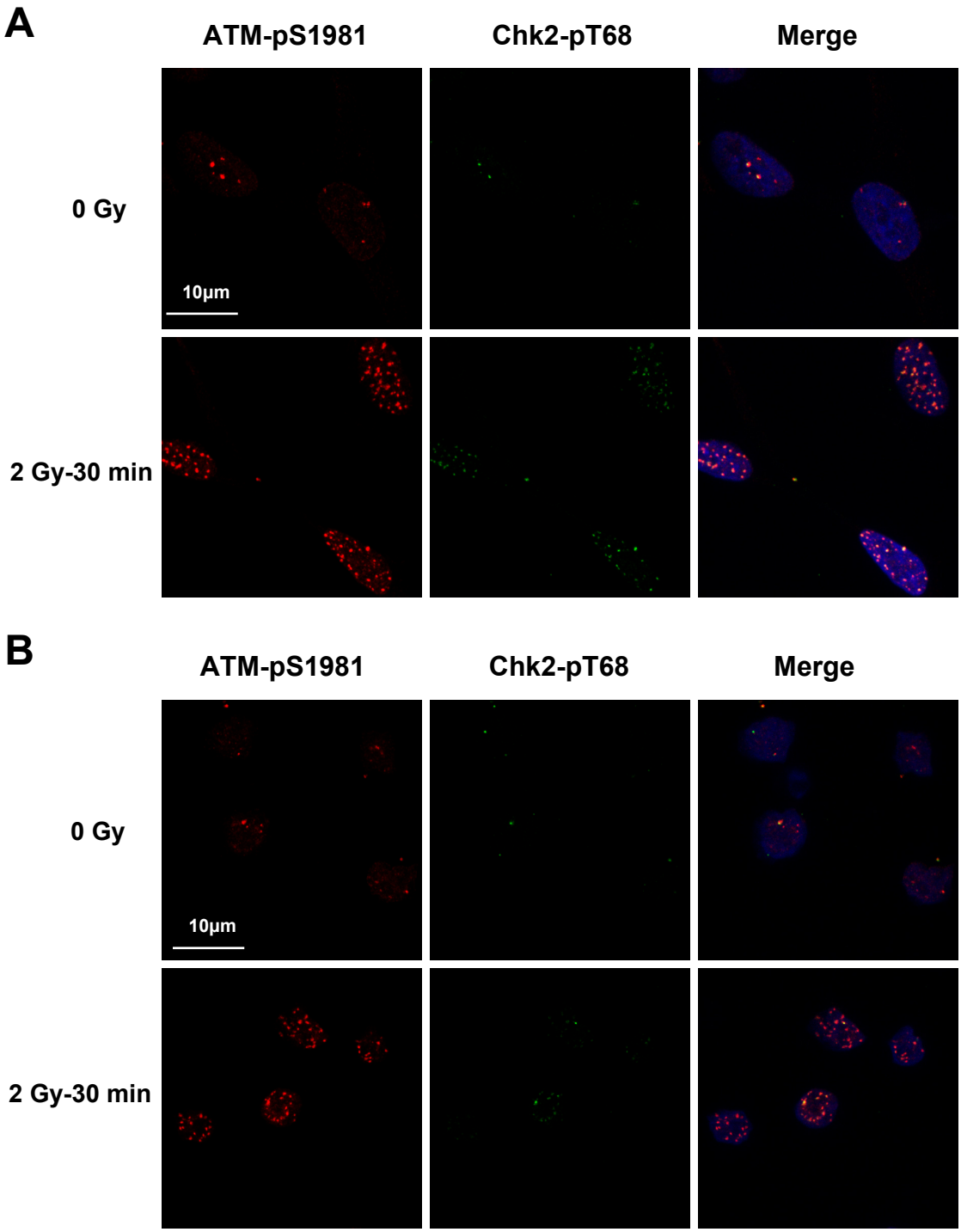

Figure 20. ATM-pS981 and Chk2-pT68 formation in Seckel syndrome cells. Exponentially F02-98 and growing DK0064 were irradiated at 2 Gy. After 30 min, the cell were fixed, permeabilized and co-stained with anti ATM-pS1981, Chk2-pT68 antibodies Images were obtained from the confocal microscope. **(A),** ATM-pS981 and Chk2-pT68 formation in F02-98 cell. **(B),** ATM-pS981 and Chk2-pT68 formation in DK0064 cell. (bar = 10 µm). **DK0064 are suspension growing cells. They could not grow on the slides. After IR, the polylysine coated cover slip was put into the dish. The dish was centrifuged at 1500 RPM 4°C for 5 min. Once the cells attached to the slip, the standard protocol for slides preparation could be followed.**

Unlike ATM-pS1981 and Chk2-pT68, discrete ATR foci, or Chk1-pS345 foci, could not be detected up to 3 h after IR in A549 cells. Although we could not find discrete ATR foci in our experiments with the staining protocols employed, some papers indeed demonstrated that ATR foci can form 4-6 h after IR (16,173,174). Since ATR is nearly constitutively present in the cell in the form of an heterodimer with ATRIP (175), ATRIP foci formation was used as a substitution to study ATR localization in the nucleus after IR.

As the results in Figure 21 indicate, ATRIP foci formation is a relatively slow process, when compared to ATM-pS1981 and γ-H2AX foci formation, and discrete foci are visible only about 1 h after IR. The number of ATRIP foci reaches a maximum 3-6 h after IR. Furthermore, ATRIP foci are found nearly exclusively in cyclin B1 positive cells, which corresponds to late S or G2-phase cells.

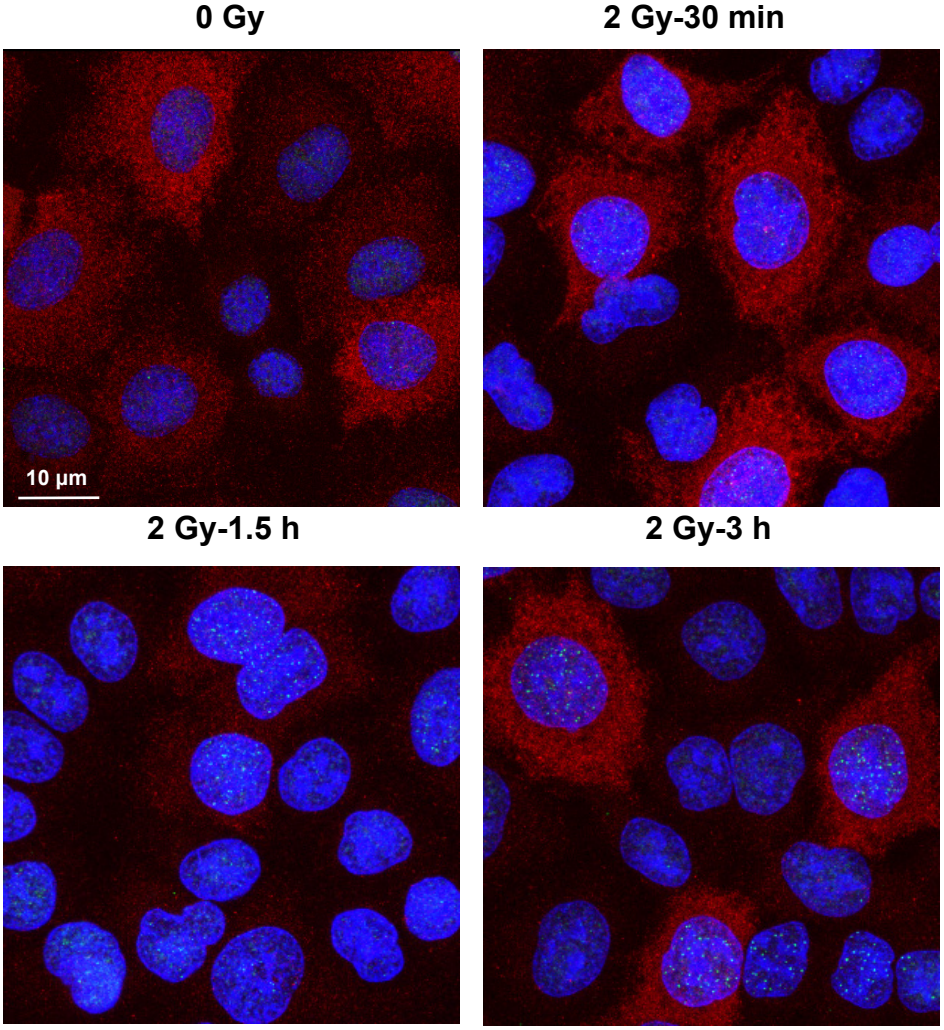

Figure 21. ATRIP foci in irradiated A549 cells. Exponentially growing A549 cells were irradiated at 2 Gy. After desired time, cells were fixed, permeabilized and co-immunostained with anti ATRIP and cyclin B1 antibodies. Green: ATRIP; Red: Cyclin B1; Blue: DAPI. (bar = 10 µm).

4.2.3 Distinct differences in the kinetics of ATM-pS1981, Chk2-pT68, and ATRIP foci formation

ATM and ATR both play central roles in IR induced G2 arrest as we described in the previous section. To compare the kinetics of G2 checkpoint activation with those of foci formation, we scored in A549 cells ATM-pS1981, Chk2-pT68 and ATRIP foci at different times after exposure to 2 Gy IR. The results are summarized in Figure 22. In agreement with results shown above, ATM-pS1981 foci formation after IR and remain rather stable in numbers for about 1 h (Figure 22A). After reaching this maximum, foci numbers start decaying with a half time of about 4 h. The foci number drops to the background level 12 h after IR. Chk2-pT68 foci form as rapidly as those of ATM-pS1981 but decay much sooner and no foci are detectable 4 h after IR (Figure 22B). In contrast to the fast kinetics of ATM-pS1981 and Chk2-pT68 foci formation, ATRIP foci form slower. As the results in Figure 22C indicate, foci formation reaches a maximum at about 1 h and remains constant for about 2 h.

Although ATR plays a dominant role in G2 checkpoint signaling, its activation for G2 arrest may not coincide with foci formation since visible foci form relatively late (1 h after IR). Such a time frame is too slow for checkpoint activation. Instead of foci formation, ATR may regulate G2 arrest in a different manner that remains to be elucidated. A possible expiation to this fact is that ATR-Chk1 pathway dominates G2 checkpoint after ATM-Chk2 pathway is fully activated. Together these results suggest a cooperation between ATM and ATR for the development and the maintenance of the G2 checkpoint that is in line with the cross-talk between the two kinases reviewed in the Introduction. Since ATM remains active for a long duration even after ATR is fully activated, it might still exert in regulating G2 checkpoint. We hypothesized that their existed a connection between the persistency of ATM-pS1981 foci and G2 checkpoint maintain.

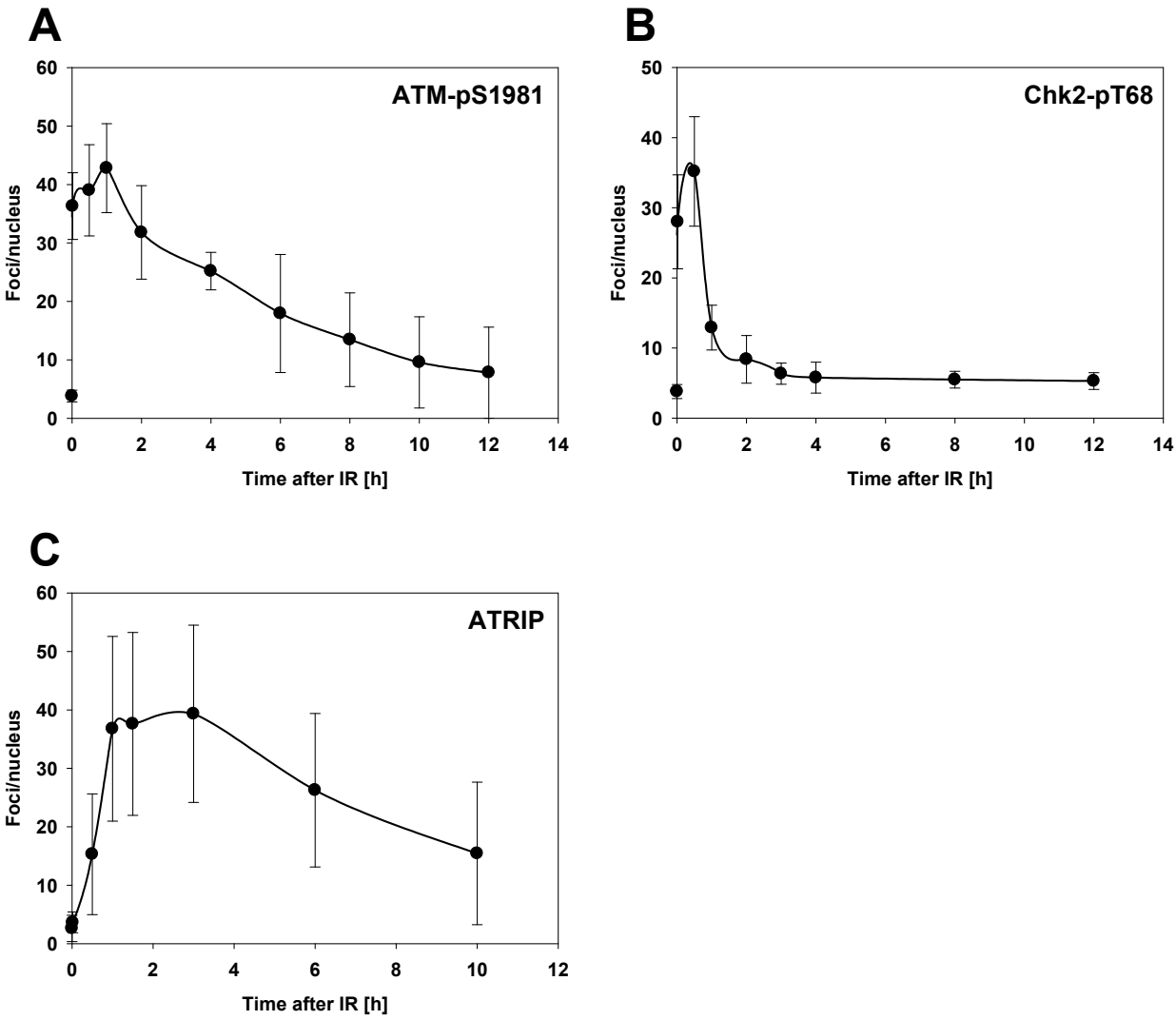

Figure 22. ATM-pS1981, Chk2-pT68 and ATRIP foci kinetics in irradiated A549 cells. Exponentially growing A549 cells were exposed to 2 Gy IR. At each time point, cells were collected, fixed, permeabilized and immunostained with anti ATM-pS1981, Chk2-pT68 or ATRIP antibodies, respectively. Foci numbers were scored. The mean foci number in each nucleus was calculated and plotted as a function of time. **(A),** ATM-pS1981 foci kinetics; **(B),** Chk2-pT68 foci kinetics; **(C),** ATRIP foci kinetics. The results are from 3 repeated experiments. Error bar stands for standard deviation.

4.2.4 ATM-pS1981 foci numbers are IR-dose and cell-cycle-phase dependent

As shown in Figure 23 a linear increase in ATM-pS1981 foci is found in A549 cells after exposure to different IR doses (0-4 Gy) in the exponential phase of growth. A similar pattern is also found when scoring γ-H2AX foci (143). Three categories of nuclei can be identified based on the number of foci scored in these experiments: nuclei with low numbers of foci, nuclei with large numbers of foci, and nuclei whose foci numbers are between these two extremes. Careful quantitative analysis hints that this variation might reflect differences in DNA content for cells irradiated in the

various phases of the cell cycle. Thus, the same radiation dose should generate twice the number of foci in a G2 as compared to a G1 cell, while S cells should lie in between.

To test this hypothesis, we scored ATM-pS1981 foci in synchronized G1 cells obtained by serum deprivation. Under these conditions, 1 Gy IR generates about 24-27 foci in G1- phase cells (Figure 23). This number is similar to that obtained for γ-H2AX foci (135). The dose response curves can not be extended above 4 Gy because above 100 foci per nucleus foci overlap causes an underestimation in the numbers of foci scored.

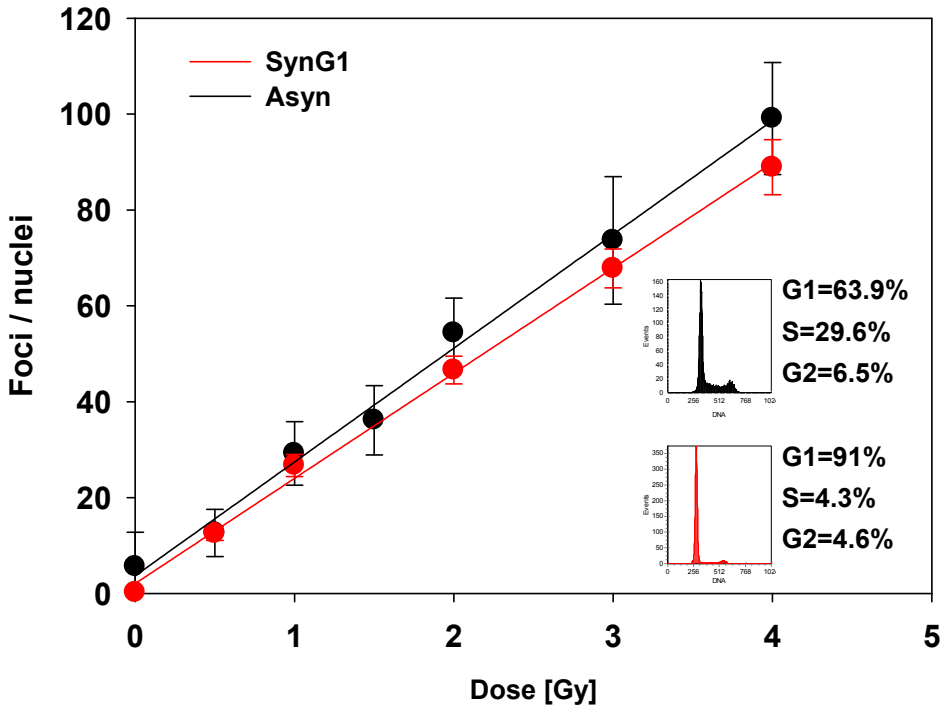

Figure 23. ATM-pS1981 foci dose response in A549 cells. Cells were exposed to IR, either in exponential phase of growing or synchronized at G1 by serum deprivation. After 1 h, cells were harvested, fixed, permeabilized and immunostained with anti ATM-pS1981 antibody. ATM-pS1981 foci numbers were scored. The mean foci number per nucleus is plotted as a function of dose. Inserted histogram together with cell cycle analysis is to show the cell cycle distributions before IR. The results are from 3 repeated experiments. Error bar stands for standard deviation.

The global G2 arrest is observed when exponentially growing cells are exposed to IR. Cells irradiated in G1, S and G2-phase may all progress through the cell cycle until they reach a specific checkpoint in G2. Therefore, for a complete analysis of the G2 checkpoint, it is necessary to consider the origin of cells eventually arrested in G2. Furthermore, when exploring the connection between foci kinetics and G2 arrest, it is

particular important to clearly discriminate between cells irradiated in the different phases of the cell cycle. This is not only because the mechanism underlying G2 arrest may be different, but also because the initial foci numbers will be different by as much as a factor of two.

4.2.5 ATM-pS1981 kinetics in irradiated G1 cells

For exponentially growing A549 cells, enriched populations of G1 cells was obtained by using serum deprivation, or by applying centrifugal elutriation to select highly enriched G1 fractions. The results in Figure 24 demonstrate that both methods can be successfully used to obtain highly enriched G1 populations of cells. However, since the elutriated cells contain actively growing G1 cells, whereas G1 cells in a serum deprived culture are in a quasi resting (G0) phase, it is not clear whether the results with these two different methods will be equivalent.

This question was tested and the results shown in Figure 24. Immediately after 2 Gy IR, the ATM-pS1981 foci number rapidly increases and reaches a maximum within 30-60 min. After this maximum, foci decay and their numbers reach background levels 6 h post IR. Similar results are obtained with elutriated-G1 populations and serum-deprived-G1 cells, which suggest that the state of growth has no influence on this cellular response. Moreover, a sophisticated staining was used to select G1 cells for analysis by excluding cyclin B1 positive cells (G2) and EdU positive cells (S) from the exponentially growing populations (explain later). It provides similar results as in synchronized G1 cells. Based on these results, we speculated that the evidence suggests ATM-pS1981 foci in G1-phase controlling the G2 arrest was very weak, since the foci decreased to the basal level before the cell moving into G2.

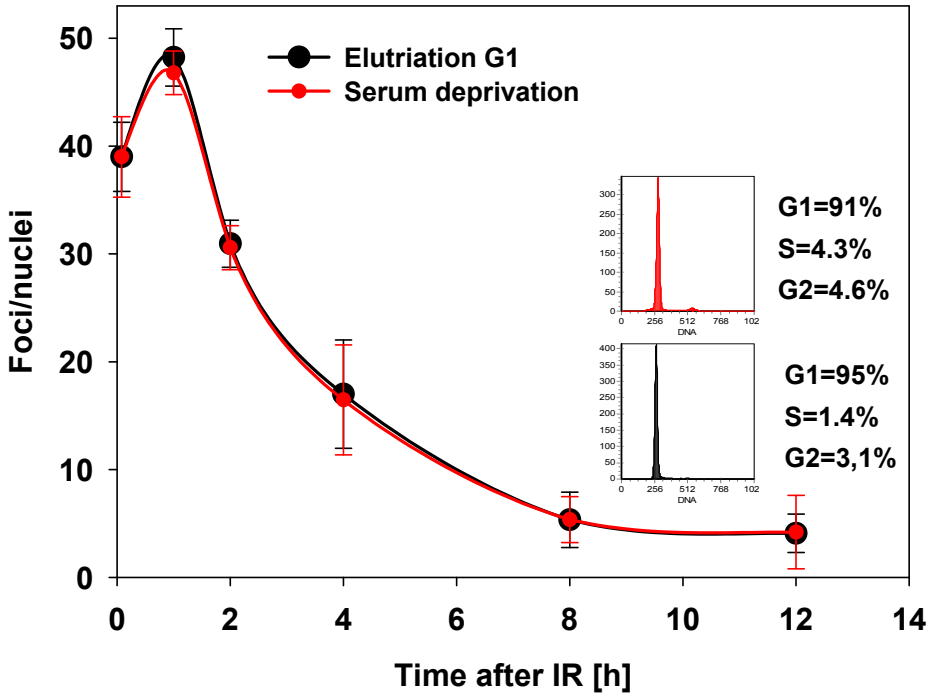

Figure 24. ATM-pS1981 foci kinetics in irradiated G1 cells. Exponentially growing A549 cells were synchronized at G1 phase either by serum deprivation or elutriation. The synchronies were examined by flow cytometry. Cells were exposed to 2 Gy IR and returned to the incubator. At the desired time, the cells were fixed, permeabilized and staining with anti ATM-pS1981 antibody. Foci numbers were scored and plotted against time. Inserted histograms indicate the cell cycle distributions before IR. The results are from 3 repeated experiments. Error bar stands for standard deviation.

4.2.6 ATM-pS1981 kinetics in irradiated G2 cells

Populations enriched in G2 cells were obtained by centrifugal elutriation from exponentially growing A549 cells. The G2 fraction was further confirmed by cyclin B1 staining. The results in Figure 25 indicate that the percent of cyclin B1 positive cells increases slightly after irradiation and then decreases at later times as cells accumulate at metaphase due to the presence of nocodazole in the medium (176). Indeed the mitotic index increases after about 2 h and reached over 50% by 8 h. The time point when the mitotic index starts increasing and the fraction cyclin B1 positive cells starts decreasing can be taken as a measure of the G2-phase and is about 2-3 h in this experiment. Follow up of ATM-pS1981 foci within these constraints provides information on the response of G2 cells. As expected, the number of ATM-pS1981 foci peaked at about 1 h after IR and then started decaying quickly. At early times (30-60 min), the number of foci is evenly distributed among nuclei and the observed range is between 80 and 100. However, the number of foci per nucleus shows a considerably larger spread after longer incubation times. Notably, the distribution of foci number in the nuclei is not continuous and nuclei with less than 20 foci are rarely

found at 4-8 h after IR, in Figure 25C. Co observation of a dramatic increase of mitotic index at these times suggests that cells have overcome G2 checkpoint and progressed into mitosis.

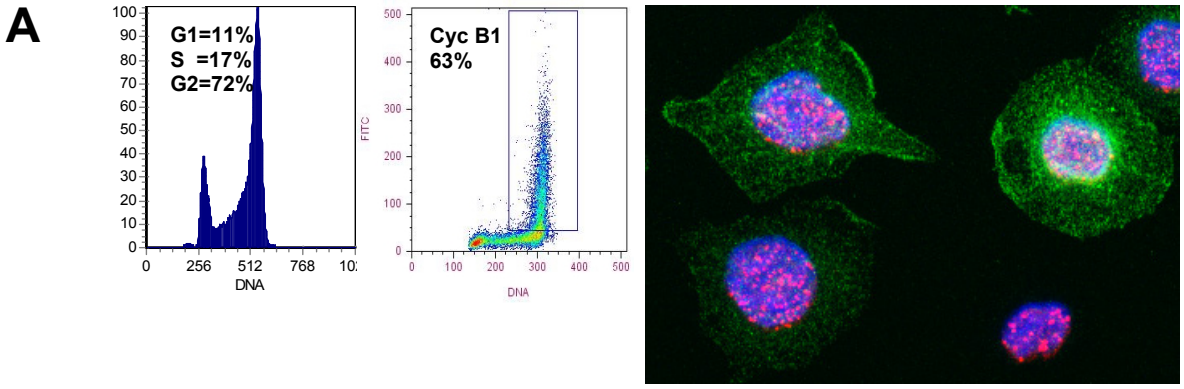

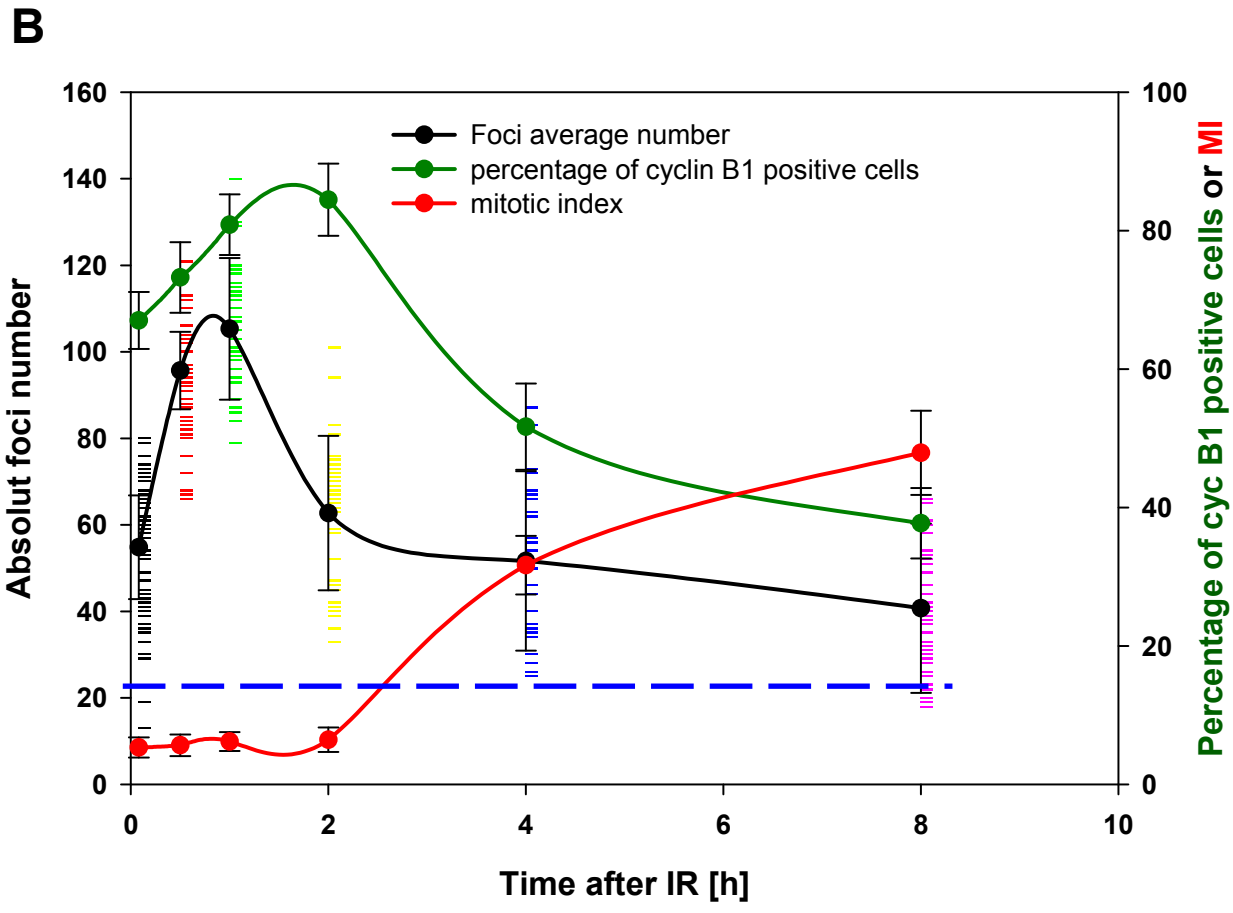

C

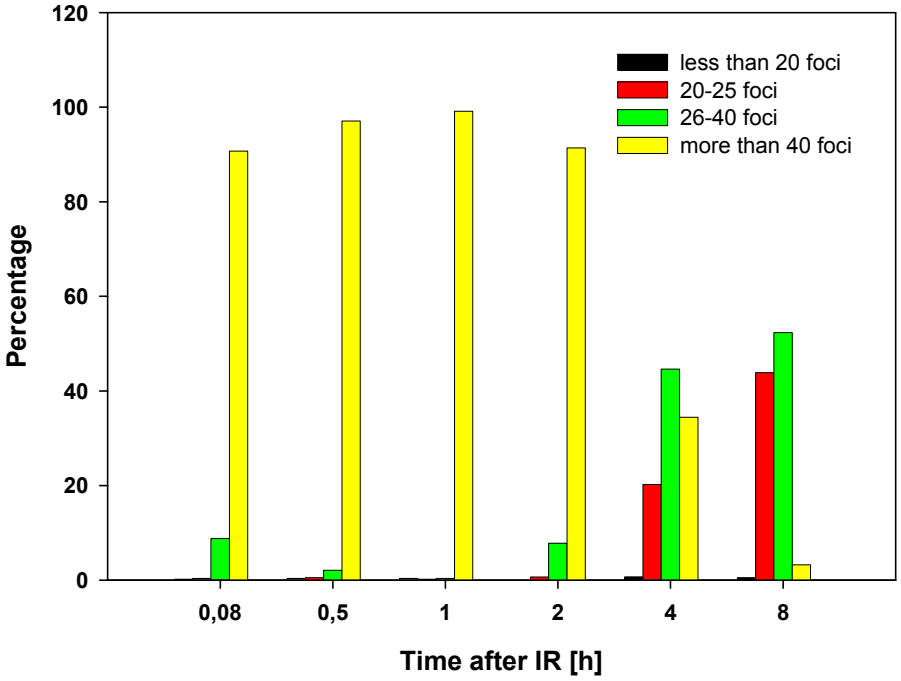

D

Dose	Time	< 20 foci	20-25 foci	25-40 foci	>40 foci	Total cell scored
2 Gy	0.08 h	1	2	51	527	581
2 Gy	0.5 h	2	3	12	557	574
2 Gy	1 h	2	1	2	556	561
2 Gy	2 h	1	4	47	551	603
2 Gy	4 h	4	117	258	199	578
2 Gy	8 h	3	243	290	18	554

Figure 25. ATM-pS1981 foci kinetics in irradiated G2-phase cells. G2 populations were enriched by centrifugal elutriation from exponentially growing A549 cultures and plated on polylysine coated cover slips in the presence of nocodazole (0.04 µg/ml). After 30 min, cells were exposed to 2 Gy IR, and returned to 37 ºC for different periods of time. After desired time, cells were fixed, permeabilized and co-immunostained with anti ATM-pS1981and cyclin B1 antibodies. ATM-pS1981 foci numbers in cyclin B1 positive cells were scored. Cyclin B1 positive fractions were calculated. The MI was measured based on the mitotic morphology. At least 500 nuclei were scored. The distributions of foci number as well as the mean foci numbers per nucleus are plotted as a function of time. MI and cyclin B1 positive fractions are also plotted against time. **(A),** Cell cycle distribution and cyclin B1 expression of the elutriated populations used in this experiment. ATM-pS1981 foci formation and cyclin B1 expression 30 min after IR (blue DAPI, Red: ATM-pS1981 and Green: cyclin B1). **(B),** Left axis: the ATM-pS1981 foci kinetics. The absolute foci number in each nucleus is shown, as well as mean foci numbers per nucleus. Right axis: cyclin B1 positive fractions and MI variations. A hypothesised threshold (foci number = 20) is drawn in blue. **(C),** The summary of foci frequency at each time point. **(D),** A detailed table about the foci frequency at each time point. **Unirradiated cells show less than 5 foci per nucleus, which are not shown here.** The results are from 3 repeated experiments. Error bar stands for standard deviation.

4.2.7 Threshold to fully maintain G2 checkpoint

On the basis of the above results we hypothesized that cyclin B1 positive cells could "ignore" 20 ATM-pS1981 foci that presumably signal to activate the checkpoint and progress to mitosis. This is compatible with requiring 20-foci either to activate or to maintain the G2 checkpoint. We previously showed that 1 Gy generates 24-27 ATM-pS1981 foci in G1 cells and 50-55 foci in the G2 cells. Thus, 20 foci in cyclin B1 positive cells are correspond to about 0.5 Gy. Hence 0.5 Gy might be a threshold radiation dose required to fully activate and then maintain the G2 checkpoint. To test this hypothesis, exponentially growing A549 cells were exposed to low radiation doses and the MI was measured by H3-pS10 staining as a function of time. The results are summarized in Figure 26. It is evident that 0.5 Gy causes a complete stop in cell progression into mitosis, which is in line with the full activation of the G2 checkpoint. This result supports therefore our threshold hypothesis. Even a dose of 0.1 and 0.2 Gy generates a clearly measurable inhibition of MI demonstrating activation of the G2 checkpoint after the induction of an estimated 5 and 10 foci per cell, respectively. In all cases examined the mitotic index recovered in a radiation dose dependent manner. For example after 2 Gy IR, which is the dosage used to study the ATM-pS1981 kinetics, the transition from G2 to M is blocked for about 4 h. After this time, MI recovers (Figure 26B), which is in line with the finding shown in Figure 25.

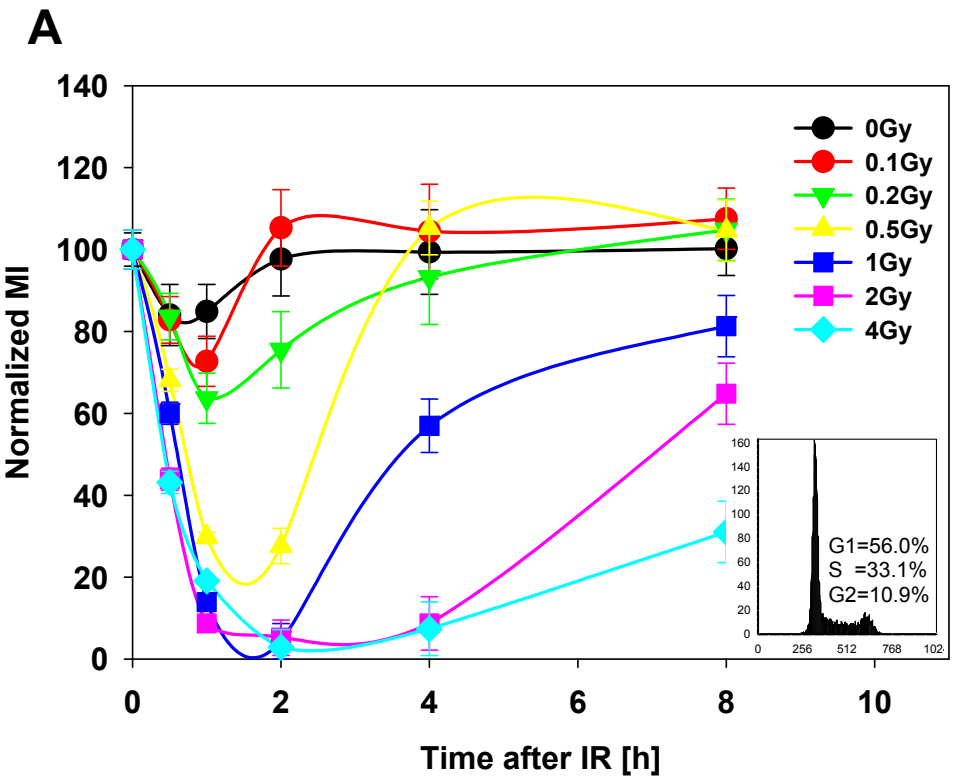

B

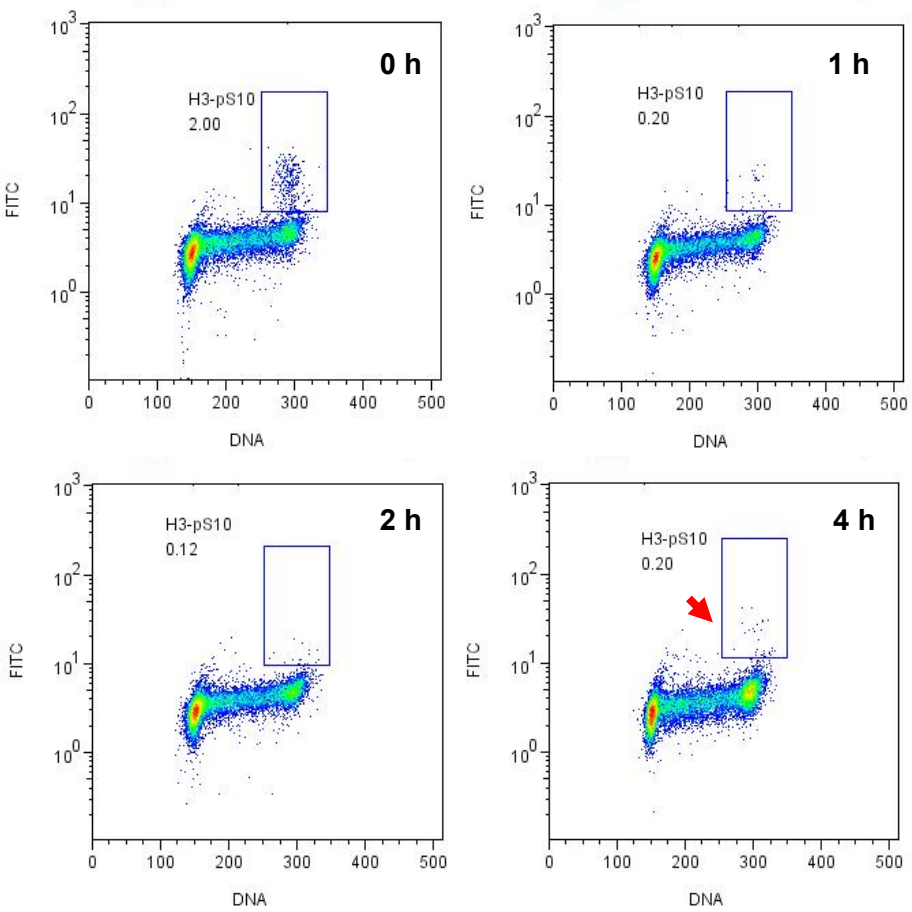

Figure 26. Mitotic index dose response in A549 cells. Exponentially growing A549 cells were exposed to different dose of IR. Samples were taken at each desired time point. Cells were fixed, permeabilized and stained with anti H3-pS10 antibody and PI. MI was measured by flow cytometry. MI is normalized by dividing against the MI from untreated samples. Normalized MI is plotted as a function of time. MI variation after 2 Gy IR is selected to show. **(A),** MI as a function of time after exposing to different IR dose Histogram indicates the cell cycle distributions before IR. **(B)** MI variation measured bivariate FACS after 2 Gy IR. The red arrow shows that some mitotic populations re-appear 4 h after IR, which indicates that some cells are released from G2 checkpoint.

4.2.8 ATM-pS1981 foci kinetics in S-phase cells

Unlike G1 and G2 cells that have a uniform DNA content, cells in S-phase have a variable DNA content depending upon how far they have advanced in replicating their DNA. Centrifugal elutriation does not allow the selection of cell populations with a narrow DNA distribution within the S-phase of the cell cycle. Typically, S-phase populations obtained by centrifugal elutriation show a wide distribution in the S-phase component and contain variable amounts of G1 and G2 phase cells. Because the number of radiation induced foci is proportional to the DNA content, S-phase cells show a wide span in the number of foci scored ranging from the number measured in G1 cells to the number measured in G2 cells. Under such circumstance, studying the

foci kinetics in S cells based on mean foci number is not meaningful. Therefore, in the analysis of the results obtained with S-phase cells, absolute foci distributions at each time point were used.

As pointed out above, BrdU pulse labeling allows identifying S-phase cells. Unfortunately, immunofluorescence detection of BrdU requires harsh treatments to denature DNA and expose BrdU to the antibody. Such treatments damage the structural integrity of the cell and seriously compromise the detection of foci formed by proteins involved in the cellular response to DNA damage. To accommodate detection of this analog with the antibody staining required in our experiments to detect radiation-induced foci, we adopted a recent modification based on the replacement for BrdU with 5-ethynyl-2′-deoxyuridine (EdU, another analog of thymidine), which can be detected under milder conditions. Under such conditions, the foci formation of proteins involved in the DNA damage response will not be dramatically altered (177).

The EdU pulse labeling protocol allows the unequivocal identification of S-phase cells. Together with the utilization of cyclin B1 staining and taking advantage of the distinct mitotic morphology, allows the identification of cells in all four phases of the cell cycle in an exponentially growing population. For instance, G1 cells lack any staining and S-phase cells have clear EdU staining; G2 cells on the other hand are cyclin B1 positive but EdU negative and do not show the typical mitotic morphology.

With the help of this sophisticated staining protocol we analyzed ATM-pS1981 foci formation throughout the cell cycle in an exponentially growing culture of A549 cells exposed to 2 Gy and analyzed 1 h later. The results obtained are summarized in Figure 27.

The similarity between foci distribution and the distribution of cells in the different phases of the cell cycle confirms previous results and provides a validation of the approach adopted here. Indeed, the foci number in G2 nuclei (cycin B1) is twice as high as the foci number in G1 nuclei, while the number of foci in S-phase cells lies between that of G1 and G2 cells.

A

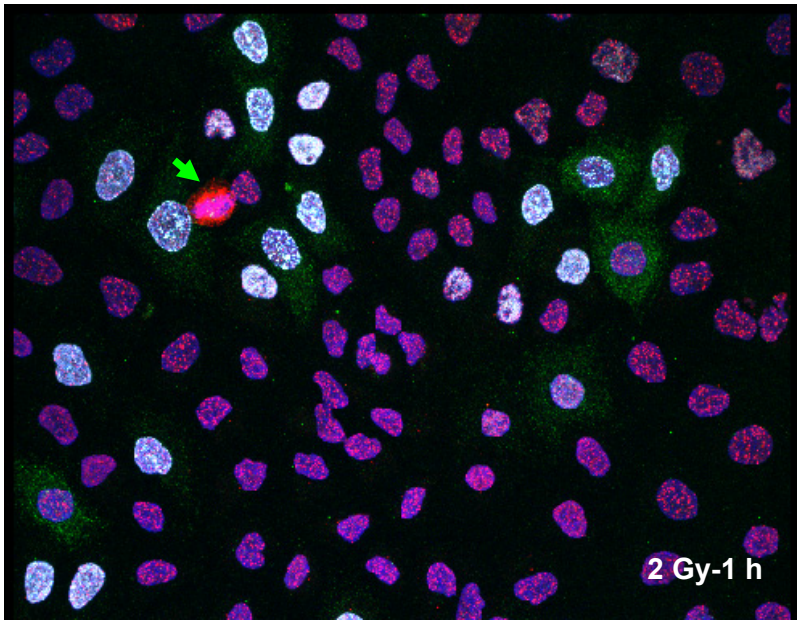

B

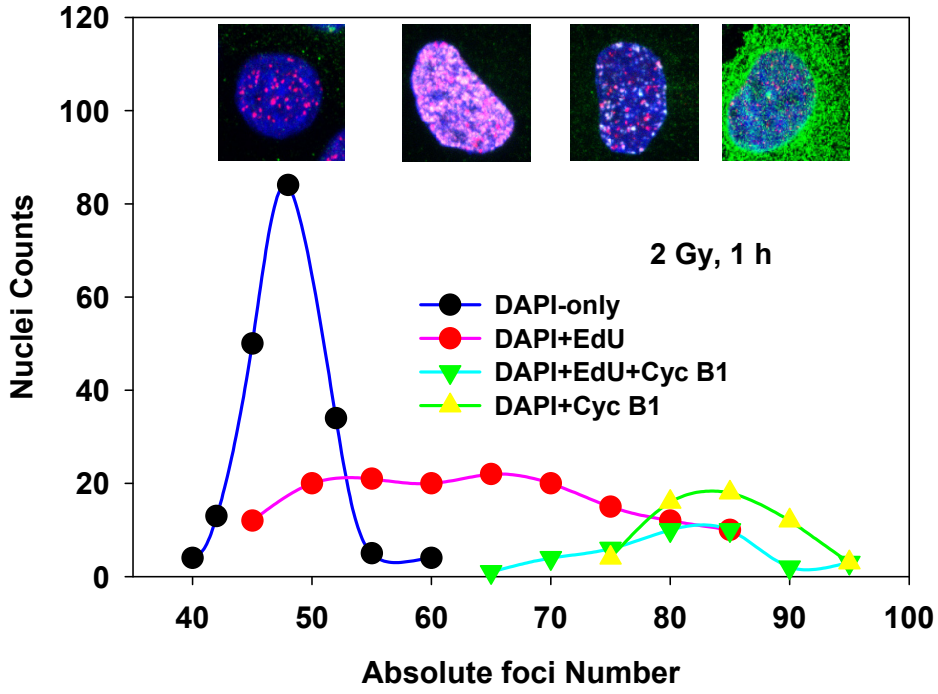

C

	Staining pattern	Nuclei counts	Percentage	Cell cycle stage
	DAPI only	1064	48,85%	G1
	DAPI+EDU	655	30,07%	S
	DAPI+EDU+Cyc B1	273	12,53%	late S
	DAPI+Cyc B1	185	8,49%	G2
	Mitotic	1	0,05%	mitosis
	Total	2178		

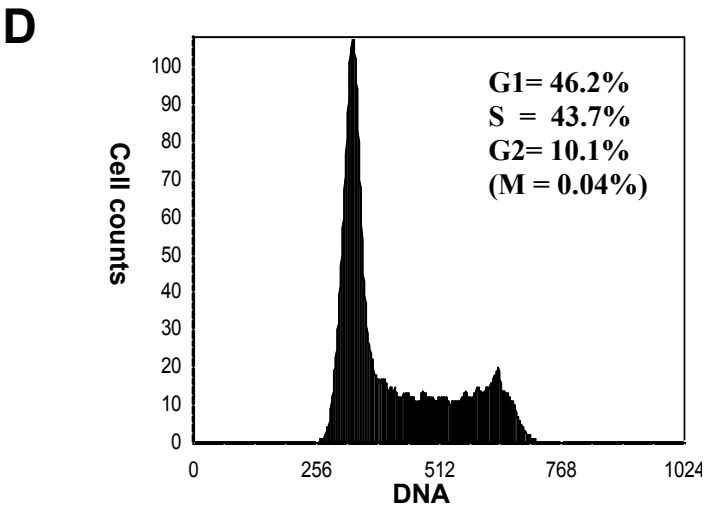

Figure 27 ATM-pS1981 foci through the cell cycle distribution. Exponentially growing A549 cells were pulsed labeled with EdU for 30 min, and exposed to 2 Gy IR followed by a fresh media change. After 1 h incubation, cells were fixed and co-immunostained with anti ATM-pS1981, cyclin B1 antibodies as well as EdU detection solution. ATM-pS1981 foci numbers in each nucleus were scored. Three experiments were carried and total of about 2000 nucleus were scored for foci. The nuclei were grouped according to their staining patterns as shown on top of the figure. The numbers of nuclei with the same foci numbers were calculated. Nuclei counts are plotted as a function of foci number. **(A),** Typical view of ATM-pS1981, cyclin B1 and EdU co-staining. Mitotic cells are distinguished by their unique morphology, as indicted by an arrow. Color scheme: Red, ATM-pS1981; Green, cyclin B1; Cyan, EdU; Blue, DAPI. ATM-pS1981 foci are observed in every nucleus, except for mitotic nuclei. **(B),** ATM-pS1981 foci numbers per nucleus show a large spread depending on the cell cycle phase when the cells were irradiated. An increase of foci number is found with the increasing of DNA contents. **(C),** The fractions of cells with unique staining pattern. **(D),** The cell cycle of the cell analyzed in this experiment. The MI was obtained from the previous experiments.

The ATM-pS1981 foci kinetics in G1-phase cells are , which refers the cells only have DAPI signals, are found comparable to those measured using synchronized G1 cells (see Figure 24). In G2-phase cells (cyclin B1 positive but without EdU signal), no nuclei with less than 20-foci are found (data not shown). Furthermore, the EdU signal migration indicated the transition of S-phase cells into subsequent phases of the cell cycle. EdU-cyclin B1 co-staining indicates the progression of S-phase cells into G2-phase, while EdU staining at mitosis indicates the progression of an S-phase cell at the time of irradiation into mitosis, Figure 28A.

An estimate of cell cycle progression can be obtained by dividing the EdU-cyclin B1 fraction by the total cyclin B1 fraction. In this way a measure of the fraction of G2 cells originating from the S-phase can be obtained, Figure 28B. A similar calculation can also provide the fraction of cells that moved from the S-phase into mitosis. In this case, the fraction of EdU-stained mitotic cells is divided by the total fraction of mitotic cells, Figure 28C.

When analyzing the absolute number of foci in EdU positive cells, ie. in cells irradiated in S-phase independently of their location in the cycle at the time of analysis, we observed a peak within 30-60 min after IR, Figure 28D. This is similar to the observations made in G1 and G2 cells. However, these foci persist for longer times than foci in G1 and G2 even when cells undergo transition into G2. This indicates that during S-phase cells retain signaling activity, possibly waiting for entry into G2 to complete repair by HRR. There is a reduction in the number of foci after 2 h, which coincides with the progression of S-phase cells into G2 and which is in line with repair occurring in this phase of the cell cycle. As S-phase cells move into M after about 6 h the number of residual foci is above 20 in line with the results obtained with G2 cells.

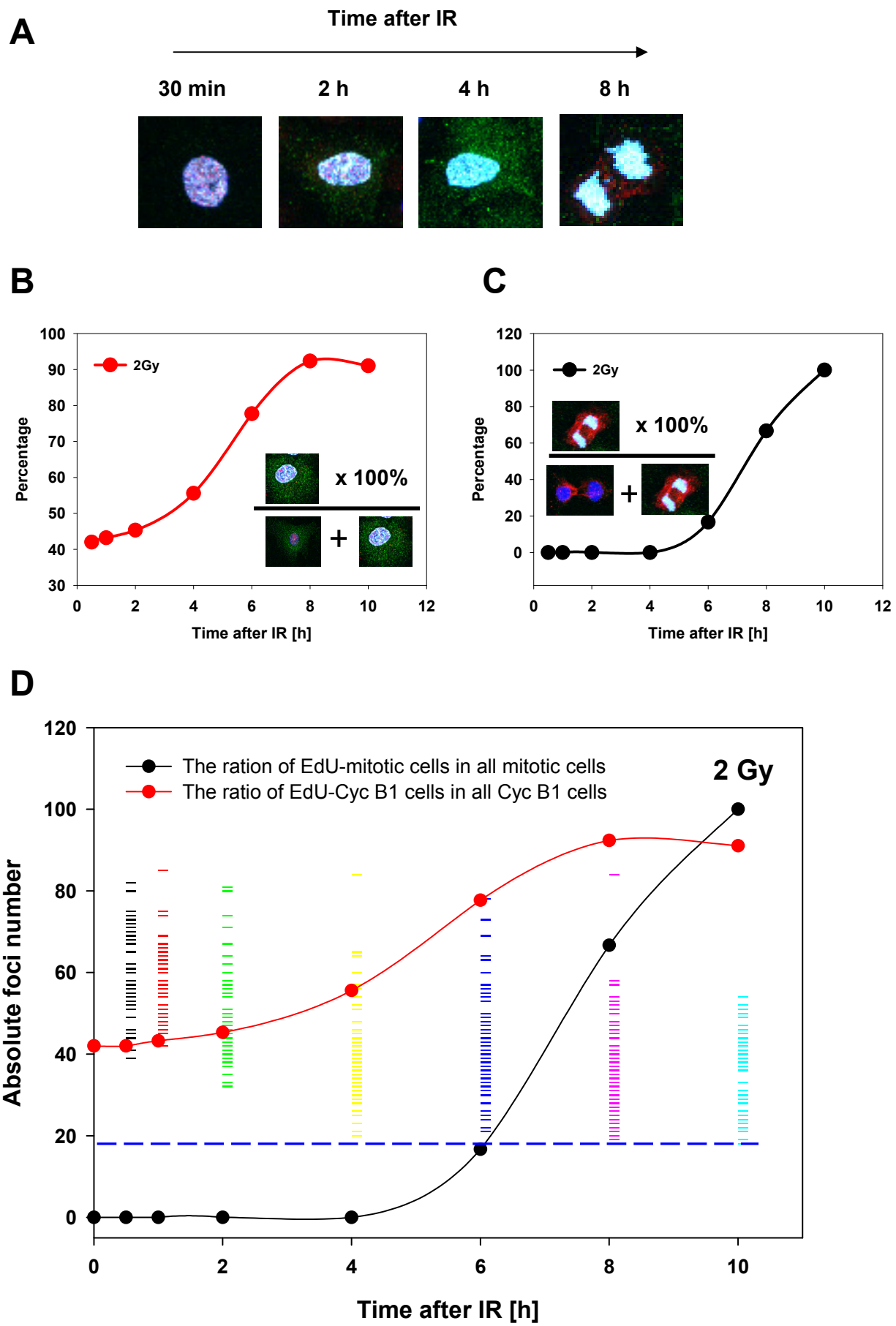
A
Time after IR
30 min
2 h
4 h
8 h
B
2Gy
x 100%
Percentage
Time after IR [h]
C
2Gy
x 100%
Percentage
Time after IR [h]
D
The ration of EdU-mitotic cells in all mitotic cells
The ratio of EdU-Cyc B1 cells in all Cyc B1 cells
2 Gy
Absolute foci number
Time after IR [h]

E

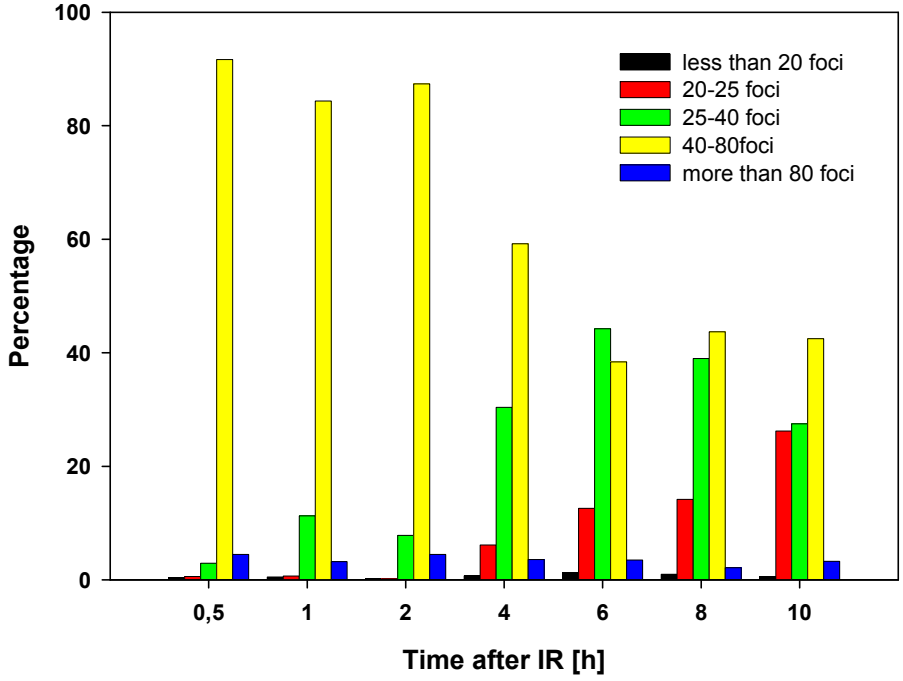

F

Dose	Time	< 18 foci	18-25 foci	25-40 foci	40-80 foci	>80 foci	Total scored
2Gy	0.5 h	2	3	15	472	23	515
2Gy	1 h	3	4	67	501	18	593
2Gy	2 h	1	11	49	546	28	635
2Gy	4 h	4	36	178	347	21	586
2Gy	6 h	7	69	242	210	19	547
2Gy	8 h	6	87	239	268	13	613
2Gy	10 h	3	145	152	235	18	553

G

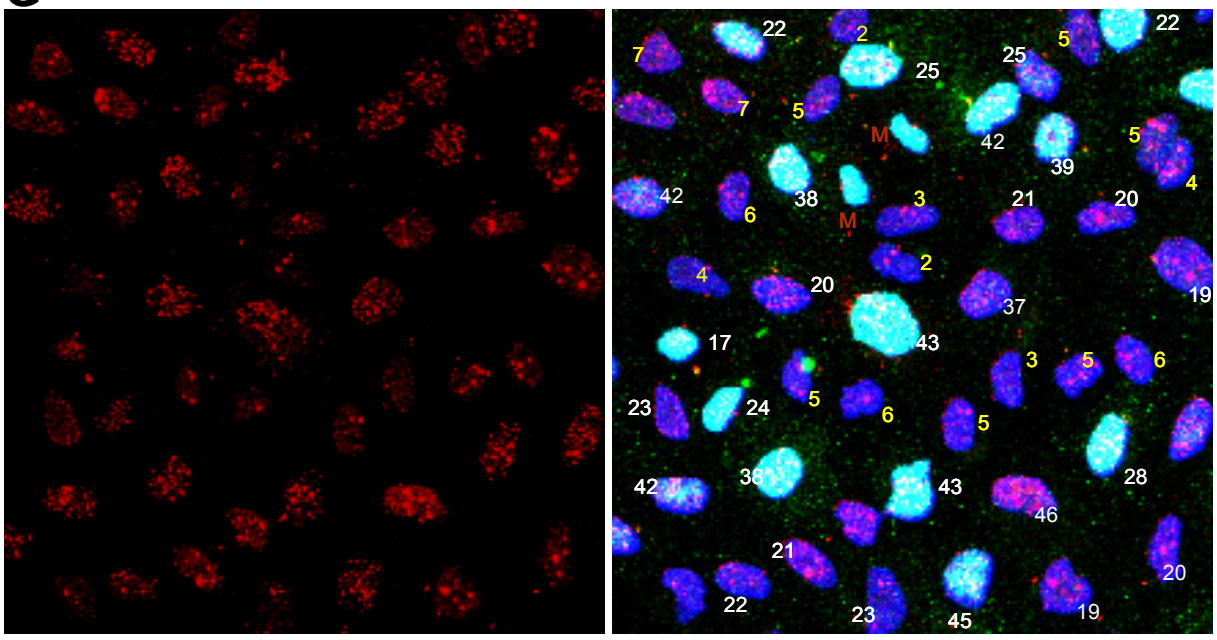

Figure 28. ATM-pS1981 foci kinetics in EdU positive cells. Exponentially growing A549 cells were pulsed labeled with EdU for 30 min, and exposed to 2 Gy IR followed by a fresh media change, as in Figure 27. Cells were returned to 37 ºC for different periods of time. Cells were collected, fixed, permeabilized and co-immunostained with anti ATM-pS1981, cyclin B1 antibodies as well as EdU detection solution. Color scheme: Red, ATM-pS1981; Green, cyclin B1; Cyan, EdU; Blue, DAPI. ATM-pS1981 foci numbers in EdU positive nuclei were enumerated. This experiment was repeated for three times and at least 500 nuclei were scored. **(A),**The transition of EdU positive cells in the cell cycle is monitored. **(B),** The transition of EdU positive cells into G2-phase is quantified according to the equation shown in the figure, and plotted as a function of time. **(C),** The transition of EdU positive cells into M-phase is quantified according to the equation shown in the figure, and plotted as a function of time. **(D),** The distributions of foci numbers in each nucleus are plotted as a function of time. A hypothesized threshold (foci number = 20) is drawn in blue. The transition of EdU positive cells into G2 and M are also incorporated. **(E),** Summary of foci distribution at each time points. **(F),** A detailed table about the foci frequency at each time point. Unirradiated cells show less than 3 foci per nucleus, which is not shown here. The results are from 3 repeated experiments. Error bar stands for standard deviation. **(G),** Foci residues of 8 hours after IR. (Yellow number: foci number in the nuclei only stained with DAPI; White number: foci number in EdU + DAPI positive cells).

5 Discussion

5.1 Are ATM and ATR working redundantly?

Although ATM and ATR belong to the same family of protein kinases, it is quite unlikely that they function redundantly in mammalian cells. Loss of ATR in the mouse causes lethality at the earliest embryonic stages, whereas humans lacking functional ATM can live for decades (93,178). These observations suggest that ATR is crucial for basic biological processes. Since ATR detects and responds primarily to ssDNA, implying that the formation of this primed ssDNA structure in unperturbed cell cycles is at the heart of the matter (18). One possibility is that ATR is activated at low levels in every cell cycle as a result of normal Okazaki-fragment dependent lagging-strand synthesis that leads to the transient formation of ssDNA. This activation might be required to enforce the order of S and M phase and to control origin timing (179). Mec1, the ATR homolog in yeast, has little to do with cell-cycle arrest or origin firing, but has fork-stabilization activity (96).

The second possibility is that there are numerous stalled replication forks in cells never exposed to DNA damaging agents, as a result of endogenous DNA damage or at DNA sequences that are difficult to replicate. So ATR might have a major role in handling these forms of DNA damage and the associated replication stress (18). Overexpression of ATRkd does not change the viability of non-irradiated GM847-ATRkd cells, while it significantly increases their radiosensitivity to killing (170). This suggests that second scenario might be true. In unperturbed mammalian cells, only a small portion of ATR might be required to handle the endogenous stress. If there was heavy loss of chromatin structure after exposure to IR, an increased activation of ATR may be required to mount a robust checkpoint response.

AT patients, whose ATM function is defect, are suffered from hypersensitivity to ionizing radiation and have disrupted cell cycle control, but can live for decades (77). Many syndromes have been reported with symptoms overlapping those of AT. For example, mutations in NBS1 and MRE11 give rise to Nijmegen breakage syndrome (NBS) and ataxia-telangiectasia-like disorder (ATLD), respectively (180,181). All syndromes are in line with a compromised proteins involved in ATM pathway (77). High frequency of alternations in the same pathway without compromising the viability of the organism may suggest the ATM is not as critical as ATR.

Our finding also suggests that ATM and ATR seem to play different roles instead of acting redundantly to sense IR induced DNA damage and activate the G2 checkpoint. Inhibition of the ATR-Chk1 pathway caused an abrogation of IR induced G2 arrest without affecting ATM-pS1981 foci formation. On the other hand, inhibition of ATM disrupts ATM-pS1981 foci formation but only affects the G2 checkpoint when cells are irradiated in specific phases of the cell cycle. The delayed G2 accumulation of irradiated AT5-BIVA cells occurs 3 h later than in ATM competent cells. This form of G2 arrest seems to be ATM-independent (172). Although strong G2 arrest is found in this case, some BrdU positive cells can escape the arrest and can migrate to the next cell cycle, Figure 12. These results suggest that the G2 arrest is only partially activated without ATM.

Overall the above results provide clear evidence for a master role of ATR-Chk1 in the checkpoint response and ATM-Chk2 exerts in maintaining the signal. Our recent data also support the view that ATR and ATM contribute to G2 checkpoint in different ways. Briefly, 30 min after irradiation, addition of caffeine elevates the decreased MI back to the normal level within 15 min; while supplying KU-55933 has no effect (data not shown). Because ATRIP and ATM-pS1981 foci have been well developed 30-60 min after IR, both pathways are believed fully activated, despite the fact that activation of the ATM pathway is faster than activation of ATR. These results suggest that ATR has to be continuously activated to enforce a G2 arrest; and that inhibition of ATM after ATM-pS1981 foci being formed does little in disrupting checkpoint response.

5.2 How is the spatial distribution of ATM controlling the G2 checkpoint?

ATM-pS1981 and γ-H2AX foci decrease as cell remove DSBs from their DNA. Such resetting of chromatin could in principle be done either by replacing γ-H2AX in the nucleosome with H2AX, or by dephosphorylating γ-H2AX directly at the nucleosome (144). The dephosphorylation seems more dominant in this case (182,183). The dephosphorylation of γ-H2AX and ATM-pS1981 are much less understood than phosphorylation. It has been shown that the removal of the phosphor group is tightly bound to DNA repair (182,184). PP2A (protein phosphatase 2A) has been documented as a player in removing γ-H2AX (182). PP2A deficient cells have been found suffered from inefficient DNA damage repair, hypersensitive to DNA damage. They also display a long duration of γ-H2AX foci persistence. These observations

suggest that a proper disassembling of the foci is as important as their assembling (182,183).

Phosphorylated protein aggregate to form foci might be a manner resisting improper dephosphorylation or disassociation, better than disperse protein. Compared with soluble form, protein foci have much smaller surface area, which limits the phosphates from accessing to them. So protein accumulated in concrete foci may be capable of maintaining signal transduction longer than disperse protein.

In response to DNA damages, a noticeable retention of ATM in the chromatin is observed, which is unaffected upon ATM inhibition though chemical inhibitors (121). Such retention of ATM might generate a “source” for G2 arrest signal transduction. Furthermore, analysis of the spatial distribution of Chk2 reveals that after phosphorylation by ATM and subsequent activation at the sites of DSBs, phosphorylated Chk2 is rapidly distributed to the undamaged parts of the nucleus to reach its physiological targets, which is allowing for a coordinated pan-nuclear response to local DNA damage (185). These results are in line with our findings that although the formation of Chk2-pT68 foci and their colocalization with ATM-pS1981 foci is a transient event (only observable 5-30 min after IR), the phosphorylation of Chk2 can be observed till 4 h after IR. On the other hand, our Western blots suggest that ATM-pS1981 can maintain its phosphor group much longer than Chk2-pT68. One possible explanation to this observation is that retention as a focus may prevent dephosphorylation as we suggested before. Hence, ATM-pS1981 spatial distribution as a focus at the site of a DSB might provide a platform for phosphorylation of Chk2, which then acts as a messenger to signal to downstream targets.

From another point of view, due to their limited surface area, protein foci may be less efficient in activating their substrates as compared to disperse proteins. Western blot suggests that the phosphor group can be maintained in ATM-pS1981 foci longer, up to 8 h. A relatively high number of ATM-pS1981 foci might provide enough surface area to phosphorylate Chk2 to maintain G2 checkpoint the signal transduction. Such response may also explain the dose response of MI variation after exposure to IR.

In vitro kinase assays suggest that 0.25 - 0.5 Gy is sufficient to activate ATM (141). In vivo, 0.5 Gy can efficiently induce ATM autophosphorylation at Ser1981, within 5 min after irradiation (78). Our findings suggest that although notable G2 arrest can be observed as low as 0.1 Gy IR, 0.5 Gy (20 foci) is the minimal dose to maintain/activate the “full scale” G2 checkpoint in irradiated G2-phase cells. Using γ-

H2AX as DSB index, cells with 20 γ-H2AX foci residue are found move freely into mitosis after irradiation (186). Hence, the spatial distribution of the 20 foci in a nucleus might ensure the minimal signal required to mount a complete G2 arrest; A larger number of foci (more than 20), corresponding to massive DNA damages, might help cells arrest in G2 for a longer period of time in order to signal serials events, such as HRR required to process the IR induced damages. Once the foci number drops to about 20, the phosphorylation level occurred on the total foci surface area is insufficient to maintain the G2 checkpoint signal cascade, thus releasing the cell from the block and allowing it to enter mitosis.

5.3 Are the ATM-pS1981 foci DSB markers?

γ-H2AX foci are widely used to evaluate IR induced DSBs, especially at low radiation doses (135,143). However, γ-H2AX foci formation is not IR specific (140). Other non-DSB-inducing agents such as MNNG (N-methyl-N'-nitro-N-nitrosoguanidine), adozelesin (187), UVC, UVB, HU (hydroxyurea), APC (aphidicolin) (187,188), hyperosmotic stress (189) and heat stress (190) have been reported can induce γ-H2AX foci. Spontaneous foci are also found in S-phase cells, probably due to the stalled replication forks during the replication (191). Although DSBs are not major products after these non-DSB-inducing treatments, there is no clear evidence that DSBs are absent at these γ-H2AX foci sites (187). As a result of this ambiguity, scoring γ-H2AX foci is still considered acceptable for analyzing induction and processing of DSBs. Since ATM-pS1981 foci colocalize with γ-H2AX, ATM-pS1981 can be an alternative in this kind of assay.

Even if γ-H2AX foci formation shows unequivocally the induction of DSBs, the reduction of γ-H2AX foci does not reflect the actual removal of the physical DSBs. When plateau-phase A549 cells are exposed to 1 Gy of X-rays, the full development of γ-H2AX foci requires 30 min and there is no reduction before 1 h. However PFGE shows an immediate reduction of the DSBs (induced by 20 Gy), proceeding with half times of 20 min and with at least 80% of the DSBs being rejoined after 1 h (144). Similar results to γ-H2AX were obtained by studying ATM-pS1981 kinetics in our experiments.

One possible explanation for the above discrepancy is that ATM-pS1981 or γ-H2AX foci, might not be appropriate markers for DSBs, but rather indicators of cellular metabolic activities initiated to facilitate and optimize DSB repair (144,192). In yeast,

the loss of γ-H2A foci (equivalent to γ-H2AX in higher eukaryotes) does not signify the removal of the discontinuity in the DNA (184). Therefore, it can be hypothesized that γ-H2AX or ATM-pS1981 foci continue marking the sites of some DSBs after processing and joining by NHEJ to facilitate additional processing, such as HRR (193,194).

If this hypothesis is true, it will be particularly significant for ATM-pS1981 foci. ATM might be a key regulator of checkpoint, but instead of key player for DSB repair, since AT cells have been disrupted checkpoint activation but without gross defect in DSB repair (195). The formation of ATM-pS1981 foci (activated ATM) indicates that all DSBs induced by IR actually signal for checkpoint. And the persistence of ATM-pS1981 foci indicates that the processing of DSBs is not completed even after they are rejoined by NHEJ; persistent foci may facilitate checkpoint maintaining or other events.

5.4 What is the role of persist ATM-pS1981 foci in G2 checkpoint?

ATM-pS1981 foci kinetics in G1 cells seems to be a relatively simple event. Foci distribution in each G1 nucleus is quite even, and 6 h after irradiation only background level of foci is observed. At this time, the cells are still in G1 or in S-phase.

The relationship between ATM activation and G2 arrest in cells irradiated during S-phase seems to be a quite complex event. Since the S-phase cells have DNA content between that of G1 and G2 cells, the most straightforward model is to hypothesize that the ATM-pS1981 kinetics will be categorized as G1-like and G2-like. A 20-focus threshold is found in G2-like subpopulations in S-phase cells. There are no subpopulations in S-phase cells that share the fast ATM-pS1981 kinetics of G1 cells. Another subpopulation of cells in the irradiated S-phase can maintain their foci and arrest in G2 for at least 6-8 h. Since these cells maintain 40-50 foci, it is quite likely they were irradiated in early S-phase. Furthermore 6-8 h maintenance of foci correlates well with the time frame required for maximal formation of Rad51 foci (our unpublished data), and for maximal interaction between ATR and ATRIP. Thus, a possible linkage between ATM/ATR activation and homologous recombination repair (HRR) is suggested.

5.5 A possible model is raised.

Our results indicate that ATR is always involved in the maintenance of the G2 checkpoint but can not come to the fore when cells are irradiated close to mitosis and ATM is not active. This result is in line with a linear transition of the G2 checkpoint responsibility from ATM to ATR: The lesion is first detected by DNA-PKcs and processed in such a way that it can be handed over to ATM. ATM in turn process further and hands it over to ATR after it has made it appropriate for HRR. All of these results allow us generating a hypothesized sequential model DNA-PKcs-ATM-ATR-HRR in the processing of DSBs and as a consequence in the modulation of the cell cycle progression through the activation of checkpoints.

Based on this model, in response to 2 Gy IR, DSBs (about 100-110) are registered by DNA-PKcs and ATM. ATM-pS1981 initiates the G2 checkpoint within less than 5 min, and maintain the signal transduction at least 4 h. About 30 ATRIP foci are observed 3 h later indicates that ATR machinery has been recruited. By referring the initial ATM-pS1981 foci number, one can speculate that 25-30 % of the DSBs are handed over from ATM to ATR. At this time, about 10-15 Rad51 foci (Dr. Christian Staudt, unpublished data) are also observed that hints a potential direction to HRR.

6 Conclusions

ATM-Chk2 and ATR-Chk1 pathways both contribute in maintaining proper G2 arrest after IR. ATR signaling plays a dominant role in the development of a full scale G2 arrest, while ATM signaling helps in the maintenance of a full scale G2 arrest.

In response to IR, ATRIP and phosphorylated ATM at serine 1981 can form foci. Although ATR plays a dominant role in G2 checkpoint signaling, its activation for G2 arrest may not coincide with foci formation since visible foci form relatively late (1 h after IR). The contribution of ATM-pS1981 foci to G2 arrest is strongly dependent on the cell cycle phase in which the cell was irradiated. There exists an apparent requirement for about 20 foci for the maintenance of the G2 arrest for cells irradiated in G2-phase. There is no apparent correlation between ATM-pS1981 foci and G2 arrest for cells irradiated in the G1-phase, as in this case foci disappear relatively quickly. Cells irradiated throughout S-phase, show a response similar to that observed with G2 cells and not, as one would expect, a mixed response reflecting subpopulations responding like G1 and subpopulations responding like G2 cells.

7 Abbreviations

9-1-1 complex	Rad9, Rad1 and Hus1complex
APC	aphidicolin
AT	Ataxia-telangiectasia
ATM	Ataxia-telangiectasia mutated
ATM-pS1981	phosphoryaltion of ATM at Serine 1981
ATR	ATM and Rad3-related
ATRIP	ATR interaction protein
ATRkd	ATR kinase dead
ATRwt	ATR wild type
BCA	bicinchoninic acid
BrdU	5-bromo-2´-deoxyuridine
BSA	Bovin serum albumin
Chk2-pT68	Phosphorylation of Chk2 at Threonine 68
Cyc B1	Cyclin B1
DAPI	4'-6-Diamidino-2-phenylindole
ddH2O	Double distilled water
DMEM	Dulbecco's Modified Eagle Medium
DMSO	Dimethyl sulfoxide
DNA-PKcs	DNA-dependent protein kinase catalytic subunit
DSB	DNA double strand break
ECL	Enhanced chemiluminescence
EDTA	Ethylenediaminetetraacetic acid
EdU	5-ethynyl-2′-deoxyuridine
FACS	Fluorescence Activated Cell Sorting
FAT	FRAP,ATM,TRRAP
FATC	FAT C-terminal
FBS	Fetal Bovin Serum
FITC	Fluorescein isothiocyanate
FS	Forward scatter
Gy	gray
H3-pS10	phosphoryaltion of Histone H3 at Serine 10

HEAT	Huntingin, elongation factor 3 (EF3), protein phosphotase 2A (PP2A), TOR1
HRP	Horseradish peroxidase
HRR	Homologous recombination repair
HSFM	Hybridoma serum free media
HST	Histrograme
HU	Hydroxyurea
IR	Ionizing radiation
KU-55933	KUDOS55933 (2-morpholin-4-yl-6-thianthren -1-yl-pyran-4-one)
LIF	Leica image format
McAb	Monoclonal antibody
MI	Mitotic index
MNNG	N-methyl-N'-nitro-N-nitrosoguanidine
MPF	Mitosis promotion factor
MQ	Milli-Q
MRN	Mre11, Rad50 and Nbs1 complex
MW	Molecular weight
NBS	Nijmegen breakage syndrome
NHEJ	Nonhomologous end-joining
NLS	Nuclear Localizatin Signal domain
NU-7026	2-(Morpholin-4-yl)-benzo[h]chomen-4-one
PBG	PBS, BSA, Gelatine
PBS	Phosphate Buffered Saline
PBST	PBS with Tween 20
PcAb	Polyclonal antibody
PCC	Prematurely condensed chromosomes
PCNA	Proliferating cell nuclear antigen
PFA	Paraformaldehyde
PFGE	Pulsed field gel electrophoresis
PI	Propidium iodine
PI-3Ks	Phosphoinositide-3 lipid family of kinases
PMT	Photomultipliers
PP2A	Protein phosphatase 2A
PVDF	Polyvinylidene Fluoride Transfer Membranes

Rnase	Ribonuclease
RPM	Rounds per minute
RT	Room temperature
SDS-PAGE	Sodium dodecyl sulfate polyacrylamide gel electrophoresis
Ser	Serine
SS	Side scatter
ssDNA	Single-stranded DNA
TAg	Tumor antigen
tet	Tetracycline
Thr	Threonine
TIFF	Tagged Image File Format
TOPBP1	Topoisomerase-binding protein-1
Tyr	Tyrosine
UCN-01	7-hydroxystaurosporine
UV	Ultraviolet
γ-H2AX	Phosphoryaltion of Histone H2AX at Serine 139

8 Reference

1. Elledge, S.J. (1996) Cell Cycle Checkpoints: Preventing an Identity Crisis. *Science*, **274**, 1664-1672.
2. Niida, H. and Nakanishi, M. (2006) DNA damage checkpoints in mammals. *Mutagenesis*, **21**, 3-9.
3. Hartwell, L.H. and Weinert, T.A. (1989) Checkpoints: controls that ensure the order of cell cycle events. *Science*, **246**, 629-634.
4. el-Deiry, W., Tokino, T., Velculescu, V., Levy, D., Parsons, R., Trent, J., Lin, D., Mercer, W., Kinzler, K. and Vogelstein, B. (1993) WAF1, a potential mediator of p53 tumor suppression *Cell*, **75**, 817-825.
5. Sherr, C.J. and Roberts, J.M. (1995) Inhibitors of mammalian G1 cyclin-dependent kinases. *Genes & Development*, **9**, 1149-1163.
6. Harper, J., Adami, G., Wei, N., Keyomarsi, K. and Elledge, S. (1993) The p21 Cdk-interacting protein Cip1 is a potent inhibitor of G1 cyclin-dependent kinases. *Cell*, **75**, 805-816.
7. Matsushime, H., Quelle, D.E., Shurtleff, S.A., Shibuya, M., Sherr, C.J. and Kato, J.Y. (1994) D-type cyclin-dependent kinase activity in mammalian cells. *Mol. Cell. Biol.*, **14**, 2066-2076.
8. Amon, A. (1999) The spindle checkpoint. *Curr Opin Genet Dev*, **9**, 69-75.
9. Wilson, G.D. (2004) Radiation and the cell cycle, revisited. *Cancer Metastasis Rev*, **23**, 209-225.
10. O'Connell, M., Walworth, N. and Carr, A. (2000) The G2-phase DNA-damage checkpoint *Trends in Cell Biology*, **10**, 296-303
11. Jackman, M. and Pines, J. (1997) Cyclins and the G2/M transition. *Cancer surveys*, **29**, 47-73.
12. O'Connor, P. (1997) Mammalian G1 and G2 phase checkpoints. *Cancer surveys*, **29**, 151-182.
13. Dunphy, W.G. (1994) The decision to enter mitosis. *Trends Cell Biol*, **4**, 202-207.
14. Agarwal, M., Agarwal, A., Taylor, W. and Stark, G. (1995) p53 controls both the G2/M and the G1 cell cycle checkpoints and mediates reversible growth arrest in human fibroblasts. *Proc. Natl. Acad. Sci. USA*, **92**, 8493-8497.

15. Hermeking, H., Lengauer, C., Polyak, K., He, T., Zhang, L., Thiagalingam, S., Kinzler, K. and Vogelstein, B. (1997) 14-3-3σ Is a p53-Regulated Inhibitor of G2/M Progression *Molecula Cell*, **1**, 3-11.
16. Adams, K.E., Medhurst, A.L., Dart, D.A. and Lakin, N.D. (2006) Recruitment of ATR to sites of ionising radiation-induced DNA damage requires ATM and components of the MRN protein complex. *Oncogene*, **25**, 3894-3904.
17. Ahn, J.Y., Schwarz, J.K., Piwnica-Worms, H. and Canman, C.E. (2000) Threonine 68 phosphorylation by ataxia telangiectasia mutated is required for efficient activation of Chk2 in response to ionizing radiation. *Cancer Res*, **60**, 5934-5936.
18. Cimprich, K. and Cortez, D. (2008) ATR: an essential regulator of genome integrity. *Nat Rev Mol Cell Biol*, **9**, 616-627.
19. Kurose, A., Tanaka, T., Huang, X., Traganos, F., Dai, W. and Z., D. (2006) Effects of hydroxyurea and aphidicolin on phosphorylation of ataxia telangiectasia mutated on Ser 1981 and histone H2AX on Ser 139 in relation to cell cycle phase and induction of apoptosis. *Cytometry Part A*, **69A**, 212-221.
20. Olive, P.L. and Banath, J.P. (1993) Detection of DNA double-strand breaks through the cell cycle after exposure to X-rays, bleomycin, etoposide and 125IdUrd. *Int J Radiat Biol*, **64**, 349-358.
21. Kanaar, R., Hoeijmakers, J.H. and van Gent, D.C. (1998) Molecular mechanisms of DNA double strand break repair. *Trends Cell Biol*, **8**, 483-489.
22. Cui, X. and Meek, K. (2007) Linking double-stranded DNA breaks to the recombination activating gene complex directs repair to the nonhomologous end-joining pathway. *Proceedings of the National Academy of Sciences*, **104**, 17046-17051.
23. Arnaudeau, C., Lundin, C. and Helleday, T. (2001) DNA double-strand breaks associated with replication forks are predominantly repaired by homologous recombination involving an exchange mechanism in mammalian cells. *J Mol Biol*, **307**, 1235-1245.
24. Bassing, C.H., Swat, W. and Alt, F.W. (2002) The mechanism and regulation of chromosomal V(D)J recombination. *Cell*, **109 Suppl**, S45-55.
25. Jackson, S.P. (2002) Sensing and repairing DNA double-strand breaks. *Carcinogenesis*, **23**, 687-696.

26. Pardo, B., Gomez-Gonzalez, B. and Aguilera, A. (2009) DNA double-strand break repair: how to fix a broken relationship. *Cell Mol Life Sci*.
27. Fleck, O. and Nielsen, O. (2004) DNA repair. *J Cell Sci*, **117**, 515-517.
28. O'Connell, M.J. and Cimprich, K.A. (2005) G2 damage checkpoints: what is the turn-on? *J Cell Sci*, **118**, 1-6.
29. Burma, S., Chen, B.P., Murphy, M., Kurimasa, A. and Chen, D.J. (2001) ATM Phosphorylates Histone H2AX in Response to DNA Double-strand Breaks. *J. Biol. Chem.*, **276**, 42462-42467.
30. Bakkenist, C.J. and Kastan, M.B. (2004) Initiating cellular stress responses. *Cell*, **118**, 9-17.
31. Savitsky, K., Bar-Shira, A., Gilad, S., Rotman, G., Ziv, Y., Vanagaite, L., Tagle, D.A., Smith, S., Uziel, T., Sfez, S. *et al.* (1995) A single ataxia telangiectasia gene with a product similar to PI-3 kinase. *Science*, **268**, 1749-1753.
32. Keegan, K.S., Holtzman, D.A., Plug, A.W., Christenson, E.R., Brainerd, E.E., Flaggs, G., Bentley, N.J., Taylor, E.M., Meyn, M.S., Moss, S.B. *et al.* (1996) The Atr and Atm protein kinases associate with different sites along meiotically pairing chromosomes. *Genes Dev*, **10**, 2423-2437.
33. O'Neill, T., Dwyer, A.J., Ziv, Y., Chan, D.W., Lees-Miller, S.P., Abraham, R.H., Lai, J.H., Hill, D., Shiloh, Y., Cantley, L.C. *et al.* (2000) Utilization of oriented peptide libraries to identify substrate motifs selected by ATM. *J Biol Chem*, **275**, 22719-22727.
34. Traven, A. and Heierhorst, J. (2005) SQ/TQ cluster domains: concentrated ATM/ATR kinase phosphorylation site regions in DNA-damage-response proteins. *Bioessays*, **27**, 397-407.
35. Anderson, C.W. and Lees-Miller, S.P. (1992) The nuclear serine/threonine protein kinase DNA-PK. *Crit Rev Eukaryot Gene Expr*, **2**, 283-314.
36. Kim, S.T., Lim, D.S., Canman, C.E. and Kastan, M.B. (1999) Substrate specificities and identification of putative substrates of ATM kinase family members. *J Biol Chem*, **274**, 37538-37543.
37. Yang, J., Yu, Y., Hamrick, H.E. and Duerksen-Hughes, P.J. (2003) ATM, ATR and DNA-PK: initiators of the cellular genotoxic stress responses. *Carcinogenesis*, **24**, 1571-1580.
38. Jiang, G. and Sancar, A. (2006) Recruitment of DNA Damage Checkpoint Proteins to Damage in Transcribed and Nontranscribed Sequences. *Mol. Cell. Biol.*, **26**, 39-49.

39. Yoshioka, K.-i., Yoshioka, Y. and Hsieh, P. (2006) ATR Kinase Activation Mediated by MutS± and MutL± in Response to Cytotoxic O6-Methylguanine Adducts. **22**, 501-510.
40. Zou, L. and Elledge, S.J. (2003) Sensing DNA damage through ATRIP recognition of RPA-ssDNA complexes. *Science*, **300**, 1542-1548.
41. Ball, H.L. and Cortez, D. (2005) ATRIP oligomerization is required for ATR-dependent checkpoint signaling. *J Biol Chem*, **280**, 31390-31396.
42. Ball, H.L., Ehrhardt, M.R., Mordes, D.A., Glick, G.G., Chazin, W.J. and Cortez, D. (2007) Function of a Conserved Checkpoint Recruitment Domain in ATRIP Proteins. *Mol. Cell. Biol.*, **27**, 3367-3377.
43. Cortez, D., Guntuku, S., Qin, J. and Elledge, S.J. (2001) ATR and ATRIP: partners in checkpoint signaling. *Science*, **294**, 1713-1716.
44. Ball, H.L., Myers, J.S. and Cortez, D. (2005) ATRIP binding to replication protein A-single-stranded DNA promotes ATR-ATRIP localization but is dispensable for Chk1 phosphorylation. *Mol Biol Cell*, **16**, 2372-2381.
45. Stokes, M.P., Van Hatten, R., Lindsay, H.D. and Michael, W.M. (2002) DNA replication is required for the checkpoint response to damaged DNA in Xenopus egg extracts. *J Cell Biol*, **158**, 863-872.
46. MacDougall, C., Byun, T., Van, C., Yee, M. and Cimprich, K. (2007) The structural determinants of checkpoint activation. *Genes Dev.* , **21**, 898-903.
47. Parrilla-Castellar, E.R., Arlander, S.J.H. and Karnitz, L. Dial 9-1-1 for DNA damage: the Rad9-Hus1-Rad1 (9-1-1) clamp complex. *DNA Repair*, **3**, 1009-1014.
48. Kumagai, A. and Dunphy, W.G. (2000) Claspin, a Novel Protein Required for the Activation of Chk1 during a DNA Replication Checkpoint Response in Xenopus Egg Extracts *Molecular Cell*, **6**, 839-849.
49. Bermudez, V.P., Lindsey-Boltz, L.A., Cesare, A.J., Maniwa, Y., Griffith, J.D., Hurwitz, J. and Sancar, A. (2003) Loading of the human 9-1-1 checkpoint complex onto DNA by the checkpoint clamp loader hRad17-replication factor C complex in vitro. *Proc Natl Acad Sci U S A*, **100**, 1633-1638.
50. Zou, L., Cortez, D. and Elledge, S.J. (2002) Regulation of ATR substrate selection by Rad17-dependent loading of Rad9 complexes onto chromatin. *Genes Dev*, **16**, 198-208.

51. Zhao, H. and Piwnica-Worms, H. (2001) ATR-Mediated Checkpoint Pathways Regulate Phosphorylation and Activation of Human Chk1. *Mol. Cell. Biol.*, **21**, 4129-4139.

52. Majka, J., Niedziela-Majka, A. and Burgers, Peter M.J. (2006) The Checkpoint Clamp Activates Mec1 Kinase during Initiation of the DNA Damage Checkpoint. **24**, 891-901.

53. Lee, J., Kumagai, A. and Dunphy, W.G. (2007) The Rad9-Hus1-Rad1 checkpoint clamp regulates interaction of TopBP1 with ATR. *J. Biol. Chem.*, M704635200.

54. Delacroix, S., Wagner, J., Kobayashi, M., Yamamoto, K. and Karnitz, L. (2007) The Rad9–Hus1–Rad1 (9–1–1) clamp activates checkpoint signaling via TopBP1. *Genes Dev.*, **21**, 1472-1477.

55. Kumagai, A., Lee, J., Yoo, H.Y. and Dunphy, W.G. (2006) TopBP1 Activates the ATR-ATRIP Complex. **124**, 943-955.

56. Kumagai, A., Lee, J., Yoo, H.Y. and Dunphy, W.G. (2006) TopBP1 Activates the ATR-ATRIP Complex. *Cell*, **124**, 943-955.

57. Mordes, D., Glick, G., Zhao, R. and Cortez, D. (2008) TopBP1 activates ATR through ATRIP and a PIKK regulatory domain. *Genes Dev.*, **22**, 1416-1421.

58. Ward, I.M., Minn, K. and Chen, J. (2004) UV-induced ataxia-telangiectasia-mutated and Rad3-related (ATR) activation requires replication stress. *J Biol Chem*, **279**, 9677-9680.

59. Fanning, E., Klimovich, V. and Nager, A.R. (2006) A dynamic model for replication protein A (RPA) function in DNA processing pathways. *Nucl. Acids Res.*, **34**, 4126-4137.

60. van den Bosch, M., Bree, R.T. and Lowndes, N.F. (2003) The MRN complex: coordinating and mediating the response to broken chromosomes. *EMBO Rep*, **4**, 844-849.

61. Costanzo, V., Shechter, D., Lupardus, P.J., Cimprich, K.A., Gottesman, M. and Gautier, J. (2003) An ATR- and Cdc7-Dependent DNA Damage Checkpoint that Inhibits Initiation of DNA Replication. *Molecular Cell*, **11**, 203-213.

62. Liu, Q., Guntuku, S., Cui, X.-S., Matsuoka, S., Cortez, D., Tamai, K., Luo, G., Carattini-Rivera, S., DeMayo, F., Bradley, A. *et al.* (2000) Chk1 is an essential kinase that is regulated by Atr and required for the G2/M DNA damage checkpoint. *Genes & Development*, **14**, 1448-1459.

63. Lopez-Girona, A., Tanaka, K., Chen, X.-B., Baber, B.A., McGowan, C.H. and Russell, P. (2001) Serine-345 is required for Rad3-dependent phosphorylation and function of checkpoint kinase Chk1 in fission yeast. *Proceedings of the National Academy of Sciences of the United States of America*, **98**, 11289-11294.

64. Chen, M.S., Ryan, C.E. and Piwnica-Worms, H. (2003) Chk1 kinase negatively regulates mitotic function of Cdc25A phosphatase through 14-3-3 binding. *Mol Cell Biol*, **23**, 7488-7497.

65. Uto, K., Inoue, D., Shimuta, K., Nakajo, N. and Sagata, N. (2004) Chk1, but not Chk2, inhibits Cdc25 phosphatases by a novel common mechanism. *Embo J*, **23**, 3386-3396.

66. Smits, V.A.J., Reaper, P.M. and Jackson, S.P. (2006) Rapid PIKK-Dependent Release of Chk1 from Chromatin Promotes the DNA-Damage Checkpoint Response. *Current Biology*, **16**, 150-159.

67. Rhind, N. and Russell, P. (2000) Chk1 and Cds1: linchpins of the DNA damage and replication checkpoint pathways. *J Cell Sci*, **113 (Pt 22)**, 3889-3896.

68. Bartek, J. and Lukas, J. (2003) Chk1 and Chk2 kinases in checkpoint control and cancer. *Cancer Cell*, **3**, 421-429.

69. Capasso, H., Palermo, C., Wan, S., Rao, H., John, U.P., O'Connell, M.J. and Walworth, N.C. (2002) Phosphorylation activates Chk1 and is required for checkpoint-mediated cell cycle arrest. *J Cell Sci*, **115**, 4555-4564.

70. Latif, C., Elzen, N.R.d. and O'Connell, M.J. (2004) DNA damage checkpoint maintenance through sustained Chk1 activity. *J Cell Sci*, **117**, 3489-3498.

71. Shiloh, Y. and Kastan, M.B. (2001) ATM: genome stability, neuronal development, and cancer cross paths. *Adv Cancer Res*, **83**, 209-254.

72. Shiloh, Y. (2003) ATM and related protein kinases: safeguarding genome integrity. *Nat Rev Cancer*, **3**, 155-168.

73. Canman, C.E., Lim, D.S., Cimprich, K.A., Taya, Y., Tamai, K., Sakaguchi, K., Appella, E., Kastan, M.B. and Siliciano, J.D. (1998) Activation of the ATM kinase by ionizing radiation and phosphorylation of p53. *Science*, **281**, 1677-1679.

74. de Jager, M., van Noort, J., van Gent, D.C., Dekker, C., Kanaar, R. and Wyman, C. (2001) Human Rad50/Mre11 Is a Flexible Complex that Can Tether DNA Ends. *Molecular Cell*, **8**, 1129-1135.

75. Berkovich, E., Monnat, R.J. and Kastan, M.B. (2007) Roles of ATM and NBS1 in chromatin structure modulation and DNA double-strand break repair. *Nat Cell Biol*, **9**, 683-690.

76. You, Z., Bailis, J., Johnson, S., Dilworth, S. and Hunter, T. (2007) Rapid activation of ATM on DNA flanking double-strand breaks. *Nat Cell Biol*, **9**, 1311-1318.

77. Lavin, M.F. (2008) Ataxia-telangiectasia: from a rare disorder to a paradigm for cell signalling and cancer. *Nat Rev Mol Cell Biol*, **9**, 759-769.

78. Bakkenist, C.J. and Kastan, M.B. (2003) DNA damage activates ATM through intermolecular autophosphorylation and dimer dissociation. *Nature*, **421**, 499-506.

79. Chun, H.H., Cary, R.B., Lansigan, F., Whitelegge, J., Rawlings, D.J. and Gatti, R.A. (2004) ATM protein purified from vaccinia virus expression system: DNA binding requirements for kinase activation. *Biochem Biophys Res Commun*, **322**, 74-81.

80. Berkovich, E., Monnat, R.J., Jr. and Kastan, M.B. (2007) Roles of ATM and NBS1 in chromatin structure modulation and DNA double-strand break repair. *Nat Cell Biol*, **9**, 683-690.

81. You, Z., Bailis, J.M., Johnson, S.A., Dilworth, S.M. and Hunter, T. (2007) Rapid activation of ATM on DNA flanking double-strand breaks. *Nat Cell Biol*, **9**, 1311-1318.

82. Banin, S., Moyal, L., Shieh, S., Taya, Y., Anderson, C.W., Chessa, L., Smorodinsky, N.I., Prives, C., Reiss, Y., Shiloh, Y. *et al.* (1998) Enhanced phosphorylation of p53 by ATM in response to DNA damage. *Science*, **281**, 1674-1677.

83. Chehab, N.H., Malikzay, A., Appel, M. and Halazonetis, T.D. (2000) Chk2/hCds1 functions as a DNA damage checkpoint in G(1) by stabilizing p53. *Genes Dev*, **14**, 278-288.

84. Lavin, M.F. ATM and the Mre11 complex combine to recognize and signal DNA double-strand breaks. *Oncogene*, **26**, 7749-7758.

85. Spycher, C., Miller, E.S., Townsend, K., Pavic, L., Morrice, N.A., Janscak, P., Stewart, G.S. and Stucki, M. (2008) Constitutive phosphorylation of MDC1 physically links the MRE11-RAD50-NBS1 complex to damaged chromatin. *J. Cell Biol.*, **181**, 227-240.

86. Carson, C.T., Schwartz, R.A., Stracker, T.H., Lilley, C.E., Lee, D.V. and Weitzman, M.D. (2003) The Mre11 complex is required for ATM activation and the G2/M checkpoint. *Embo J*, **22**, 6610-6620.

87. Chaturvedi, P., Eng, W.K., Zhu, Y., Mattern, M.R., Mishra, R., Hurle, M.R., Zhang, X., Annan, R.S., Lu, Q., Faucette, L.F. *et al.* (1999) Mammalian Chk2 is a downstream effector of the ATM-dependent DNA damage checkpoint pathway. *Oncogene*, **18**, 4047-4054.

88. Matsuoka, S., Rotman, G., Ogawa, A., Shiloh, Y., Tamai, K. and Elledge, S.J. (2000) Ataxia telangiectasia-mutated phosphorylates Chk2 in vivo and in vitro. *Proc Natl Acad Sci U S A*, **97**, 10389-10394.

89. Hosing, A.S., Kundu, S.T. and Dalal, S.N. (2008) 14-3-3 Gamma is required to enforce both the incomplete S phase and G2 DNA damage checkpoints. *Cell Cycle*, **7**, 3171-3179.

90. Matsuoka, S., Huang, M. and Elledge, S.J. (1998) Linkage of ATM to Cell Cycle Regulation by the Chk2 Protein Kinase. *Science*, **282**, 1893-1897.

91. Castedo, M., Perfettini, J.L., Roumier, T., Yakushijin, K., Horne, D., Medema, R. and Kroemer, G. (2004) The cell cycle checkpoint kinase Chk2 is a negative regulator of mitotic catastrophe. *Oncogene*, **23**, 4353-4361.

92. Xu, X., Tsvetkov, L.M. and Stern, D.F. (2002) Chk2 Activation and Phosphorylation-Dependent Oligomerization. *Mol. Cell. Biol.*, **22**, 4419-4432.

93. Brown, E.J. and Baltimore, D. (2000) ATR disruption leads to chromosomal fragmentation and early embryonic lethality. *Genes & Development*, **14**, 397-402.

94. Alderton, G.K., Joenje, H., Varon, R., Borglum, A.D., Jeggo, P.A. and O'Driscoll, M. (2004) Seckel syndrome exhibits cellular features demonstrating defects in the ATR-signalling pathway. *Hum. Mol. Genet.*, **13**, 3127-3138.

95. Culligan, K., Tissier, A. and Britt, A. (2004) ATR Regulates a G2-Phase Cell-Cycle Checkpoint in Arabidopsis thaliana. *Plant Cell*, **16**, 1091-1104.

96. Tercero, J.A., Longhese, M.P. and Diffley, J.F.X. (2003) A Central Role for DNA Replication Forks in Checkpoint Activation and Response. **11**, 1323-1336.

97. Niida, H., Tsuge, S., Katsuno, Y., Konishi, A., Takeda, N. and Nakanishi, M. (2005) Depletion of Chk1 Leads to Premature Activation of Cdc2-cyclin B and Mitotic Catastrophe. *J. Biol. Chem.*, **280**, 39246-39252.

98. Zachos, G., Rainey, M.D. and Gillespie, D.A.F. (2003) Chk1-deficient tumour cells are viable but exhibit multiple checkpoint and survival defects. *The Embo Journal*, **22**, 713-723.

99. Shiloh, Y. (1997) Ataxia-telangiectasia and the Nijmegen breakage syndrome: related disorders but genes apart. *Annu Rev Genet*, **31**, 635-662.

100. Kastan, M.B. and Lim, D.S. (2000) The many substrates and functions of ATM. *Nat Rev Mol Cell Biol*, **1**, 179-186.

101. Takai, H., Naka, K., Okada, Y., Watanabe, M., Harada, N., Saito, S., Anderson, C.W., Appella, E., Nakanishi, M., Suzuki, H. *et al.* (2002) Chk2-deficient mice exhibit radioresistance and defective p53-mediated transcription. *Embo J*, **21**, 5195-5205.

102. Hirao, A., Cheung, A., Duncan, G., Girard, P.-M., Elia, A.J., Wakeham, A., Okada, H., Sarkissian, T., Wong, J.A., Sakai, T. *et al.* (2002) Chk2 Is a Tumor Suppressor That Regulates Apoptosis in both an Ataxia Telangiectasia Mutated (ATM)-Dependent and an ATM-Independent Manner. *Mol. Cell. Biol.*, **22**, 6521-6532.

103. McPherson, J.P., Lemmers, B., Hirao, A., Hakem, A., Abraham, J., Migon, E., Matysiak-Zablocki, E., Tamblyn, L., Sanchez-Sweatman, O., Khokha, R. *et al.* (2004) Collaboration of Brca1 and Chk2 in tumorigenesis. *Genes Dev*, **18**, 1144-1153.

104. Lee, S.B., Kim, S.H., Bell, D.W., Wahrer, D.C.R., Schiripo, T.A., Jorczak, M.M., Sgroi, D.C., Garber, J.E., Li, F.P., Nichols, K.E. *et al.* (2001) Destabilization of CHK2 by a Missense Mutation Associated with Li-Fraumeni Syndrome. *Cancer Res*, **61**, 8062-8067.

105. Bi, X., Srikanta, D., Fanti, L., Pimpinelli, S., Badugu, R., Kellum, R. and Rong, Y.S. (2005) Drosophila ATM and ATR checkpoint kinases control partially redundant pathways for telomere maintenance. *Proc Natl Acad Sci U S A*, **102**, 15167-15172.

106. Choudhury, A., Cuddihy, A. and Bristow, R.G. (2006) Radiation and new molecular agents part I: targeting ATM-ATR checkpoints, DNA repair, and the proteasome. *Semin Radiat Oncol*, **16**, 51-58.

107. Zglinicki, T.v., Saretzki, G., Ladhoff, J., Fagagna, F.d.A.d. and Jackson, S.P. (2005) Human cell senescence as a DNA damage response. *Mechanisms of Ageing and Development*, **126**, 111-117.

108. Takata, H., Kanoh, Y., Gunge, N., Shirahige, K. and Matsuura, A. (2004) Reciprocal Association of the Budding Yeast ATM-Related Proteins Tel1 and Mec1 with Telomeres In Vivo. **14**, 515-522.

109. Craven, R.J., Greenwell, P.W., Dominska, M. and Petes, T.D. (2002) Regulation of Genome Stability by TEL1 and MEC1, Yeast Homologs of the Mammalian ATM and ATR Genes. *Genetics*, **161**, 493-507.

110. Heffernan, T.P., Simpson, D.A., Frank, A.R., Heinloth, A.N., Paules, R.S., Cordeiro-Stone, M. and Kaufmann, W.K. (2002) An ATR- and Chk1-dependent S checkpoint inhibits replicon initiation following UVC-induced DNA damage. *Mol Cell Biol*, **22**, 8552-8561.

111. Suzuki, K., Kodama, S. and Watanabe, M. (1999) Recruitment of ATM protein to double strand DNA irradiated with ionizing radiation. *J Biol Chem*, **274**, 25571-25575.

112. Unsal-Kacmaz, K., Makhov, A.M., Griffith, J.D. and Sancar, A. (2002) Preferential binding of ATR protein to UV-damaged DNA. *Proc Natl Acad Sci U S A*, **99**, 6673-6678.

113. Smith, G.C., Cary, R.B., Lakin, N.D., Hann, B.C., Teo, S.H., Chen, D.J. and Jackson, S.P. (1999) Purification and DNA binding properties of the ataxia-telangiectasia gene product ATM. *Proc Natl Acad Sci U S A*, **96**, 11134-11139.

114. Helt, C.E., Cliby, W.A., Keng, P.C., Bambara, R.A. and O'Reilly, M.A. (2005) Ataxia Telangiectasia Mutated (ATM) and ATM and Rad3-related Protein Exhibit Selective Target Specificities in Response to Different Forms of DNA Damage. *J. Biol. Chem.*, **280**, 1186-1192.

115. Nakada, D., Hirano, Y., Tanaka, Y. and Sugimoto, K. (2005) Role of the C Terminus of Mec1 Checkpoint Kinase in Its Localization to Sites of DNA Damage. *Mol. Biol. Cell*, **16**, 5227-5235.

116. Tibbetts, R., Cortez, D., Brumbaugh, K., Scully, R., Livingston, D., Elledge, S. and Abraham, R. (2000) Functional interactions between BRCA1 and the checkpoint kinase ATR during genotoxic stress. *Genes Dev.*, **14**, 2989-3002.

117. Tibbetts, R., Brumbaugh, K., Williams, J., Sarkaria, J., Cliby, W., Shieh, S., Taya, Y., Prives, C. and Abraham, R. (1999) A role for ATR in the DNA damage-induced phosphorylation of p53. *Genes Dev.*, **13**, 152-157.

118. Yajima, H., Lee, K.-J. and Chen, B.P.C. (2006) ATR-Dependent Phosphorylation of DNA-Dependent Protein Kinase Catalytic Subunit in Response to UV-Induced Replication Stress. *Mol. Cell. Biol.*, **26**, 7520-7528.

119. Jazayeri, A., Falck, J., Lukas, C., Bartek, J., Smith, G.C.M., Lukas, J. and Jackson, S.P. (2006) ATM- and cell cycle-dependent regulation of ATR in response to DNA double-strand breaks. *Nat Cell Biol*, **8**, 37-45.

120. Wang, X.Q., Redpath, J.L., Fan, S.T. and Stanbridge, E.J. (2006) ATR dependent activation of Chk2. *J. Cell. Physiol.*, **208**, 613-619.

121. Cuadrado, M., Martinez-Pastor, B., Murga, M., Toledo, L.I., Gutierrez-Martinez, P., Lopez, E. and Fernandez-Capetillo, O. (2006) ATM regulates ATR chromatin loading in response to DNA double-strand breaks. *J. Exp. Med.*, jem.20051923.

122. Stiff, T., Walker, S.A., Cerosaletti, K., Goodarzi, A.A., Petermann, E., Concannon, P., O'Driscoll, M. and Jeggo, P.A. (2006) ATR-dependent phosphorylation and activation of ATM in response to UV treatment or replication fork stalling. *The Embo Journal*, **25**, 5775–5782.

123. Chen, X., Zhao, R., Glick, G.G. and Cortez, D. (2007) Function of the ATR N-terminal domain revealed by an ATM/ATR chimera. *Exp Cell Res*, **313**, 1667-1674.

124. Wakabayashi, M., Ishii, C., Inoue, H. and Tanaka, S. (2008) Genetic analysis of CHK1 and CHK2 homologues revealed a unique cross talk between ATM and ATR pathways in Neurospora crassa. *DNA Repair (Amst)*, **7**, 1951-1961.

125. Zaugg, K., Su, Y.W., Reilly, P.T., Moolani, Y., Cheung, C.C., Hakem, R., Hirao, A., Liu, Q., Elledge, S.J. and Mak, T.W. (2007) Cross-talk between Chk1 and Chk2 in double-mutant thymocytes. *Proc Natl Acad Sci U S A*, **104**, 3805-3810.

126. Gatei, M., Sloper, K., Sorensen, C., Syljuasen, R., Falck, J., Hobson, K., Savage, K., Lukas, J., Zhou, B.-B., Bartek, J. *et al.* (2003) Ataxia-telangiectasia-mutated (ATM) and NBS1-dependent Phosphorylation of Chk1 on Ser-317 in Response to Ionizing Radiation. *J. Biol. Chem.*, **278**, 14806-14811.

127. Daboussi, F., Dumay, A., Delacote, F. and Lopez, B.S. (2002) DNA double-strand break repair signalling: the case of RAD51 post-translational regulation. *Cell Signal*, **14**, 969-975.

128. Balajee, A.S. and Geard, C.R. (2004) Replication protein A and gamma-H2AX foci assembly is triggered by cellular response to DNA double-strand breaks. *Exp Cell Res*, **300**, 320-334.

129. Balajee, A.S. and Geard, C.R. (2001) Chromatin-bound PCNA complex formation triggered by DNA damage occurs independent of the ATM gene product in human cells. *Nucleic Acids Res*, **29**, 1341-1351.

130. Anderson, L., Henderson, C. and Adachi, Y. (2001) Phosphorylation and rapid relocalization of 53BP1 to nuclear foci upon DNA damage. *Mol Cell Biol*, **21**, 1719-1729.

131. Whalen, M.K., Gurai, S.K., Zahed-Kargaran, H. and Pluth, J.M. (2008) Specific ATM-mediated phosphorylation dependent on radiation quality. *Radiat Res*, **170**, 353-364.

132. Rogakou, E.P., Pilch, D.R., Orr, A.H., Ivanova, V.S. and Bonner, W.M. (1998) DNA double-stranded breaks induce histone H2AX phosphorylation on serine 139. *J Biol Chem*, **273**, 5858 - 5868.

133. Chen, H.T., Bhandoola, A., Difilippantonio, M.J., Zhu, J., Brown, M.J., Tai, X., Rogakou, E.P., Brotz, T.M., Bonner, W.M., Ried, T. *et al.* (2000) Response to RAG-Mediated V(D)J Cleavage by NBS1 and {gamma}-H2AX. *Science*, **290**, 1962-1964.

134. Fernandez-Capetillo, O., Celeste, A. and Nussenzweig, A. (2003) Focusing on foci: H2AX and the recruitment of DNA-damage response factors. *Cell Cycle*, **2**, 426-427.

135. Rogakou, E.P., Pilch, D.R., Orr, A.H., Ivanova, V.S. and Bonner, W.M. (1998) DNA Double-stranded Breaks Induce Histone H2AX Phosphorylation on Serine 139. *J. Biol. Chem.*, **273**, 5858-5868.

136. Redon, C., Pilch, D., Rogakou, E., Sedelnikova, O., Newrock, K. and Bonner, W. (2002) Histone H2A variants H2AX and H2AZ. *Curr Opin Genet Dev*, **12**, 162-169.

137. Sedelnikova, O.A., Horikawa, I., Zimonjic, D.B., Popescu, N.C., Bonner, W.M. and Barrett, J.C. (2004) Senescing human cells and ageing mice accumulate DNA lesions with unrepairable double-strand breaks. *Nat Cell Biol*, **6**, 168-170.

138. Rothkamm, K., Kruger, I., Thompson, L.H. and Lobrich, M. (2003) Pathways of DNA Double-Strand Break Repair during the Mammalian Cell Cycle. *Mol. Cell. Biol.*, **23**, 5706-5715.

139. Sedelnikova, O.A., Rogakou, E.P., Panyutin, I.G. and Bonner, W.M. (2002) Quantitative detection of (125)IdU-induced DNA double-strand breaks with gamma-H2AX antibody. *Radiat Res*, **158**, 486-492.

140. Tanaka, T., Huang, X., Jorgensen, E., Gietl, D., Traganos, F., Darzynkiewicz, Z. and Albino, A. (2007) ATM activation accompanies histone H2AX phosphorylation in A549 cells upon exposure to tobacco smoke. *BMC Cell Biology*, **8**, 26.

141. Buscemi, G., Perego, P., Carenini, N., Nakanishi, M., Chessa, L., Chen, J., Khanna, K. and Delia, D. (2004) Activation of ATM and Chk2 kinases in relation to the amount of DNA strand breaks. *Oncogene*, **23**, 7691-7700.

142. Gradzka, I. and Iwanenko, T. (2005) A non-radioactive, PFGE-based assay for low levels of DNA double-strand breaks in mammalian cells. *DNA Repair*, **4**, 1129-1139.

143. Nakamura, A., Sedelnikova, O.A., Redon, C., Pilch, D.R., Sinogeeva, N.I., Shroff, R., Lichten, M., Bonner, W.M. and Judith L. Campbell, a.P.M. (2006), *Methods in Enzymology*. Academic Press, Vol. Volume 409, pp. 236-250.

144. Kinner, A., Wu, W., Staudt, C. and Iliakis, G. (2008) {gamma}-H2AX in recognition and signaling of DNA double-strand breaks in the context of chromatin. *Nucl. Acids Res.*, **36**, 5678-5694.

145. Young, D.B., Jonnalagadda, J., Gatei, M., Jans, D.A., Meyn, S. and Khanna, K.K. (2005) Identification of domains of ataxia-telangiectasia mutated required for nuclear localization and chromatin association. *J Biol Chem*, **280**, 27587-27594.

146. Bencokova, Z., Kaufmann, M.R., Pires, I.M., Lecane, P.S., Giaccia, A.J. and Hammond, E.M. (2009) ATM Activation and Signaling under Hypoxic Conditions. *Mol. Cell. Biol.*, **29**, 526-537.

147. Suzuki, K., Okada, H., Yamauchi, M., Oka, Y., Kodama, S. and Watanabe, M. (2006) Qualitative and Quantitative Analysis of Phosphorylated ATM Foci Induced by Low-Dose Ionizing Radiation. *Radiation Research*, **165**, 499-504.

148. Hesse, J.E., Faulkner, M.F. and Durdik, J.M. (2009) Increase in double-stranded DNA break-related foci in early-stage thymocytes of aged mice. *Experimental Gerontology*, **44**, 676-684.

149. Golubnitschaja, O. (2007) Cell cycle checkpoints: the role and evaluation for early diagnosis of senescence, cardiovascular, cancer, and neurodegenerative diseases. *Amino Acids.*, **32**, 359-371.

150. Zou, Y., Misri, S., Shay, J.W., Pandita, T.K. and Wright, W.E. (2009) Altered States of Telomere Deprotection and the Two-Stage Mechanism of Replicative Aging. *Mol. Cell. Biol.*, **29**, 2390-2397.

151. Fernandez-Capetillo, O., Chen, H., Celeste, A., Ward, I., Romanienko, P., Morales, J., Naka, K., Xia, Z., Camerini-Otero, R., Motoyama, N. *et al.* (2002) DNA damage-induced G2-M checkpoint activation by histone H2AX and 53BP1. *Nat Cell Biol*, **4**, 277-279.

152. Yamauchi, M., Oka, Y., Yamamoto, M., Niimura, K., Uchida, M., Kodama, S., Watanabe, M., Sekine, I., Yamashita, S. and Suzuki, K. (2008) Growth of persistent foci of DNA damage checkpoint factors is essential for amplification of G1 checkpoint signaling. *DNA Repair*, **7**, 405-417.

153. Rowley, R. (1992) Reduction of radiation-induced G2 arrest by caffeine. *Radiat Res.*, **129**, 224-227.

154. Playle, L.C., Hicks, D.J., Qualtrough, D. and Paraskeva, C. (2002) Abrogation of the radiation-induced G2 checkpoint by the staurosporine derivative UCN-01 is associated with radiosensitisation in a subset of colorectal tumour cell lines. *British Journal of Cancer*, **87**, 352-358.

155. Zhao, Y., Lu, Y., Newell, D.R., O'Connor*, M., Lau*, A., Harris, N., Smith, G.C.M. and Curtin, N.J. (2006) Chemo-sensitization by the novel ATM inhibitor (KU-55933) is p53 independent. *AACR Meeting Abstracts*, **2006**, 486-b-.

156. Arienti, K.L., Brunmark, A., Axe, F.U., McClure, K., Lee, A., Blevitt, J., Neff, D.K., Huang, L., Crawford, S., Pandit, C.R. *et al.* (2005) Checkpoint Kinase Inhibitors: SAR and Radioprotective Properties of a Series of 2-Arylbenzimidazoles. *J. Med. Chem.*, **48**, 1873-1885.

157. Sarkaria, J.N., Busby, E.C., Tibbetts, R.S., Roos, P., Taya, Y., Karnitz, L.M. and Abraham, R.T. (1999) Inhibition of ATM and ATR Kinase Activities by the Radiosensitizing Agent, Caffeine. *Cancer Res*, **59**, 4375-4382.

158. Bache, M., Pigorsch, S., Dunst, J., Würl, P., Meye, A., Bartel, F., Schmidt, H., Rath, F.W. and Taubert, H. (2001) Loss of G2/M arrest correlates with radiosensitization in two human sarcoma cell lines with mutant p53. *International Journal of Cancer*, **96**, 110-117.

159. Matsuoka, S., Rotman, G., Ogawa, A., Shiloh, Y., Tamai, K. and Elledge, S.J. (2000) Ataxia telangiectasia-mutated phosphorylates Chk2 in vivo and in vitro. *Proceedings of the National Academy of Sciences*, **97**, 10389-10394.

160. Luo, C.-M., Tang, W., Mekeel, K.L., DeFrank, J.S., Anné, P.R. and Powell, S.N. (1996) High Frequency and Error-prone DNA Recombination in Ataxia Telangiectasia Cell Lines. *J. Biol. Chem.*, **271**, 4497-4503.

161. Block, W.D., Merkle, D., Meek, K. and Lees-Miller, S.P. (2004) Selective inhibition of the DNA-dependent protein kinase (DNA-PK) by the radiosensitizing agent caffeine. *Nucl. Acids Res.*, **32**, 1967-1972.

162. Collis, S.J., DeWeese, T.L., Jeggo, P.A. and Parker, A.R. (2004) The life and death of DNA-PK. *Oncogene*, **24**, 949-961.

163. Mahaney, B.L., Meek, K. and Lees-miller, S.P. (2009) Repair of ionizing radiation-induced DNA double-strand breaks by non-homologous end-joining. *Biochem J*, **417**, 639-650.

164. Burma, S., Chen, B.P.C. and Chen, D.J. (2006) Role of non-homologous end joining (NHEJ) in maintaining genomic integrity. *DNA Repair*, **5**, 1042-1048.

165. Holgersson, Å., Heiden, T., Castro, J., Edgren, M.R., Lewensohn, R. and Meijer, A.E. (2005) Different G2/M accumulation in M059J and M059K cells after exposure to DNA double-strand break-inducing agents. *International Journal of Radiation Oncology*Biology*Physics*, **61**, 915-921.

166. Nutley, B.P., Smith, N.F., Hayes, A., Kelland, L.R., Brunton, L., Golding, B.T., Smith, G.C.M., Martin, N.M.B., Workman, P. and Raynaud, F.I. Preclinical pharmacokinetics and metabolism of a novel prototype DNA-PK inhibitor NU7026. *Br J Cancer*, **93**, 1011-1018.

167. Veuger, S.J., Curtin, N.J., Smith, G.C.M. and Durkacz, B.W. (2004) Effects of novel inhibitors of poly(ADP-ribose) polymerase-1 and the DNA-dependent protein kinase on enzyme activities and DNA repair. *Oncogene*, **23**, 7322-7329.

168. Chan, D., Gately, D., Urban, S., Galloway, A., Lees-Miller, S., Yen, T. and Allalunis-Turner, J. (1998) Lack of correlation between ATM protein expression and tumour cell radiosensitivity. *Int J Radiat Biol.*, **74**, 217-224.

169. Tsuchida, R., Yamada, T., Takagi, M., Shimada, A., Ishioka, C., Katsuki, Y., Igarashi, T., Chessa, L., Delia, D., Teraoka, H. *et al.* (2002) Detection of ATM gene mutation in human glioma cell line M059J by a rapid frameshift/stop codon assay in yeast. *Radiat Res.*, **158**, 195-201.

170. Cliby, W.A., Roberts, C.J., Cimprich, K.A., Stringer, C.M., Lamb1, J.R., Schreiber, S.L. and Friend, S.H. (1998) Overexpression of a kinase-inactive ATR protein causes sensitivity to DNA-damaging agents and defects in cell cycle checkpoints. *The EMBO Journal* 159-169.

171. Crissman, H.A. and Steinkamp, J.A. (1987) A new method for rapid and sensitive detection of bromodeoxyuridine in DNA-replicating cells. *Experimental Cell Research*, **173**, 256-261.

172. Xu, B., Kim, S.-T., Lim, D.-S. and Kastan, M.B. (2002) Two Molecularly Distinct G2/M Checkpoints Are Induced by Ionizing Irradiation. *Mol. Cell. Biol.*, **22**, 1049-1059.

173. Venere, M., Snyder, A., Zgheib, O. and Halazonetis, T.D. (2007) Phosphorylation of ATR-Interacting Protein on Ser239 Mediates an Interaction with Breast-Ovarian Cancer Susceptibility 1 and Checkpoint Function. *Cancer Res*, **67**, 6100-6105.

174. Peng, A. and Chen, P.-L. (2005) NFBD1/Mdc1 Mediates ATR-Dependent DNA Damage Response. *Cancer Res*, **65**, 1158-1163.

175. Ball, H.L., Myers, J.S. and Cortez, D. (2005) ATRIP Binding to Replication Protein A-Single-stranded DNA Promotes ATR-ATRIP Localization but Is Dispensable for Chk1 Phosphorylation. *Mol. Biol. Cell*, **16**, 2372-2381.

176. Jordan, M.A., Thrower, D. and Wilson, L. (1992) Effects of vinblastine, podophyllotoxin and nocodazole on mitotic spindles. Implications for the role of microtubule dynamics in mitosis. *J Cell Sci*, **102**, 401-416.

177. Buck, S.B., Bradford, J., Gee, K.R., Agnew, B.J., Clarke, S.T. and Adrian, S. (2008) Detection of S-phase cell cycle progression using 5-ethynyl-2′-deoxyuridine incorporation with click chemistry, an alternative to using 5-bromo-2′-deoxyuridine antibodies. *BioTechniques*, **44**, 927-929.

178. de Klein, A., Muijtjensa, M., van Os, R., Verhoevena, Y., Smit, B., CarrA, M., LehmannA, R. and Hoeijmakersa, J.H.J. (2000) Targeted disruption of the cell-cycle checkpoint gene ATR leads to early embryonic lethality in mice. *Current Biology*, **10**, 479-482.

179. Shechter, D., Costanzo, V. and Gautier, J. Regulation of DNA replication by ATR: signaling in response to DNA intermediates. *DNA Repair*, **3**, 901-908.

180. Carney, J.P., Maser, R.S., Olivares, H., Davis, E.M., Le Beau, M., Yates, J.R., Hays, L., Morgan, W.F. and Petrini, J.H.J. (1998) The hMre11/hRad50 Protein Complex and Nijmegen Breakage Syndrome: Linkage of Double-Strand Break Repair to the Cellular DNA Damage Response. **93**, 477-486.

181. Stewart, G.S., Maser, R.S., Stankovic, T., Bressan, D.A., Kaplan, M.I., Jaspers, N.G.J., Raams, A., Byrd, P.J., Petrini, J.H.J. and Taylor, A.M.R. (1999) The

DNA Double-Strand Break Repair Gene hMRE11 Is Mutated in Individuals with an Ataxia-Telangiectasia-like Disorder. **99**, 577-587.

182. Chowdhury, D., Keogh, M.-C., Ishii, H., Peterson, C.L., Buratowski, S. and Lieberman, J. (2005) ³-H2AX Dephosphorylation by Protein Phosphatase 2A Facilitates DNA Double-Strand Break Repair. **20**, 801-809.
183. Chowdhury, D., Xu, X., Zhong, X., Ahmed, F., Zhong, J., Liao, J., Dykxhoorn, D.M., Weinstock, D.M., Pfeifer, G.P. and Lieberman, J. (2008) A PP4-Phosphatase Complex Dephosphorylates ³-H2AX Generated during DNA Replication. **31**, 33-46.
184. Keogh, M.-C., Kim, J.-A., Downey, M., Fillingham, J., Chowdhury, D., Harrison, J.C., Onishi, M., Datta, N., Galicia, S., Emili, A. *et al.* (2006) A phosphatase complex that dephosphorylates [gamma]H2AX regulates DNA damage checkpoint recovery. *Nature*, **439**, 497-501.
185. Lukas, C., Falck, J., Bartkova, J., Bartek, J. and Lukas, J. (2003) Distinct spatiotemporal dynamics of mammalian checkpoint regulators induced by DNA damage. *Nat Cell Biol*, **5**, 255 - 260.
186. Deckbar, D., Birraux, J., Krempler, A., Tchouandong, L., Beucher, A., Walker, S., Stiff, T., Jeggo, P. and Lobrich, M. (2007) Chromosome breakage after G2 checkpoint release. *J. Cell Biol.*, **176**, 749-755.
187. Akihisa, T. and Takeo, O. (2005) Does Î³H2AX foci formation depend on the presence of DNA double strand breaks? *Cancer letters*, **229**, 171-179.
188. Hammond, E.M., Green, S.L. and Giaccia, A.J. (2003) Comparison of hypoxia-induced replication arrest with hydroxyurea and aphidicolin-induced arrest. *Mutation Research/Fundamental and Molecular Mechanisms of Mutagenesis*, **532**, 205-213.
189. Dmitrieva, N.I., Bulavin, D.V. and Burg, M.B. (2003) High NaCl causes Mre11 to leave the nucleus, disrupting DNA damage signaling and repair. *Am J Physiol Renal Physiol*, **285**, F266-274.
190. Takahashi, A., Matsumoto, H., Nagayama, K., Kitano, M., Hirose, S., Tanaka, H., Mori, E., Yamakawa, N., Yasumoto, J.-i., Yuki, K. *et al.* (2004) Evidence for the Involvement of Double-Strand Breaks in Heat-Induced Cell Killing. *Cancer Res*, **64**, 8839-8845.
191. Balajee, A.S. and Geard, C.R. (2004) Replication protein A and [gamma]-H2AX foci assembly is triggered by cellular response to DNA double-strand breaks. *Experimental Cell Research*, **300**, 320-334.

192. Schultz, L.B., Chehab, N.H., Malikzay, A. and Halazonetis, T.D. (2000) p53 Binding Protein 1 (53BP1) Is an Early Participant in the Cellular Response to DNA Double-Strand Breaks. *J. Cell Biol.*, **151**, 1381-1390.

193. Asaad, N.A., Zeng, Z.-C., Guan, J., Thacker, J. and Iliakis, G. (2000) Homologous recombination as a potential target for caffeine radiosensitization in mammalian cells: reduced caffeine radiosensitization in XRCC2 and XRCC3 mutants. *Oncogene*, **19**, 5788-5800.

194. Wang, H., Zeng, Z.-C., Bui, T.-A., Sonoda, E., Takata, M., Takeda, S. and Iliakis, G. (2001) Efficient rejoining of radiation-induced DNA double-strand breaks in vertebrate cells deficient in genes of the RAD52 epistasis group. *Oncogene*, **20**, 2212-2224.

195. Riballo, E., Kühne, M., Rief, N., Doherty, A., Smith, G.C.M., Recio, M.a.-J., Reis, C., Dahm, K., Fricke, A., Krempler, A. *et al.* (2004) A Pathway of Double-Strand Break Rejoining Dependent upon ATM, Artemis, and Proteins Locating to ³-H2AX Foci. **16**, 715-724.

9 Appendix

9.1 Appendix 1: Buffers and Solutions

1. **1X Phosphate Buffered Saline (PBS)**

   Dissolve the following in 800ml Double distilled water (ddH_2O).

   - 8 g of NaCl
   - 0.2 g of KCl
   - 1.44 g of Na2HPO4
   - 0.24 g of KH2PO4

   Adjust pH to 7.4.

   Adjust volume to 1 L with additional ddH_2O.

   Sterilize by autoclaving and store at 4°C.

2. **Trypsin-EDTA (Trypsin0.05%, EDTA 0.02%)**

   0.5 g of Trypsin

   0.2 g of EDTA

   Adjust the volume to 1 L with 1X PBS.

   Sterilize by passing through 0.22 µm filter and store at -20°C.

3. **Sodium azide (NaN_3 0.02%)**

   10 g of NaN_3

   Adjust the volume to 100 ml with ddH_2O.

   Store at RT.

4. **BrdU stock solution (10mM)**

   0.307 g of BrdU

   Adjust the volume to 100 ml with 1X PBS.

   Sterilize by passing through 0.22 µm filter and store at -20°C in dark.

5. **100X Propidium iodine. (4 mg/ml)**

   400 mg of PI

Adjust the volume to 100 ml with ddH_2O.

Store at -20°C in dark.

6. 100X RNase. (6.2 mg/ml)

620 mg of BrdU

Adjust the volume to 100 ml with MQ

Store at -20°C in dark.

7. 100X Nocodazole (40 µg/ml)

400 µg of Nocodazole

Adjust the volume to 10ml with DMSO.

Store at -20°C in dark.

8. 1M HCl

Add 10 ml 12M HCl to 50 ml ddH_2O.

Adjust the volume to 120ml with ddH_2O.

Store at RT.

9. 4x Tris/SDS pH 6.8 stacking gel buffer

Dissolve 6.05 g Tris-base in 40ml ddH_2O.

Adjust pH to 6.8 with 1 N HCl.

Add H20 to 100 ml.

Add 0.4 g SDS.

Store at 4°C.

10. 4x Tris/SDS pH 8.8 resolving gel buffer

Dissolve 91 g Tris-base in 300 ml ddH_2O.

Adjust to pH 8.8 with 1 N HCl.

Add H2O to 500 ml.

Add 2 g SDS.

Store at room temperature

11. 5x SDS electrophoresis buffer

15.1 g Tris-base

72.0 g glycine

5.0 g SDS

Add ddH_2O to 1000 ml.

Store at room temperature.

12. 6x SDS sample buffer

7 ml 4x Tris/SDS pH 6.8 stacking gel buffer

3.0 ml glycerol

1 g SDS

0.93 g DTT (dithio-threitol)

1.2 mg bromophenol blue

Add ddH_2O to 10 ml.

Store in 1 ml aliquots at -20°C.

13. 1X Transfer Buffer (Western blot transfer buffer)

Dissolve the following in 1600ml ddH2O.

- 28.8 g of glycine
- 6.04 g Tris base

Add 200 ml methanol.

Adjust the volume to 2000 ml with ddH2O.

Store at 4°C.

14. Tween-20 20%

200 ml Tween-20

Adjust the volume to 1000ml with ddH2O.

Store the solution at RT in dark.

15. PBST (PBS+0.05% ,Tween-20, washing buffer)

2.5 ml 20% Tween-20

Adjust the volume to 1000 ml with PBS.

Store the solution at RT in dark.

16. PBST-milk (PBST+5% ,Tween-20, washing buffer)

5g of milk (blot grade)

Adjust the volume to 1000 ml with ddH2O.

Store the solution at 4°C in dark.

17. 2% PFA (paraformaldehyde, fixation solution)

10 g PFA

450 ml ddH_2O

Heat to 50°C

Add a drop 1 N NaOH to bring PFA into solution.

Adjust the volume to 500 ml with ddH_2O.

Store the solution at -20°C in dark.

18. PBG (PBS-BSA 0.5%-Gelatin 0.2%, blocking buffer)

450 ml ddH_2O

1g Gelatine (boil at 50°C to dissolve and cool down)

2.5 g BSA

Adjust the volume to 500 ml with ddH_2O.

Store the solution at -20°C in dark.

19. P-solution (Permeabilization buffer)

2.43 g Tris-base

3.72 g EDTA

1 ml Triton X-100

Adjust pH7.4 with 1 M HCl.

Add ddH_2O to 200 ml.

Store the solution at 4°C in dark.

20. DAPI stock solution

10 mg DAPI

10 ml ddH2O

Store the solution at -20°C in dark.

21. FACS Permeabilization solution (PBS + 0.25% Triton X-100)

2.5 ml Triton X-100

Adjust the volume to 1000 ml with PBS.

Store the solution at RT in dark.

22. FACS blocking buffer (PBS + 0.05% Tween-20 + 1% BSA)

10 g BSA

2.5 ml 20% Tween-20

Adjust the volume to 1000 ml with PBS.

Store the solution at RT in dark.

9.2 Appendix 2: Cell line information

Cells were maintained at 37°C with 5% CO_2. 10% FBS were supplemented to the media.

Cell line	Doubling time	Mean size (µm)	Media	Initial Number	cell type	Genotype
A549	20 h	14,6	McCoy's	0,5 M	adenocarcinoma	wt
AT5BIVA	30 h	16,67	MEM	1 M	fibroblast	ATM deficient
GM847 ATRkd	30 h	18,65	MEM	1 M	fibroblast	ATR kinase dead
MO59 J	30 h	13,8	DMEM	1 M	glioblastoma	DNA-PKcs deficient
MO59 K	20 h	15,5	DMEM	0,4 M	glioblastoma	wt
HCT116 DNA-PKcs-/-	31 h	14,7	McCoy's	1 M	carcinoma	DNA-PKcs deficient
HCT116 wt	24 h	13,2	McCoy's	0,5 M	carcinoma	wt
F0298	35 h	16,2	MEM	2M	fibroblast	ATR defect
DK0064*	22 h	11,3	DMEM	0,3M	lymphoblastoid	ATR defect

** DK0064 grows in a suspension form.

9.3 Appendix 3: Settings for cell cycle analysis

Cell cycle analysis programme settings

Flow cytometry: COULTER EPICS XL

Sheath Speed: middle

Total cells sampled: 20000

Maximal running duration: 900 seconds

Working mode: carousel

cell line / Paramater	A549	AT5-BIVA	GM847 wt	GM847 ATRkd	F0298	DK0064	MO59 J	MO59 K	HCT116 DNAPkcs-/-	HCT116 wt
Exicitation (nm)	488	488	488	488	488	488	488	488	488	488
Filter spectrum (nm)	655-735	655-735	655-735	655-735	655-735	655-735	655-735	655-735	655-735	655-735
FS-PMT (volt)	55	55	55	55	55	55	55	55	55	55
FS-Gain	2	2	2	2	2	2	2	2	2	2
SS-PMT (volt)	400	400	400	400	400	400	400	400	400	400
SS-Gain	1	1	1	1	1	1	1	1	1	1
AUX-PMT (volt)	300	300	300	300	300	300	300	300	300	300
AUX-Gain	2	2	2	2	2	2	2	2	2	2
PI-PMT (volt)	530	520	520	520	530	530	540	545	560	550
PI-Gain	2	2	2	2	2	2	2	2	2	2
Discriminator	PI>3	PI>3	PI>3	PI>3	PI>3	PI>3	PI>3	PI>3	PI>3	PI>3
Gate	single cell	single cell	single cell	single cell	single cell	single cell	single cell	single cell	single cell	single cell

9.4 Appendix 4: Settings for bivariate flow cytometry

Flow cytometry: COULTER EPICS XL

Sheath Speed: middle

Total cells sampled: 20000

Maximal running duration: 900 seconds

Working mode: Manual

Programe / Paramater	DNA-PI BrdU-FITC	DNA-PI Cylin B1-FITC	DNA-PI H3-pS10-FITC
FS-PMT (volt)	55	55	55
FS-Gain	2	2	2
SS-PMT (volt)	400	400	400
SS-Gain	1	1	1
AUX-PMT (volt)	300	300	300
AUX-Gain	2	2	2
Excitation of PI	488nm	488nm	488nm
PI- Filter spectrum	655-735nm	655-735nm	655-735nm
PI-PMT (volt)	530	520	520
PI-Gain	2	2	2
PI signal	Linear	Linear	Linear
PI-GATE	single cell	single cell	single cell
Discriminator	PI>3	PI>3	PI>3
Excitation of FITC	488nm	488nm	488nm
FITC Filter	490-550nm	490-550nm	490-550nm
FITC-PMT (volt)	530	520	520
FITC-Gain	2	2	2
FITC signal	Logarithm	Linear	Linear
FITC-GATE	FITC positive	FITC positive	FITC positive

9.5 Appendix 5: Settings for western blot and immunofluorescence

1. Setting for SDS-PAGE

Protein	Gel conc	Constant Voltage (V)	Running time (min)	Temp	MW (KD)
ATM	8%	150	90	RT	370
ATM-pS1981	8%	150	90	RT	370
ATR	8%	150	90	RT	301
ATRIP	10%	150	90	RT	85
Chk2	12%	150	90	RT	68
Chk2-pT68	12%	150	90	RT	62
GAPDH	12%	150	90	RT	38
LAMIN	12%	150	90	RT	70

2. Setting for electrotransfer

Protein Name	Membrane	Transfer Voltage (V)	Transfer time (min)	Temp (°C)
ATM	PVDF	110	75	0
ATM-pS1981	PVDF	110	75	0
ATR	PVDF	110	75	0
ATRIP	PVDF	110	75	0
Chk2	PVDF	100	60	0
Chk2-pT68	PVDF	100	60	0
GAPDH	PVDF	100	60	0
LAMIN	PVDF	100	60	0

3. Antibody dilution for western blot and ECL exposure duration

Protein Name	Primary Antibody	Secondary Antibody	Image exposure duration (seconds)
GAPDH	1:20000	1:20000	50
ATM	1:800	1:1500	120
ATM-pS1981	1:800	1:1500	165
ATR	1:800	1:1500	150
ATRIP	1:10 **	1:1000	120
Chk2	1:1000	1:2000	120
Chk2-pT68	1:800	1:2000	160
LAMIN	1:500	1:1000	120

** ATRIP hybridoma culture supernatant

4. Antibody dilution for immunofluorescence

Protein Name	Primary Antibody	Secondary Antibody
ATM-pS1981	McAb 1:300	1:400
ATM-pS1981	PcAb 1:300	1:400
ATRIP	1:5**	1:400
Chk2-pT68	1:300	1:400
Cyclin B1	PcAb 1:300	1:400

** ATRIP hybridoma culture supernatant

5. Antibody dilution for bivariate flow cytometry

Protein Name	Primary Antibody	Secondary Antibody
BrdU	McAb 1:200	1:300
H3-pS10	PcAb 1:150	1:200
Cyclin B1	PcAb 1:150	1:200

9.6 Appendix 6: Settings for microscope and Imaris

Settings for Leica SP5 confocal microscope

Instrument Parameter Setting:	Confocal LDM			**Argon laser intensity:**	50%
Objective:	HCX PL APO lambda blue 63.0x1.40 OIL UV			**Speed:**	400Hz
Image size:	246.03 µm x 246.03 µm				
Pixel size:	481.46 nm x 481.47nm				
Sequential Scan:	between stacks				
Lineal Average:	1	**Accum:**	1		
Frame Average:	1	**Accum:**	1		
Scan direction:	bidirection			**Step size:**	0.5 µm
Resolution:	512x512				

Programe / Paramater	DAPI	ATM-pS1981 Alexa 488	ATM-pS1981 Alexa 568	Chk2-pT68 Alexa 488	Chk2-pT68 Alexa 568	ATRIP Alexa 488	Cyclin B1 Alexa 488	Cyclin B1 Alexa 568	EdU Alexa 647
Excitation	405 nm	488 nm	561 nm	488 nm	561 nm	488 nm	488 nm	561 nm	633 nm
Laser intensity	16%	23%	32%	23%	32%	23%	23%	32%	29%
Filter range	420-530nm	495-550 nm	620-700 nm	495-550 nm	620-700 nm	495-550 nm	495-550 nm	620-700 nm	646-733 nm
PMT	850 V	540 V	720 V	580 V	720 V	580 V	650 V	780 V	480 V
Smart gain offset	-2%	-5%	-5%	-5%	-5%	-5%	-2%	-2%	-2%
minimal foci size (Imaris)		0,5µm	0,5µm	0,5µm	0,5µm	0,5µm			
Imaris threshold		17	17	21	23	19			

Acknowledgement

I would like to express my deepest appreciation to my supervisor, Professor Dr. George Iliakis. His continuous and convincing guidance was a great benefit to me and helped me complete this project. Professor Iliakis, with his persistent help allowed me to resolve many issues and complications that arose during the preparation of this dissertation. His steady encouragement was a constant inspiration for me and helped me recover from setbacks. Finally, his generosity gave me enough freedom to carry out my research.

I would also like to thank my colleagues. Thank you all for creating an atmosphere full of harmony. Thank you for providing me with all the help I needed to resolve technical problems. Thank you for helping me by preparing many working solutions and growth media that I needed. Special thanks go to Frau Müller for all the administrative support she provided during my tenure as a Ph.D. student.

My sincere thanks go also to my parents. Thanks to them for giving me life to enjoy the diversity of this world.

At last, I would like to dedicate this thesis to my deeply beloved wife. During the last decade I am lucky to have her unconditional support, no matter where I am or what the circumstances might be.

Erklärung:

Hiermit erkläre ich, gem. § 6 Abs. 2, Nr. 8 der Promotionsordnung der Math.-Nat.-Fachbereiche zur Erlangung der Dr. rer. nat., dass ich das Arbeitgebiet, dem das Thema „**Interplay between ATM and ATR for the regulation of cellular responses to DNA damage**“ zuzuordnen ist, in Forschung und Lehre vertrete und den Antrag von (Herr Xiaoxiang Fan) befürworte.

Essen, den _____ _____

Unterschrift d. wissenschaftl. Betreuers/Mitglieds
der Universität Duisburg-Essen

Erklärung:

Hiermit erkläre ich, gem. § 6 Abs. 2, Nr. 6 der Promotionsordnung der Math.-Nat.-Fachbereiche zur Erlangung des Dr. rer. nat., dass ich die vorliegende Dissertation selbständig verfasst und mich keiner anderen als der angegebenen Hilfsmittel bedient habe.

Essen, den _____ _____

Unterschrift des/r Doktoranden/in

Erklärung:

Hiermit erkläre ich, gem. § 6 Abs. 2, Nr. 7 der Promotionsordnung der Math.-Nat.-Fachbereiche zur Erlangung des Dr. rer. nat., dass ich keine anderen Promotionen bzw. Promotionsversuche in der Vergangenheit durchgeführt habe und dass diese Arbeit von keiner anderen Fakultät abgelehnt worden ist.

Essen, den _____ _____

Unterschrift des Doktoranden